Investigating Lebercilin Interacting Proteins TTC30A/B and SSNA1 in Cilia Related Processes

Dissertation

der Mathematisch-Naturwissenschaftlichen Fakultät

der Eberhard Karls Universität Tübingen

zur Erlangung des Grades eines

Doktors der Naturwissenschaften

(Dr. rer. nat.)

vorgelegt von

Felix Hoffmann

aus Gera

Tübingen

2022

Gedruckt mit Genehmigung der Mathematisch-Naturwissenschaftlichen Fakultät der Eberhard Karls Universität Tübingen.

Tag der mündlichen Qualifikation:	05.04.2023
Dekan:	Prof. Dr. Thilo Stehle
1. Berichterstatter:	Prof. Dr. Robert Lukowski
2. Berichterstatter:	Prof. Dr. Marius Ueffing

Table of contents

List of figures

List of tables

Abbreviations

%	Percentage
A	adenine
Å	Ångström
aa	amino acid(s)
ABC	ammonium bicarbonate
ACN	acetonitrile
Amp	ampicillin
AP	affinity purification
APS	ammonium persulfate
ATP	adenosine 5'-triphosphate
BB	basal body
bp	base pair(s)
BSA	bovine serum albumin
C	cytosine
Cas9	CRISPR-associated protein 9
CC	connecting cilium
CCP5	cytoplasmic carboxypeptidase 5
CMLE	Classical Maximum Likelihood Estimation
CMV	cytomegalovirus
Cr	*Chlamydomonas reinhardtii*
CRISPR	clustered regularly interspaced short palindromic repeats
Da	Dalton
DAPI	4,6-diamidin-2-phenylindol
dATP	2'-deoxyadenosine 5'-triphosphate
ddH_2O	ultra-pure water
dH_2O	deionized water
DPBS	Dulbecco's phosphate-buffered saline
DMEM	Dulbecco's modified Eagle medium
DMSO	dimethylsulfoxid
DNA	deoxyribonucleic acid
dNTP	2'-deoxynucleotide 5'-triphosphate
dsDNA	double-stranded DNA
DTT	dithiotreitol
ECL	enhanced chemiluminescence
E. coli	*Escherichia coli*
e.g.	for example
ERG	electroretinogram
EtOH	ethanol
ESI	electrospray ionisation
Ex	exon
FA	formic acid
FBS	fetal bovine serum
flr	*fleer*
g	gram
G	guanine
GFP	green fluorescent protein
h	hour
HAc	acetic acid
HCD	higher-energy collisional dissociation
HCl	hydrochloric acid
HPLC	high performance liquid chromatography
HRP	horseradish peroxidase
HyD	hybrid detector
IAA	iodoacetamide
IFT	Intraflagellar Transport
IP	Immunoprecipitation
IS	inner segment
Kan	kanamycin
kb	kilo base(s)
kDa	kilo Dalton
KO	knockout
L	litre
LB	lysis buffer
LB-medium	lysogeny broth medium
LFQ	label free quantification
LCA	Leber congenital amaurosis
LCA5	Lebercilin
LC-MS/MS	liquid chromatography-tandem mass spectrometry
mAb	monoclonal antibody
MeOH	methanol
min	minute(s)
mRNA	messenger RNA
MS	mass spectrometry
MS/MS	tandem mass spectrometry

MTOC	microtubule organizing center
m/z	mass to charge ratio
NA	numeric apertur
NaCl	sodium chloride
NGS	normal goat serum
NP-40	Nonidet P-40
nt	nucleotide
OD	optical density
OMIM	Online Mendelian Inheritance in Man
OS	outer segment
pAb	polyclonal antibody
PAM	protospacer adjacent motif
PCR	polymerase chain reaction
PEI	polyethylenimine
PFA	paraformaldehyde
Puro	puromycin
PVDF	polyvinylidene difluoride
RNA	ribonucleic acid
RPE	retinal pigment epithelium
rpm	round per minute
RT	room temperature
SDS	sodium dodecyl sulfate
SDS-PAGE	SDS-polyacrylamide gel electrophoresis
SDM	site directed mutagenesis
sec	second(s)
SF-TAP	Strep/Flag tandem affinity purification
SOC	super optimal broth with glucose
ssDNA	single stranded DNA
StageTips	stop and go extraction tips
STED	stimulated emission depletion
T	thymine
Taq	Thermus aquaticus
TBS	tris-buffered saline
TBST	TBS-Tween
TEMED	N,N,N',N'-tetramethylethylene-diamine
TFA	trifluoroacetic acid
TPR	tetratricopeptide repeat
tRNA	transfer RNA
TTLL	tubulin tyrosine ligase-like
TZ	transition zone
U	unit(s)
UV/Vis	ultraviolet/visible
V	volt
v/v	volume per volume
WB	washing buffer
wt	wildtype
w/v	weight per volume

Amino acids

Alanine	A
Arginine	R
Asparagine	N
Aspartic acid	D
Cysteine	C
Glutamic acid	E
Glutamine	Q
Glycine	G
Histidine	H
Isoleucine	I
Leucine	L
Lysine	K
Methionine	M
Phenylalanine	F
Proline	P
Serine	S
Threonine	T
Tryptophan	W
Tyrosine	Y
Valine	V

Summary

Cilia are elongated compartments, emerging from the cellular surface of most eukaryotic cells. These organelles can be classified into motile and non-motile (primary or sensory) subtypes which are highly conserved across species [1-6]. Further, cilia consist of specific domains with distinct functions. The basal body derives from the centrosome, nucleates axonemal growth and is the starting point for intraciliary protein trafficking [7]. For cilium assembly, proteins are imported from the cytoplasm while free diffusion of proteins into the cilium is restricted by the transition zone [7]. The intraflagellar transport (IFT) system is a microtubule-based bidirectional transport process which moves cargo (e.g., tubulins) along the axoneme from the base to the tip of the cilium where they are incorporated into the growing axoneme [1, 8-10]. The process of IFT involves the movement of large protein complexes with the help of motor proteins [11]. The IFT particles are organized in two subcomplexes called complexes A and B consisting of 6 (A) and 16 (B) distinct proteins [8, 11, 12]. One of the core proteins of IFT-B is IFT70/TTC30, which comprises the two paralogues TTC30A and TTC30B [1, 8, 9, 13].

In the human retina, photoreceptors (rods, cones) have two major compartments: the inner segment (IS) and the outer segment (OS) [14]. The OS is a modified sensory cilium that is packed with membrane discs containing rhodopsin [14, 15]. The molecular transport between IS and OS is facilitated along the connecting cilium [16, 17]. Any biomolecule necessary for generation and maintenance of the photoreceptive outer segment is produced in the inner segment and needs to be transported by IFT via this route [17, 18]. A complete malfunction of the IFT leads to severe ciliogenesis defects, not only in the OS but in all cilia [2, 18, 19].

Defects in primary cilia structure and function are associated with a wide spectrum of inherited diseases involving various organs. Until now there are 35 of these so-called ciliopathies including Leber congenital amaurosis (LCA) [20, 21]. LCA is a rare hereditary retinal dystrophy which leads to photoreceptor degeneration in children already in the first year of life [22, 23]. To date 25 genes were identified to be associated with this disease, including *LCA5* [24, 25]. This gene is coding for Lebercilin, which was previously described (by Boldt *et al.*) to interact with the IFT machinery, including TTC30A/B. This interaction was lost due to LCA-associated mutations, resulting in an impaired IFT mediated opsin transport in

photoreceptors [26]. Further, Lebercilin was also described to interact with SSNA1 [26], which is essential for microtubule stability but is also involved in ciliary assembly and intraflagellar transport [27, 28]. In addition, both Lebercilin and SSNA1 were associated with regulators of cilia specific Sonic hedgehog (Shh) signaling [26]. This pathway regulates ciliogenesis and is dependent on intraflagellar transport [29, 30].

The study presented here investigated Lebercilin and its interacting proteins TTC30A and TTC30B as well as SSNA1 in cilia related processes. Initially, it was essential to create gene knockouts in human retinal pigment epithelium cell lines using the CRISPR/Cas9 system. Regarding TTC30, paralogue specific homozygous single knockouts as well as double knockouts were generated. By comparing KO and wildtype (wt) cell lines, structural features, differences in cilia assembly and protein function were assessed. In the TTC30A/B double knockout, the loss of cilia and tubulin polyglutamylation were observed. This phenotype resembled the previously described results of Takei *et al.* and Pathak *et al.* [31, 32]. These findings could be reversed by generating rescue cells, stably transfected with TTC30A or TTC30B wt constructs. In contrast, TTC30A/B single knockout cells had assembled cilia, but their length was reduced and they had less polyglutamylated tubulin.

In addition to these generated knockout cell lines, a paralogue specific CRISPR/Cas9 based knock-in was performed to insert a FLAG-tag on endogenous level. These tagged TTC30A/B cell lines were used for mass spectrometry analysis to define paralogue specific interactomes. Both proteins were found to interact with all IFT-B complex proteins, which was in line with previous findings [26]. Additionally, it was revealed that a TTC30 single KO did not affect complex stability, possibly due to redundancy. But a TTC30A/B double knockout led to a destabilized IFT-B complex and eventually to a disrupted intraflagellar transport as well as ciliary assembly. Further, interactome analysis revealed so far unknown paralogue specific protein interactors.

The proposed interaction of TTC30A with protein kinase A (PKA) catalytic subunit A was investigated. In TTC30A KO cells an increased PKA activity was observed plus a decreased localization of Smoothened (Smo) to the cilium. PKA and Smo are key regulators of cilia specific Shh and these findings indicate an inhibitory effect of TTC30A KO on this pathway. Next, the A375V TTC30B mutation was examined which was previously identified by Du *et al*. This mutation was described to influence Shh and possibly leading to synpolydactyly [33]. A MS analysis was performed, comparing wildtype (wt) and mutant TTC30A/B interactomes, to

evaluate the impact of this mutation on the abundance of their protein interactors. The A375V mutation led to several paralogue specific differences in protein interaction. Especially, the decreased interaction of mutant TTC30A with IFT57 is interesting and needs further investigation. This finding and the involvement of TTC30A in Shh signaling, might be possible explanations of how TTC30 is connected to synpolydactyly.

Regarding Lebercilin and SSNA1, the generation of respective knockouts in human retinal pigment epithelium cell lines was performed. LCA5 exon 3 and exon 6 as well as SSNA1 exon 1 and exon 3 knockouts were created. LCA5 and SSNA1 KO cells were compared to wt cells, to investigate the impact of these proteins on ciliary assembly and structure as well as their function. It was revealed, that LCA5 knockout led to a reduction of ciliary length and to overall less cells assembling cilia. In contrast, SSNA1 knockout led to an increase of ciliary length with no effect on the number of ciliated cells which is in line with previous findings [34]. The proposed involvement of Lebercilin and SSNA1 in Shh signaling could be partially verified as ciliary localization of Smo and Gli2 was decreased in SSNA1 KO cells [26, 28]. This result suggests an inhibitory effect of SSNA1 KO on this signaling pathway. Further, in Shh activated SSNA1 KO cells a ciliary accumulation of Lebercilin was observed, indirectly linking Lebercilin to Sonic hedgehog. These findings highlight the importance of Lebercilin-SSNA1 interaction in cilia related processes and imply that SSNA1 function is possibly connected to the misfunction of Lebercilin, which ultimately leads to photoreceptor degeneration. But to understand the protein function of Lebercilin and SSNA1 in cilia related processes and to uncover the underlying mechanism of Leber congenital amaurosis further investigations are needed.

Zusammenfassung

Zilien sind Ausstülpungen der Zellmembran, die auf der Oberfläche der meisten eukaryotischen Zellen zu finden sind. Diese Organellen können in motile und nicht-motile (primäre oder sensorische) Unterklassen eingeteilt werden und sind evolutionär stark konserviert in unterschiedlichsten Spezies [1-6]. Zilien sind weiterhin aus diversen Domänen mit spezifischen Funktionen aufgebaut. Der Basalkörper leitet sich vom Zentrosom ab und dient als Ursprung für die Ausbildung des Axonems. Gleichzeitig dient er als Startpunkt für den intraziliären Proteintransport [7]. Für Ausbildung und Wachstum eines Ziliums werden Proteine aus dem Zytoplasma ins Innere des Ziliums befördert, da passive Diffusion von Proteinen durch die Transitionszone eingeschränkt ist [7]. Das intraflagellare Transportsystem (IFT) ist ein bidirektionaler Transportprozess. Dieses System nutzt das ziliäre Grundgerüst aus Mikrotubuli um unterschiedlichste Ladung von der Basis des Ziliums zur Spitze, entlang dem Axonem, zu transportieren [1, 8-10]. Zu diesem Prozess gehört der Transport großer Proteinkomplexe (IFT Komplex A und B) mit Hilfe von Motorproteinen [11]. Der A-Komplex besteht aus 6 und der B-Komplex aus 16 verschiedenen Proteinen [8, 11, 12]. Ein Protein des B-Komplexes ist IFT70/TTC30, welches die beiden paralogen Proteine TTC30A und TTC30B zusammenfasst [1, 8, 9, 13].

In der menschlichen Retina bestehen die Fotorezeptoren (Stäbchen, Zapfen) aus zwei größeren Abschnitten: dem inneren (IS) und dem äußeren Segment (OS) [14]. Das OS ist ein modifiziertes sensorisches Zilium, dass Membrandisks mit Rhodopsin enthält [14, 15]. Jedes Biomolekül wird im inneren Segment synthetisiert und muss mittels IFT, entlang einem verbindenden Zilium, ins äußere Segment transportiert werden [16, 17]. Dort werden die Moleküle zur Ausbildung und zum Erhalt des lichtsensitiven äußeren Segments benötigt [17, 18]. Eine totale Fehlfunktion des IFT führt zu schweren Defekten der Ziliogenese, nicht nur im OS sondern in allen Zilien [2, 18, 19]. Strukturschäden und Fehlfunktionen in primären Zilien sind mit einem weiten Spektrum an erblich bedingten Krankheiten verknüpft, die unterschiedliche Organe betreffen. Bisher sind 35 dieser Ziliopathien bekannt, darunter die Leber kongenitale Amaurose (LCA) [20, 21]. LCA ist eine seltene angeborene retinale Dystrophie, die gekennzeichnet ist durch die Degeneration von Fotorezeptoren bei Kindern, während der ersten Lebensjahrs [22, 23]. Bis heute wurden 25 Gene identifiziert, die mit

dieser Krankheit assoziiert sind, darunter *LCA5* [24, 25]. Dieses Gen kodiert für Lebercilin, was von Boldt *et al.* als Interaktor des IFT-Apparats, einschließlich TTC30A/B, identifiziert wurde. In LCA-assoziierten Mutationen waren diese Interaktionen nicht vorhanden und hatten einen eingeschränkten intraflagellaren Transport von Opsinen im Fotorezeptor zur Folge [26]. Weiterhin wurde Lebercilin als Interaktor von SSNA1 beschrieben, welches essenziell ist für die Stabilität von Mikrotubuli, aber auch im Aufbau von Zilien und am IFT involviert ist [27, 28]. Zusätzlich wurden sowohl Lebercilin als auch SSNA1 mit Proteinen assoziiert, die zum Sonic hedgehog (Shh) Signalweg gehören [26]. Dieser zilienspezifische Signalweg reguliert die Ziliogenese und ist zur Signaltransduktion auf den intraflagellaren Transport angewiesen [29, 30].

Die hier vorgelegte Arbeit untersuchte die mit Lebercilin interagierenden Proteine TTC30A/B und SSNA1, sowie deren Beteiligung an ziliären Prozessen. Dazu wurden initial, mit Hilfe des CRISPR/Cas9-Systems, Gen-Knockouts in humanen retinalen Pigmentepithel-Zelllinien generiert. Zur Untersuchung von TTC30 wurden paralogspezifische homozygote TTC30A und TTC30B Einzel-Knockouts (KO) sowie Doppel-Knockouts hergestellt. Deren Vergleich mit Wildtyp-Zellen (wt) ermöglichte es Unterschiede an Strukturmerkmalen, im Zilienaufbau und der Proteinfunktion festzustellen und auszuwerten. Beim TTC30A/B Doppel-KO konnte ein Verlust von Zilien sowie der Polyglutamylierung von Tubulin beobachtet werden. Diese Ergebnisse, die bereits schon von Takei *et al.* und Pathak *et al.* beschrieben wurden, konnten durch das Erstellen von Rescue-Zellen umgekehrt werden. Diese stabilen Zelllinien wurden, durch Transfektion mit TTC30A oder TTC30B wt Konstrukten und anschließender Selektion mit Antibiotika, generiert [31, 32]. In TTC30A/B Einzel-KOs hingegen wurden Zilien exprimiert, deren Länge war jedoch reduziert und zudem wurde weniger Tubulin polyglutamyliert.

Zusätzlich zu den Knockout-Zelllinien wurden, mit Hilfe des CRISPR/Cas9 Systems, Knockin-Zelllinien erstellt. Bei diesen wurde gezielt in TTC30A oder TTC30B ein FLAG-Tag auf endogener Ebene eingeführt. Diese Zelllinien sind verwendet worden, um eine massenspektrometrische (MS) Analyse durchzuführen und ein paralogspezifisches Interaktom zu generieren. Wie bereits in der Literatur beschrieben, interagieren beide Proteine mit dem gesamten IFT-B Komplex [26]. Weiterhin konnte beobachtet werden, dass im TTC30 Einzel-Knockout, aufgrund von möglicher Redundanz der paralogen Proteine, die IFT-B Komplexstabilität nicht beeinträchtigt war. Allerdings führte der TTC30A/B Doppel-Knockout zu einem destabilisierten IFT-B Komplex und letztendlich zu einem Stopp des intraflagellaren

Transports sowie des Zilienaufbaus. Außer gemeinsamen Interaktoren, ermöglichte die MS Analyse es wahrscheinliche und bisher unbekannte Interaktoren zu identifizieren, die spezifisch für TTC30A oder TTC30B sind.

Die mögliche Interaktion von TTC30A mit der katalytische Untereinheit A der Protein Kinase A (PKA) wurde untersucht und ergab in TTC30A KO Zellen eine erhöhte Aktivität der Protein Kinase A. Außerdem war gleichzeitig die ziliäre Lokalisierung von Smoothened (Smo) reduziert. Sowohl PKA als auch Smo gehören zum zilienspezifischen Shh Signalweg und dessen Beeinflussung deutet auf einen inhibitorischen Effekt des TTC30A KOs hin. Als nächstes wurde die A375V Mutation in TTC30B untersucht, die von Du *et al.* Identifiziert wurde. Diese Mutation beeinflusst den Shh Signalweg und führt möglicherweise zu Synpolydaktylie [33]. Eine MS Analyse wurde durchgeführt um die Interaktome von Wildtyp und mutierten TTC30A/B Zelllinien zu vergleichen. Die Häufigkeit im Auftreten von Interaktoren ermöglichte es die Auswirkungen der Mutation abzuschätzen. Dabei konnten paralogspezifische Unterschiede bei einigen Interaktionen festgestellt werden. Hervorzuheben ist hier die beeinträchtigte Interaktion der TTC30A Mutante mit IFT57, die weiter erforscht werden muss. Dieses Ergebnis und die Beeinflussung des Shh Signalwegs durch TTC30A sind mögliche Erklärungen wie TTC30 und Synpolydaktylie verbunden sind.

Hinsichtlich der Untersuchung von Lebercilin und SSNA1 wurden Gen-Knockouts in humanen retinalen Pigmentepithel-Zelllinien erstellt. LCA5 Exon 3 und 6 sowie SSNA1 Exon 1 und 3 KOs wurden generiert. Diese KO-Zelllinien wurden mit wt Zelllinien verglichen, um den Einfluss dieser Proteine auf Zilienaufbau und -struktur zu beurteilen und deren Proteinfunktion zu untersuchen. Es konnte gezeigt werden, dass der LCA5 KO zu einer Reduktion der Zilienlänge führt und generell weniger Zellen ein Zilium ausbilden. Im Gegensatz dazu führte der SSNA1 KO zu einer Erhöhung der Zilienlänge, wobei aber die Zahl der zilierten Zellen unverändert blieb. Dieses Ergebnis ist identisch mit früheren Arbeiten [34]. Die vermutete Beteiligung von Lebercilin und SSNA1 am Shh Signalweg konnte teilweise bestätigt werden, da die ziliäre Lokalisierung von Smo [26, 28] und Gli2 im SSNA1 KO reduziert war. Dieses Resultat weist auf einen inhibitorischen Effekt des SSNA1 KOs auf den Shh Signalweg. Zudem konnte in SSNA1 KO Zellen gezeigt werden, das Lebercilin bei aktiviertem Signalweg im Zilium akkumuliert. Wodurch Lebercilin und Shh indirekt verbunden werden. Zusammengefasst heben diese Ergebnisse die Bedeutung der Interaktion von Lebercilin und SSNA1 in ziliären Prozessen hervor. Weiterhin wird angedeutet, dass die Funktion von SSNA1 eventuell mit der

Fehlfunktion von Lebercilin zusammenhängt, die zur Degeneration von Fotorezeptoren führt. Allerdings sind noch weitere Untersuchungen nötig, um die Funktionen von Lebercilin und SSNA1 im Zilium zu verstehen und um den zugrunde liegenden Mechanismus von Leber kongenitaler Amaurose aufzudecken.

1. Introduction

1.1. Cilia

Cilia are elongated compartments, emerging from the cellular surface of most eukaryotic cells. These organelles can be classified into motile and non-motile subtypes which are highly conserved across species [1-6]. Motile (or secondary) cilia consist of nine peripheral microtubule heterodimers (α- and β-tubulin) which are circular arranged around a central pair of single microtubules. This structure with the characteristic 9+2 microtubule pattern is called an axoneme [3-5, 35]. Furthermore, the axoneme of a motile cilium has auxiliary dynein arms and radial spokes. These structural features allow steady ciliary movement which is utilized e.g., by epithelial cilia in the lungs for mucus clearance, the sperm flagellum for propulsion or during embryonic development for left-right determination [5, 36-39]. Contrary to this, non-motile (primary or sensory) cilia are specialized in signal transduction [1, 2, 6, 40, 41]. They have a 9+0 axonemal pattern without a central pair of microtubules, dynein arms, radial spokes and therefore without ciliary movement [2, 4-6]. Other domains of the primary cilium, crucial for ciliogenesis, are the basal body (BB), the transition zone (TZ), the ciliary tip and the ciliary membrane [1-3].

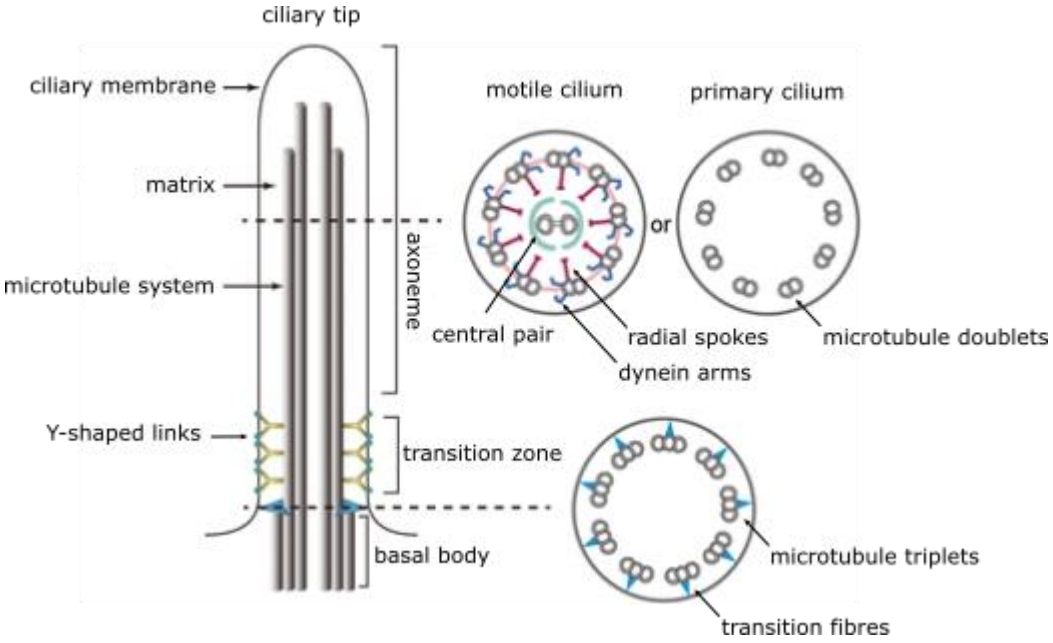

Figure 1 – Ciliary structure of motile and primary cilia – Depicted are the ciliary compartments basal body, transition zone, ciliary membrane, axoneme and the ciliary tip. Microtubule patterns of primary cilia (9+0), motile cilia (9+2) and the basal body (9+3) are shown in cross sections. Y-shaped links connect the axoneme and transition fibers the basal body to the cilia membrane. Modified after [42]

The TZ is regulating the entry of proteins by restricting their free diffusion into the cilium [7]. The BB has a cylindrical barrel-like structure with a radial layout of nine microtubule triplets (γ-tubulin; **Figure 1**) [3, 43]. It nucleates the axoneme and is the starting point for protein trafficking to the ciliary tip, where the transported cargo is used for assembly and disassembly of the cilium [7]. The plasma membrane is the outer boundary of the cilium. It has a very specific lipid and protein composition enabling the cilium in combination with the ciliary tip to be involved in photo-, mechano- or thermosensation processes. [3, 5, 7, 20, 44]. More detailed, specific transmembrane receptors and ion channels are part of unique signaling pathways (e.g., Sonic hedgehog) that initiate interaction cascades. Ultimately, affecting transcription factors in the nucleus and influencing the regulation of cellular proliferation and growth, differentiation as well as ciliogenesis [2, 3, 45, 46].

1.2. Ciliogenesis

Ciliogenesis, the formation of the cilium, starts with the centrosome migration to the cell surface. Followed by the transition into the basal body in G_1 phase and the subsequent docking of ciliary vesicles [1, 47-49]. This conversion also nucleates the axoneme [1, 47]. The BB itself is anchored at the distal end to the ciliary membrane by transition fibers [3, 46, 50]. Additionally, in the transition zone, the proximal end of the axoneme, is also connected to the ciliary membrane by Y-shaped links (**Figure 1**). Transition fibers and transition zone together form the ciliary gate [3, 46, 51]. This sub-domain regulates selective protein trafficking in and out of the cilium since proteins for synthetically inactive cilia must be imported from the cytoplasm [1, 46, 52]. This control of protein influx results in a discrete ciliary proteome [53]. Furthermore, the transition fibers are also binding sites for intraflagellar transport (IFT) complexes [3, 54]. These belong to a cilia specific transport system which carries proteins and other cargos, that are necessary for axoneme elongation, into the cilium [1, 3, 9, 46, 55]. In G_0 phase assembly and disassembly are in balance and a mature cilium is formed. This state of cell cycle arrest can be achieved by serum deprivation. After serum stimulation, cells can re-enter cell cycle (G_1 phase) and cilia start to disassemble [52, 56-58]. Finally, when going from S/G_2 phase to M phase the basal body is released from the cilium and the centrosome can then again function as microtubule organizing center (MTOC) or spindle poles (**Figure 2**) [47, 49, 52].

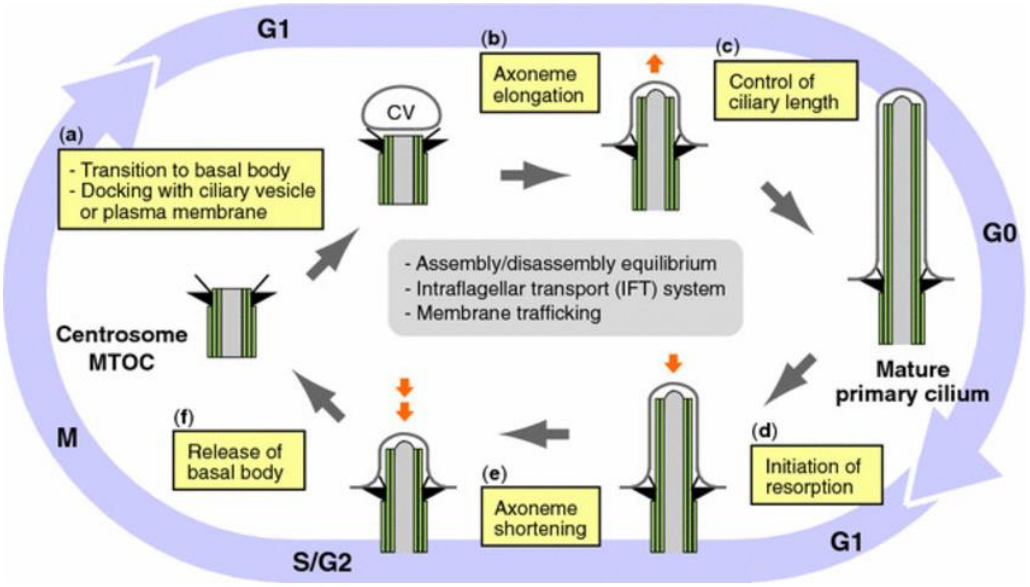

Figure 2 – Cell cycle dependent ciliary assembly and disassembly – Depicted are centrosome docking at the plasma membrane and transition to the basal body (a) in G_1. Axoneme elongation (b) and increasing ciliary length (c) in G_1. Maturation of primary cilia in G_0. Beginning of cilia resorption (d) and axoneme shortening (e) in G_1 to S/G_2. Finally, the release of the basal body to function as MTOC in M phase. [52]

1.3. Intraflagellar transport

For cilium assembly, axonemal tubulins are imported from the cytoplasm and transported by IFT to the tip of the cilium where they are incorporated into the axoneme [8]. IFT is a microtubule-based bidirectional transport process which moves cargo along the axoneme [1, 8-10]. The process of IFT involves the movement of large protein complexes with the help of motor proteins [8, 59, 60]. The anterograde transport is mediated by the hetero trimeric motor protein kinesin-2 and retrograde movement by dynein 2 (**Figure 3**) [8, 11, 61, 62]. The IFT particles are organized in two subcomplexes called complexes A and B [11] consisting of 6 (A) and 16 (B) distinct proteins [12]. The architecture of IFT-A and IFT-B is well described. IFT-A contains IFT144, -140, -139, -122, -121 and -43. IFT-B can be divided into peripheral and core subunits [8, 26, 63]. The stable IFT-B core complex is known as IFT-B1 (IFT88, -81, -74, -70, -52, -46, -27, -25, and -22) interacting with the second subcomplex known as IFT-B2 (IFT172, -80, -57, -54, -38, and -20) [8, 64].

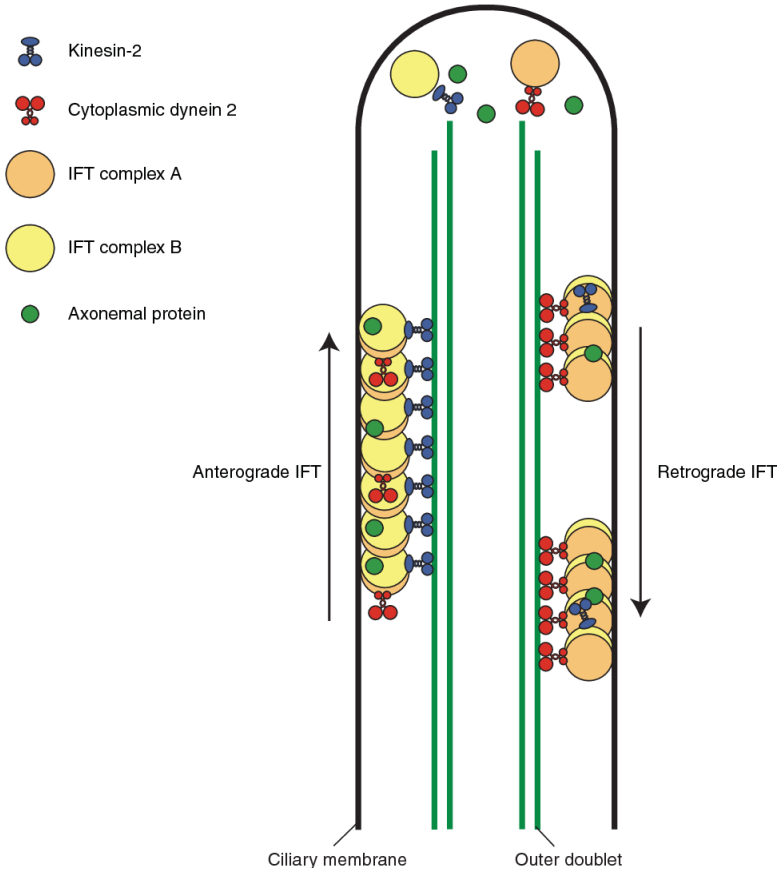

Figure 3 – Intraflagellar transport system in cilia – Depicted are kinesin-2 and IFT-B mediated anterograde transport to the ciliary tip and dynein 2 and IFT-A mediated retrograde transport from the tip to the ciliary base. [9]

The IFT-B structure consists of a complex interaction pattern. The IFT27/25 hetero-dimer binds to the N- and mainly C-terminal parts of IFT81/74 hetero-dimer and IFT22 binds to the central part of IFT81/74 [65]. The C-termini of IFT81/74 and heterodimeric IFT52/46 interact with each other, therefore connecting tetrameric IFT88/70/52/46 and pentameric IFT81/74/27/25/22 subcomplexes [66], but also the N-terminal regions of IFT81 and IFT74 crosslink to IFT88 and IFT70 [65]. IFT88 is linked to IFT70 as well as IFT52, with IFT70 also being covalently bound to IFT52 [65]. IFT-B1 and B2 are connected by IFT88/52 and IFT57/38 [13, 63]. IFT57 and IFT38 interact via their C-terminal domains. IFT54 and IFT20 are linked similarly and form with IFT57/38 an antiparallel hetero-tetramer [65]. IFT38 interacts with IFT80 and IFT57 with IFT172, whereas IFT80 and IFT172 form a hetero-dimer **(Figure 4)** [65].

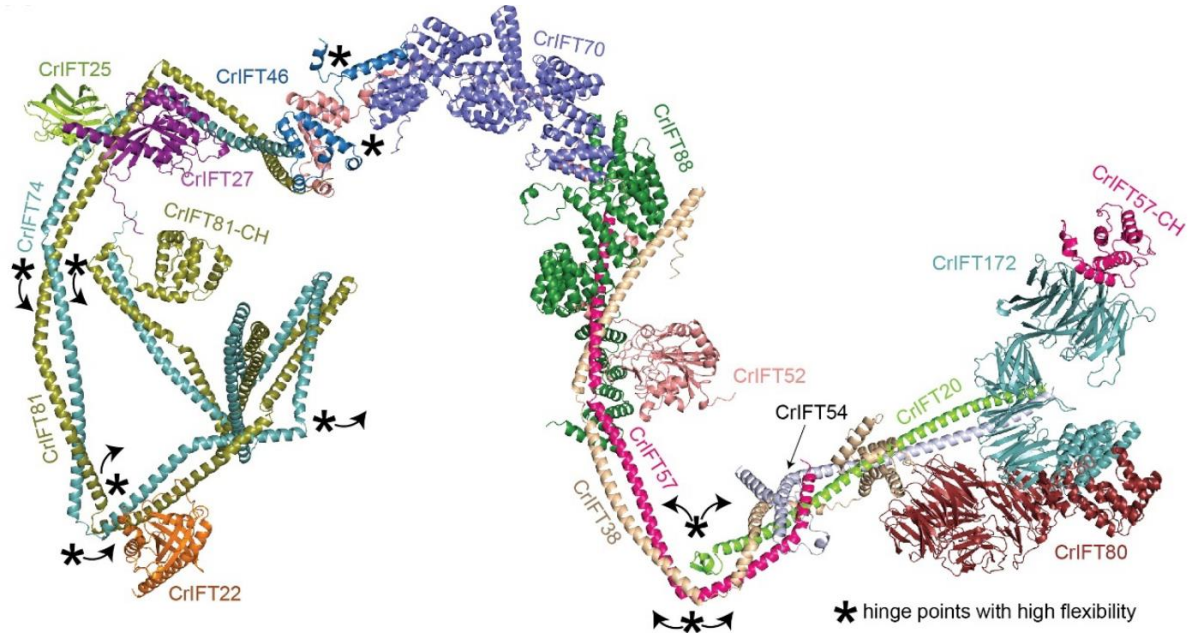

Figure 4 – Structural model of the IFT-B complex – Depicted is the is silico rigid body assembly of IFT-B complex (*Chlamydomonas reinhardtii* (Cr)) calculated from sub-complexes, predicted by AlphaFold. The structural model is assembled from CrIFT81/74$_{128\text{-}C}$/27/25/22, CrIFT88$_{120\text{-}713}$/70/52/46$_{188\text{-}319}$/81$_{587\text{-}645}$/74$_{583\text{-}C}$, CrIFT88$_{120\text{-}713}$/52$_{1\text{-}336}$/57$_{360\text{-}C}$/38$_{174\text{-}303}$, CrIFT57/54$_{135\text{-}C}$/38/20, CrIFT80/38 and CrIFT172$_{1\text{-}780}$/57. Hinge regions (*) provide most likely conformational flexibility within the IFB-B complex. [65]

1.4. TTC30

One of the core proteins of IFT-B is IFT70/TTC30, which comprises the two paralogue proteins TTC30A and TTC30B [8]. Both genes, encoding the two paralogues, consist of one large exon (665 aa) and both proteins have a molecular weight of 76 kDa. They contain tetratricopeptide repeat (TPR) structural motifs and these motifs fold together to produce a single TPR domain. Such domains usually mediate protein–protein interactions and the assembly of multiprotein complexes [8, 13, 66]. In the tetrameric IFT88/70/52/46 subcomplex, IFT70 interacts with IFT88 by their TPRs [65] and IFT88 forms a hetero-dimer with IFT52 [31, 65]. The TPRs of IFT70 wrap around IFT52 as a superhelix [66]. The N-terminus of IFT70 is covalently connected to the C-termini of IFT52 and IFT46, which interact with each other to form a hetero-dimer [65]. TTC30A and B share highly similar nucleotide sequences (**Appendix 1**) and subsequently protein structure (**Figure 5**), which are conserved throughout several species [8, 33]. Each paralogue is sufficient to support cilia assembly [31] and is able to interact with IFT-B complex components [8, 26, 67]. Further, Taschner *et al.* showed the direct interaction of the *Chlamydomonas reinhardtii* IFT70/DYF-1 orthologue with IFT52 [8, 66, 68]. DYF-1 depletion in *C. reinhardtii* leads to extremely shortened cilia, demonstrating its importance for

IFT-B-mediated ciliary assembly [8, 67]. This phenotype was also observed in zebrafish (*Danio rerio*) *fleer* (*flr*, IFT70 orthologue) mutants, additionally linked to an ultrastructural defect in the axoneme. This defect likely results from a reduced level of glutamylated tubulin [8, 32]. Polyglutamylated tubulin, a post-translational modification, was previously shown to be involved in stabilizing axonemes [8, 69, 70]. These findings suggest a role of *flr* in ciliogenesis as a structural component of IFT-B and a function as an IFT cargo adapter for a tubulin tyrosine ligase-like (TTLL) enzyme that catalyzes tubulin glutamylation [8, 32, 71]. The knockdown of cytoplasmic carboxypeptidase 5 (CCP5), restoring ciliary tubulin glutamylation in *flr* mutants and rescuing cilia assembly, indicates that polyglutamylation is a key driver of ciliogenesis [8, 72].

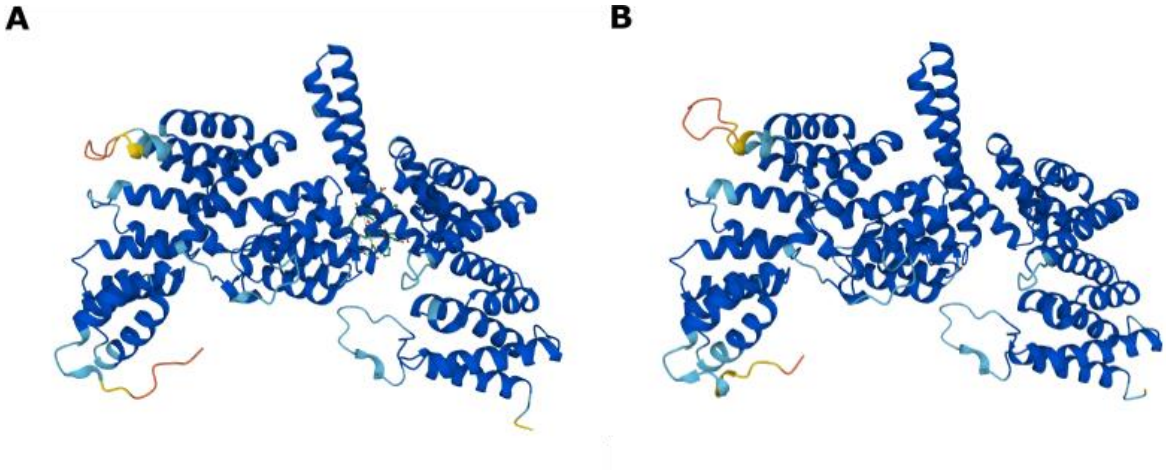

Figure 5 – Protein structure of paralogue TTC30A and TTC30B – The picture shows the highly similar protein structure of TTC30A (**A**) and TTC30B (**B**) calculated by AlphaFold (via UniProt). Regions with very high confidence (per residue confidence score, pLDDT > 90) are depicted dark blue. Regions with high confidence (90 > pLDDT > 70) are depicted light blue, low confidence is depicted yellow (70 > pLDDT > 50) and very low shown in orange (pLDDT < 50).

1.5. Retinal cilia

The eyes of nearly all animals, humans in particular, are capable of visual perception. They collect and focus light rays onto the retina which is the innermost, light-sensitive tissue of the eye. In the human retina the primary light-sensing cells are the photoreceptor cells, which are of two types: rods and cones [15]. They are specialized neuroepithelial cells that develop unique sensory cilia for phototransduction [15, 73]. Photoreceptors have two major compartments: the biosynthetically active inner segment (IS) and the outer segment (OS). The OS is a modified sensory cilium that has stacks of membrane discs which contain rhodopsin [14, 15]. This particle is a chromophore (11-cis retinal) covalently bound to the

transmembrane protein opsin [15]. The molecular transport between IS and OS is facilitated along the connecting cilium (CC; Figure 6) [16, 17]. Its structure is comparable to the transition zone of primary cilia [17, 74].

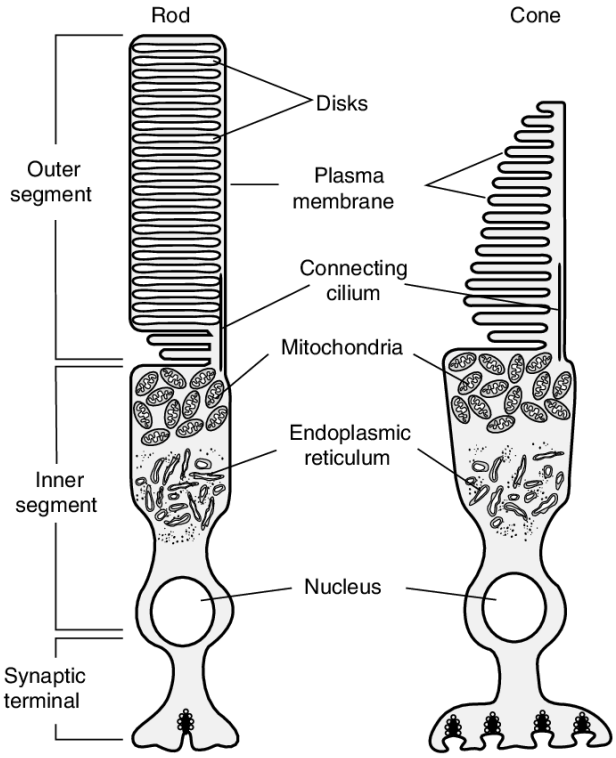

Figure 6 – Structure of rod and cone photoreceptor cells – Depicted are the two major compartments of rods (**left**) and cones (**right**): the bioactive inner segment and the outer segment, linked by the connecting cilium. The outer segment, derived from a sensory cilium, is packed with rhodopsin containing discs. [75]

Any biomolecule necessary for generation and maintenance of the photoreceptive outer segment is produced in the inner segment and needs to be transported via this route. Especially the demand of rhodopsin as well as the daily shedding of discs necessitates a massive transport [17, 18]. Along the microtubular system of the CC, the transport is driven by the IFT together with the motor proteins dynein and kinesin [61, 62]. Also, membrane associated molecules and membrane integral receptors, which enable the cilium to serve as the cell's signalling hub, need to be transported via the IFT to reach their destination. A complete malfunction of the IFT leads to severe ciliogenesis defects due to the ciliary composition of microtubular structures, not only in the OS but in all cilia [2, 18, 19].

1.6. Leber congenital amaurosis

Defects in primary cilia structure and function are associated with a wide spectrum of inherited diseases involving various organs. Until now there are 35 of these so-called ciliopathies including many syndromes like Joubert syndrome (JS) or Bardet-Biedl syndrome (BBS) [19-21]. These disorders are genetically and phenotypically heterogeneous but also share common clinical features demonstrating their complexity [45]. Individually, ciliopathies are quite uncommon, but collectively these diseases with so far 190 known ciliopathy genes add up to 1 in 2000 affected people [76, 77].

Leber congenital amaurosis (LCA) is a rare hereditary retinal dystrophy which leads to photoreceptor degeneration in children, already in the first year of life [22, 23]. The typical disease characteristics are early visual loss, sensory nystagmus, amaurotic pupils and absence of scotopic and photopic electroretinogram (ERG) [78]. To date 25 genes were identified to be associated with this disease [24, 25]. Nine of these are genes that either localize or are essential for the function of the connecting cilium, the ciliary transport within photoreceptors or primary cilia in cultures of mammalian cells, including *LCA5* [79, 80].

1.6.1. Lebercilin

Mutations in Leber congenital amaurosis 5 (*LCA5*, Lebercilin, OMIM: 611408) gene accounts for about 1%-2% of LCA [23]. *LCA5* consists of nine exons (697 aa; 80.5 kDa), whereas exon 1 and exon 2 are not translated [79]. The protein structure is poorly characterized. So far only disordered and coiled coil regions could be identified (Figure 7) [79]. Recently, it was revealed that Lebercilin forms tetramers or even higher order oligomers due to interaction of their coiled coil domains [81], which is common for centrosomal proteins [82].

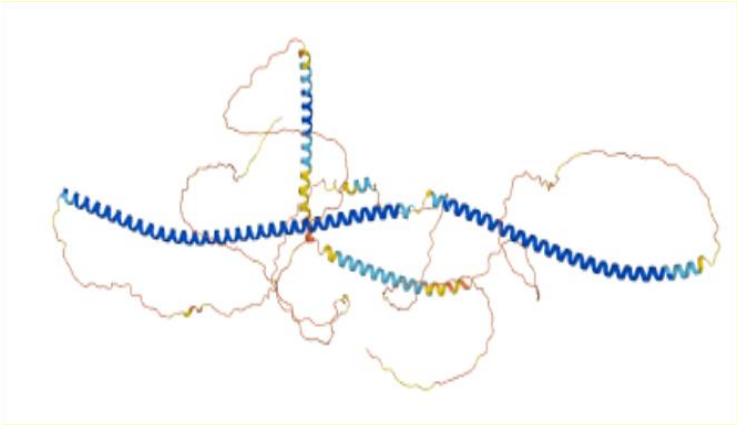

Figure 7 – Protein structure of LCA5 – The picture shows the protein structure of Lebercilin calculated by AlphaFold (via UniProt). Regions with very high confidence (per residue confidence score, pLDDT > 90) are depicted dark blue. Regions with high confidence (90 > pLDDT > 70) are depicted light blue, low confidence is depicted yellow (70 > pLDDT > 50) and very low shown in orange (pLDDT < 50).

Lebercilin function is essential to maintain the highly active ciliary transport of the CC, including intraflagellar transport mechanisms [80]. Malfunction of the connecting cilium results in either failure to generate outer segments in developing photoreceptors or in degeneration of those when light reception sets in [79, 80]. Although Lebercilin is widely expressed throughout different tissues and developmental stages, the disease phenotype is only restricted to the eye [79].

Mutations in Lebercilin were described to be the cause of LCA. To date, four mutations, causing LCA, and affecting either the protein sequence or its expression, were described (P384QfsX17, P493TfsX1, Q279X and a deletion, encompassing 1,077 bp of the promoter region and noncoding exon 1) [79, 80]. These mutations (in exon 5, 6, 9) either lead to a loss of expression or to the expression of a truncated Lebercilin form. The function of Lebercilin as well as the mechanism by which these mutations lead to LCA are not clear yet [23, 79, 80]. However, it was already reported, that the interaction of Lebercilin with the IFT machinery, including TTC30A/B, is lost due to LCA-associated mutations resulting in an impaired IFT transport in photoreceptors [79, 80]. Additionally, in mice, a knockout of Lebercilin leads to failure in generating normal outer segments and to a loss of rhodopsin as well as opsin in the outer segments. Taken together with the fact that both light induced translocation of Arrestin and Transducin is clearly impaired, demonstrates that it is truly a transport defect [79, 80]. Nevertheless, the role of Lebercilin in these mechanisms remains unknown.

1.6.2. SSNA1

Syscilia (www.syscilia.org) generated a comprehensive interaction network of cilia and gave novel insights into the interactions of Lebercilin [83]. After stringent filtering of the data and computational analysis using both, socio-affinity as well as a novel protein complex detection approach, additional interactions of Lebercilin with SSNA1 were revealed [84]. The functional relevance of this interaction is not known and needs to be elucidated.

Sjögren's syndrome nuclear autoantigen-1 (SSNA1) is a rather small protein, with three exons (119 aa) and a mass of 13.6 kDa, that mainly consists of one large coiled coil domain (**Figure 8**) [28, 85]. SSNA1 can be found at the spindle poles and has a role in cell division [27, 86]. It localizes to the axoneme and mainly to the centrosome/basal body [27, 28]. SSNA1 forms like Lebercilin higher order oligomers [87] and has a function in ciliary assembly and intraflagellar transport [27, 28]. In neuronal cells it is involved in axon outgrowth and branching [86]. These functions are depending on microtubular nucleation and assembly, which are also promoted by SSNA1 [87]. More recently, SSNA1 was shown to stabilize microtubules by decreasing microtubule growth rate, shrinkage and sudden catastrophe. Furthermore, it detects naturally and induced (by Spastin) damages in the microtubule complex [34].

Figure 8 – Protein structure of SSNA1 – The picture shows the protein structure of LCA5 calculated by AlphaFold (via UniProt). Regions with very high confidence (per residue confidence score, pLDDT > 90) are depicted dark blue. Regions with high confidence (90 > pLDDT > 70) are depicted light blue, low confidence is depicted yellow (70 > pLDDT > 50) and very low shown in orange (pLDDT < 50).

Based on the previous findings of Lai *et al.* it was clear that SSNA1 is involved in Shh. But so far it remains unclear how SSNA1 downregulates ciliary localization of Smo and Gli3 [28]. The Syscilia protein network revealed the strong interaction with ciliopathy associated Lebercilin. Additional protein interactors of Lebercilin (KIF7) and SSNA1 (SuFu) could be identified. Both

proteins are related to cilia specific Sonic hedgehog signaling pathway (Shh). These findings suggest how Lebercilin and SSNA1 could be involved in Shh. Additionally, Lebercilin and SSNA1 are both involved in ciliogenesis and intraflagellar transport [27, 28, 79, 80]. Therefore, the aim was to investigate SSNA1 function and by that to uncover the nature of Lebercilin-SSNA1 interaction and the underlying mechanism of Leber congenital amaurosis.

1.7. Ciliary signaling and Sonic hedgehog pathway

The membrane of a sensory (primary) cilium is packed with transmembrane receptors and ion channels which let cells respond to different external stimuli. Signaling cascades are initiated and regulation takes place at the basal body or transition zone. A variety of signaling pathways has been linked to the cilium e.g., Wnt, Notch, Hippo, GPCR and TGF-β. With Sonic hedgehog being the best studied primary cilia signaling pathway [3, 44, 46].

In the Shh off state, the receptor Patched1 (Ptch1) is located at the ciliary membrane inhibiting the localization of Smoothened (Smo) to the primary cilium [3, 44, 88, 89]. Additionally, tubby-like protein 3 (TULP3) and IFT-A mediate the localization of GPR161 to the cilium [90]. The activity of this G protein-coupled receptor leads to increased ciliary cAMP level [91]. Protein kinase A (PKA) is a tetrameric holoenzyme consisting of two regulatory and two catalytic subunits (PKAcat). Upon binding of cAMP, the regulatory subunits dissociate from PKA and relieve the inhibition of the catalytic subunits [92]. Activated PKAcat in conjunction with glycogen synthase kinase 3β (GSK3β) and casein kinases (CK) are involved in the proteolytic cleavage of full length Gli2 and Gli3 (GliFL) transcription factors into their repressed form (GliR) (Figure 9) [93-96].

Upon binding of Hedgehog (Hh) ligand to Patched1, the protein exits the cilium and the inhibition of pathway components entering, followed by their migration to the tip, is relieved. This includes Smo, suppressor of Fused (SuFu) and glioma associated oncogene (Gli1) transcription factors [88, 94, 97-99]. Ciliary enrichment of Smo leads to the dissociation of SuFu from GliFL transcription factors. This is followed by their phosphorylation and subsequent formation of Gli transcriptional activator (GliA) [98-100]. This process is highly dependent on the IFT in the primary cilium [101-103]. Furthermore, due to Hh activation GPR161 exits the cilium. This leads to a decrease of cAMP level and to an inhibition of PKA and subsequently GliR downregulation [104]. Upon activation of Shh, the ratio of GliA/R is

shifted towards GliA, resulting in a transcriptional induction of nuclear Hh target genes (e.g., Ptch1 and Gli1; Figure 9) [30, 88, 91, 98, 105]. Thus, Hh signaling regulates ciliogenesis but also embryonic development and tissue homeostasis [29, 30, 106].

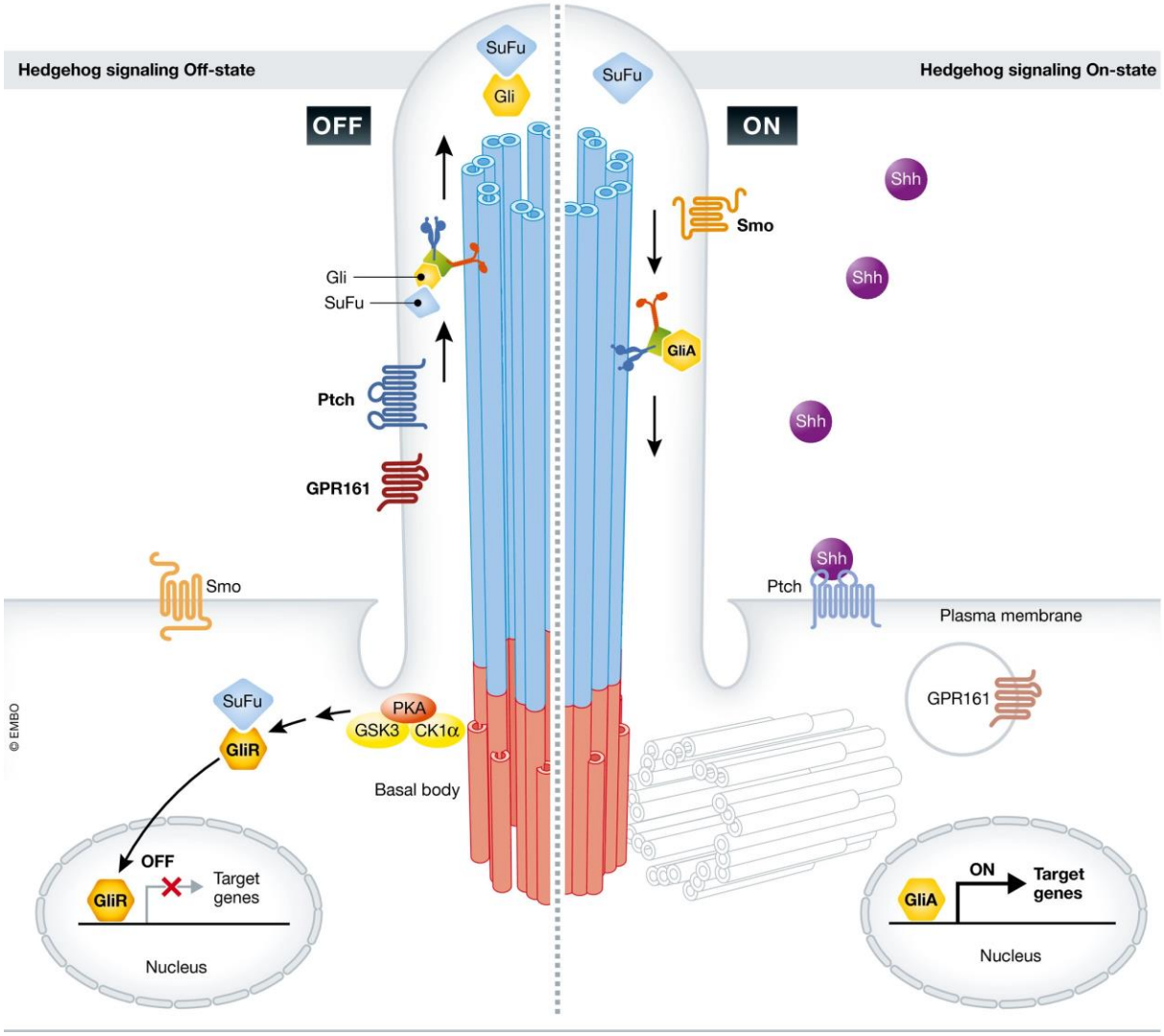

Figure 9 – Sonic hedgehog signaling in primary cilia – In the absence of Hh ligands negative hedgehog regulators Ptch1 and GPR161 are present on the ciliary membrane. In this off-state (left), SuFu forms a complex with the Gli transcription factors at the ciliary tip. Upon phosphorylation by the kinases PKA, GSK3 and CK1α at the basal body, Gli is processed to GliR. Hh ligand binding to Ptch1 induces its translocation out of the cilium and promotes the entry of Smo. In this on-state (right) also GPR161 exits the cilium, decreasing cAMP level and leaving PKA inactive. Therefore, Gli is no longer processed to GliR, but rather to GliA mediated by Smo. Either GliR or GliA migrate to the nucleus repressing or activating Shh target genes. [107]

2. Aim of the study

Cilia are elongated compartments, emerging from the cellular surface of most eukaryotic cells. To assemble these highly conserved organelles, protein cargo is transferred by the intraflagellar transport (IFT) from the base to the tip of the cilium, where they are incorporated into the growing cilium [1, 8-10]. This anterograde transport is mediated by IFT-B complex and driven by motor protein kinesin 2 [11]. One of the core proteins of IFT-B is IFT70/TTC30, which comprises the two paralogues TTC30A and TTC30B [1, 8, 9, 13]. Defects in primary cilia structure and IFT are associated with a wide spectrum of inherited diseases involving various organs. Until now there are 35 of these so-called ciliopathies including Leber congenital amaurosis (LCA) [20, 21]. To date 25 genes were identified to be associated with this disease, including *LCA5* [23]. This gene is coding for Lebercilin protein, which was previously described to interact with the IFT machinery, including TTC30A/B [26]. This interaction was lost due to LCA-associated mutations resulting in an impaired IFT mediated opsin transport in photoreceptors [80]. Further, Lebercilin was also described to interact with SSNA1, which is essential for microtubule stability but is also involved in ciliary assembly and intraflagellar transport [26-28]. In addition, both Lebercilin and SSNA1 were associated with cilia specific Sonic hedgehog signaling which regulates ciliogenesis and is dependent on intraflagellar transport [26, 30]. The aim of the study here is to investigate Lebercilin and its interacting proteins TTC30A and TTC30B as well as SSNA1 in cilia related processes.

To investigate Lebercilin, SSNA1, TTC30A/B function in human retinal pigment epithelium cell lines (hTERT-RPE1) knockout (KO) cell lines will be created with the CRISPR/Cas9 method. Therefore, a prediction tool (CCTop) is used to design corresponding sgRNAs that specifically target the gene of interest. Specificity is particularly important for TTC30A and TTC30B, due to the similarity of their nucleotide sequences. The transfection of sgRNAs is followed by single clone selection to create KO cell lines with a homozygous genome. Knockouts are then verified by Sanger sequencing, western blot and localization studies.

Regarding TTC30A/B the aim is to investigate whether these paralogues have redundant and/or individual functions in primary cilia [8]. Further, TTC30A and B will be characterized according to their effect on ciliogenesis, especially ciliary length and the number of ciliated cells. The influence of TTC30A/B single and double knockouts on IFT-B complex stability will

be examined by analyzing IFT88 and IFT140 localization to the cilium and their total protein level. To shed light onto paralogue specific functions, the CRISPR/Cas9 system is used to generate endogenously FLAG-tagged TTC30A and TTC30B HEK293T cells [8]. This will be followed by immunoprecipitation and mass spectrometry (MS) analysis to determine if the TTC30 paralogues can be detected separately and to identify shared and individual protein interactors. Dependent on these results, shared interactors would hint at redundant functions whereas newly found interacting proteins might reveal additional paralogue specific functions. Abundance of mutual proteins, especially of IFT-B proteins, will give new insights on how TTC30A/B redundancy protects IFT complex B integrity and hence intraflagellar transport in TTC30 single knockout cells [8].

Recently, the TTC30B mutation A375V was discovered and linked to Sonic hedgehog signaling (Shh), possibly causing synpolydactyly [29, 33]. To investigate and characterize the involvement of TTC30A/B in Shh, fluorescence constructs harboring Smoothened or Patched1, early regulators of Shh, will be stably transfected into hTERT-RPE1 TTC30A/B wildtype and knockout cells. These cells are chemically treated to activate (Smoothened agonist; SAG) or inhibit (Forskolin) Shh and differences in localization of Smo and Ptch1 are visualized by immunofluorescence microscopy. In addition, any observed phenotype will be validated in rescue cells, stably transfected with wildtype (wt) and mutant TTC30A/B. Further, the discovered TTC30A/B A375V mutation is recreated by site directed mutagenesis (SDM). SDM is applied on Strep/FLAG-tag TTC30A or B expression vectors to introduce this mutation. These constructs are then transiently transfected into HEK293T cells and an affinity purification will be performed with subsequent MS analysis. By comparing wt and mutant TTC30A/B interactomes, differences might hint at the underlying mechanism connecting TTC30A/B, Shh and synpolydactyly.

To uncover the underlying mechanism of Leber congenital amaurosis leading to rapid photoreceptor degeneration, the function of Lebercilin and interactor SSNA1 will be investigated. Ciliary length and the number of ciliated cells will be analyzed in LCA5 and SSNA1 hTERT-RPE1 KO cell lines to evaluate their effect on ciliogenesis. Since, both Lebercilin and SSNA1 were linked to different components (KIF7, SuFu) of Sonic hedgehog signaling [26], the generated knockouts will be investigated to characterize their involvement in this pathway. Therefore, localization studies of Shh proteins, Smo and Gli2, in LCA5 and SSNA1 KO cells will provide insights in understanding how both proteins affect Sonic hedgehog.

Furthermore, the impact of Shh on Lebercilin and SSNA1 is analyzed. By activating this signaling pathway with an agonist, its effect on Lebercilin in SSNA1 KO cells and vice versa, SSNA1 in Lebercilin knockout cells will be investigated. These localization studies might help to characterize Lebercilin and SSNA1 function in cilia related processes.

3. Material

3.1. Equipment

Equipment	Company
2 Channel Jumbo Display Clock Timer	Carl Roth GmbH & Co.KG
µPAC nano column (50 cm, C18)	Thermo Scientific
µPAC trapping column	Thermo Scientific
Mini-PROTEAN® Tetra-Cell	Bio-Rad Laboratories, Inc.
BioRad T100™ Thermal Cycler	Bio-Rad Laboratories, Inc.
Mini Trans-Blot® Electrophoretic Transfer Cell	Bio-Rad Laboratories, Inc.
Brand® Accu-jet® Pipetboy	Sigma-Aldrich
Centrifuge 5415 R	Eppendorf AG
Chemi Imager Fusion FX	Vilber
Ecotron Incubation Shaker	Infors HT
FIBERLite® F15-8x50C	Thermo Scientific
Filter system	Millipore Filterunit Express Plus
Gel Documentation System	Herolab GmbH
HERACell 150i CO2 Incubator	Thermo Scientific
Heraeus Fresco 17 Centrifuge	Thermo Scientific
Heraeus Multifuge X3R Centrifuge	Thermo Scientific
Wärmeschrank UM 200	Memmert GmbH & CO.KG
Laboport® Mini Vacuum Pump	KNF Neuberger, Inc.
Leica TCS SP8 Scanning Microscope	Leica Microsystems IR GmbH
MiniStar Centrifuge	VWR
MSC-Advantage	Thermo Fisher Scientific
MWG Biotech Inc Primus 25 Thermal Cycler	Cole-Parmer GmbH
NanoDrop 1000 Spectrophotometer	PeqLab
NeoLab Intelli-Mixer	NeoLab
Orbitrap Fusion™ Tribrid	Thermo Scientific
Pipetman classic P10, P20, P200, P1000	Gilson
PowerPac™ Basic	Bio-Rad Laboratories, Inc.
PrimoVert microscope	Carl Zeiss Microscopy GmbH
Savant RVT400 Refrigerated Vapor Trap	Thermo Scientific
Savant SPD111V SpeedVac Concentrator	Thermo Scientific
Swivel Roller Mixer RM5F	Paul Marienfeld GmbH & Co. KG
Systec DX-150, DX-23 Autoclave	Systec GmbH
Tecan Spark 10M Luminescence Reader	Tecan Group AG
Thermo-Shaker Incubator MT-100	Universal Labortechnik GmbH & KO.KG
Ultimate3000 RSLCnano systems	Thermo Scientific
Vortex-Genie2	Scientific Industries, Inc.
Water bath VWB 18	VWR
Zeiss Axio Imager Z1 ApoTome Microscope	Carl Zeiss Microscopy GmbH

3.2. Software

Software	Company/Developer
Adobe Illustrator CS5 v15.0.0	Adobe System Inc.
Adobe Photoshop CS5 v12.0	Adobe System Inc.
BioEdit v7.0.5.3	Tom Hall
EASYWin32 5.17.295	Herolab GmbH
EndNote X8	Thomson Reuters
FIJI (ImageJ) 1.53q	Wayne Rasband
Graphpad Prism 5.01	GraphPad Software Inc.
Huygens Professional 19.04	Scientific Volume Imaging B.V.
Inkscape 0.92.3	Free Software Foundation, Inc.
Leica Application Suite X (LasX; 3.5.7)	Leica Microsystems
Mascot 1.6.1.0	Matrix Science
MaxQuant 1.6.1.0; 1.6.3.3; 1.6.5.0	MPI of Biochemistry
Microsoft Office 2016	Microsoft Corporation
NeuronJ (Plugin; FIJI) 1.4.3.	Erik Meijering
Perseus 1.6.2.3; 1.6.5.0; 1.6.14.0	MPI of Biochemistry
Scaffold 4.0	Proteome Software Inc.
Serial Cloner 2.6.1	Serial Basics Software
SparkControl 2.2	Tecan Group AG
ZEN 3.0 (blue edition)	Carl Zeiss Microscopy GmbH

3.3. Websites, online tools and databases

Name	Web links
BioGRID	https://thebiogrid.org/
CCTop	https://cctop.cos.uni-heidelberg.de/index.html
CRAPome	https://reprint-apms.org/?q=chooseworkflow
Ensembl	http://www.ensembl.org/index.html
Expasy	https://web.expasy.org/translate/
GetGo	http://getgo.russelllab.org
ICE Analysis	https://ice.synthego.com/#/
ImageJ documentation	https://imagej.nih.gov/ij/docs/index.html
MultAlin	http://multalin.toulouse.inra.fr/multalin/
NCBI BLAST	https://blast.ncbi.nlm.nih.gov/Blast.cgi
NCBI Primer-BLAST	https://www.ncbi.nlm.nih.gov/tools/primer-blast/
NCBI PubMed	https://pubmed.ncbi.nlm.nih.gov/
PrimerQuest™ Tool	https://eu.idtdna.com/pages/tools/primerquest
Protein Atlas	https://www.proteinatlas.org/
Reactome	https://reactome.org/
Reverse Complement	https://www.bioinformatics.org/sms/rev_comp.html
SysCilia Gold Standard	http://www.syscilia.org/goldstandard.shtml
Uniprot	http://www.uniprot.org/
Sequencing	https://www.eurofinsgenomics.eu/de/home/ https://www.microsynth.com/home-de.html
Signaling pathways	https://www.genome.jp/kegg/pathway.html
String	https://string-db.org/

3.4. Consumables

Consumable	Company
BD 3 mL Syringe Luer-Lok™ Tip	Becton Dickinson
BD Microlance™ 3	Becton Dickinson
Cell Chip™	Tecan Group AG
Colour coded insert, mixed	Sarstedt AG & Co. KG
Cover Glasses Ø 12mm	VWR
Cultube sterile culture tubes Tube with cap, polystyrene, 25/tray 17 mm x 95mm H.	Simport; Sarstedt AG & Co. KG
Disposal Bags SEKUROKA® PP 40 µm, 50 µm 600 x 800 mm	Carl Roth GmbH & Co.KG
Eppendorf CombiTips	Eppendorf AG
Gel blotting paper Whatman® 3MM	Carl Roth GmbH & Co.KG
Gel Loading Tips 0.5-200 µl, round	VWR
Gilson TowerPack D10, D200, D1000 tips	Gilson
Gloves Nitrile M	ABENA
High Precision Microscope Cover Glasses	Carl Roth GmbH & Co.KG
Hybond-P PVDF Transfer membrane	GE Healthcare
Microscope slides 26 x76mm	R. Langenbrinck GmbH
Multiply® -µStrip 8-strip	Sarstedt AG & KO. KG
Multiply®-Pro cup 0.2 ml	Sarstedt AG & Co. KG
Nitrile /Powder-Free Medical Examination Gloves M	Abena
Parafilm M	Bemis Company, Inc.
Pasteur Capillary Pipettes 230 mm	Wilhelm Ulbrich GdbR
Peha-soft nitrile Guard M	Paul Hartmann AG
Pipet tips with microcapillary for loading gels 1-200 µL	VWR
PP Cryo Tubes 1.8 mL	NUNC; Sarstedt AG & Co. KG
PP Insert with bottom spring 0.20 mL	Sigma Aldrich
PP Tubes 15 mL	Sarstedt AG & Co. KG
PP Tubes 50 mL	Greiner Bio-One
Precision Wipes Kimtech Science	Kimberly Clark® Professional
Receiver Columns 20 µm, 35 µm	Macherey-Nagel GmbH & Co. KG
Safe-Lock Tubes 0.5 mL, 1.5 mL, 2 mL	Eppendorf AG
Cell Scraper	Sarstedt AG & Co. KG
Falcon ® serological pipet 2 mL, 5 mL, 10 mL, 25 mL, 50 mL	Corning; Sarstedt AG & Co. KG
StageTips 200 µL pipette tip	Thermo Scientific
Tissue dishes 10 cm, 14 cm	Thermo Scientific
VWR® Tissue Culture Plates with 96, 48, 24, 12 and 6 wells	VWR; Sarstedt AG & Co. KG

3.5. Chemicals, reagents, buffer and solutions

3.5.1. Cloning

• Agar-Agar	Carl-Roth GmbH & Co. KG
• ATP (10 mM)	Fermentas GmbH
• Ampicillin sodium salt (100 mg/mL)	Carl-Roth GmbH & Co. KG
• Chloramphenicol (100 mg/mL)	Carl-Roth GmbH & Co. KG
• 1,4-Dithiothreitol (DTT)	Merck KGaA
• DNA Loading Dye (6x)	Thermo Fisher Scientific
• dNTP Mix (10 mM)	Thermo Fisher Scientific
• DpnI (20 U/µl)	New England BioLabs® Inc.
• FastDigest BpiI (BbsI; 10 U/µL)	Thermo Fisher Scientific
• FastDigest Buffer	Thermo Fisher Scientific
• Gateway® BP Clonase™ II	Thermo Fisher Scientific
• Gateway® LR Clonase™ II	Thermo Fisher Scientific
• GC Buffer (5x)	Thermo Fisher Scientific
• HF Buffer (5x)	Thermo Fisher Scientific
• Kanamycin Sulfate (100 mg/mL)	Carl-Roth GmbH & Co. KG
• Nuclease free water (ddH_2O)	Promega GmbH
• Phusion High Fidelity DNA Polymerase (20 U/µL)	Thermo Fisher Scientific
• PlasmidSafe ATP-dependent DNase (10 U/µL)	Epicentre®
• PlasmidSafe buffer (10x)	Epicentre®
• Polynucleotide kinase Buffer (PNK) (10x)	Epicentre®
• S.O.C Medium	Invitrogen
• Sodium Chloride (NaCl)	Merck KGaA
• T4 DNA-Ligase (1U/µL)	Roche Holding AG
• T4 polynucleotide Kinase (PNK; 10 U/µL)	New England BioLabs® Inc.
• Tryptone/Peptone from Casein	Carl-Roth GmbH & Co. KG
• Yeast Extract	Carl-Roth GmbH & Co. KG

1. LB-Medium

Tryptone	50 g
Yeast Extract	25 g
NaCl	50 g
dH_2O	5 L

➔ stir until dissolved; adjust to pH 7.0; autoclave

2. LB-Agar

LB-Medium	400 mL
Agar-Agar	6 g

➔ autoclave

➔ to cast LB-Agar plates: boil up and cool down (55-60 °C) to add antibiotics (1:1000), then pour into plates

3. Ampicillin Solution (100 mg/mL)	
Ampicillin	1 g
HPLC water	10 mL

4. Chloramphenicol Solution (100 mg/mL)	
Chloramphenicol	1 g
Ethanol p.a.	10 mL

5. Kanamycin Solution (50 mg/mL)	
Kanamycin	500 mg
HPLC water	10 mL

3.5.2. Nucleic acid methods

- Agarose — Lonza Group AG
- Deoxynucleotide (dNTP) Solution (10 mM) — New England BioLabs® Inc.
- Dimethylsulfoxide (DMSO) — Thermo Fisher Scientific
- Dream Taq DNA Polymerase (5 U/µL) — Thermo Fisher Scientific
- Dream Taq Green Buffer (10x) — Thermo Fisher Scientific
- Ethidium Bromide — AppliChem GmbH
- Gene Ruler 1 kb Plus — Thermo Fisher Scientific

6. Agarose Gel (1 %)	
Agarose	1 g
TBE (1x)	100 mL
Ethidium Bromide	4 µL

➔ boil up to dissolve agarose
➔ cool down before adding Ethidium Bromide and casting gel

3.5.3. Cell culture

- Dimethylsulfoxide (DMSO) 100 % — Carl Roth GmbH & Co. KG
- Dulbecco's Modified Eagle Medium (DMEM) high glucose — Sigma Aldrich
- Dulbecco's Phosphate Buffered Saline, [-] $CaCl_2$, [-] $MgCl_2$ — Thermo Fisher Scientific
- Fetal Bovine Serum (FBS) — Sigma Aldrich

• Geneticidinsulfate (G418) solution (50 mg/mL)	Carl Roth GmbH & Co. KG
• Lipofectamine™ 3000 transfection kit	Thermo Fisher Scientific
• Penicillin/Streptomycin (P/S) (10,000 Units/mL; 10 mg/mL)	Thermo Fisher Scientific
• Puromycin (10 mg/mL)	Life Technologies
• QuickExtract™ DNA extraction solution	Lucigen Coorporation
• Trypsin-EDTA (0.05 %)	Thermo Fisher Scientific

7. Culturing Medium

DMEM	500 mL
FBS	50 mL
P/S	2.5 mL

➔ gently homogenize

8. Cryo Medium

FBS	3.6 mL
DMSO (100 %)	0.4 mL

➔ gently homogenize

3.5.4. Localization studies

• Bovine Serum Albumin	Carl-Roth GmbH & Co. KG
• Diamidino-Phenylindole (DAPI) (1 mg/mL) (1:10000 in DPBS)	Sigma Aldrich
• Fluoromount-G®	SouthernBiotech
• Methanol (MeOH)	Honeywell
• Normal Goat Serum	Merck KGaA
• Paraformaldehyde (PFA)	Sigma Aldrich
• Smoothened Agonist (SAG) HCl	Abmole BioSciences
• 2,2'-Thiodiethanol (TDE) mounting medium	Abberior
• Triton® X-100	Sigma Aldrich

9. PBST (0.1/0.3 %)

PBS	25 mL
Triton® X-100	25/75µL

➔ stir for 5 min

10. PFA (4 %)	
PFA	4 g
PBS	100 mL

➔ dissolve in 50 mL PBS at 55 °C; ad 50 mL and stir for 45 min
➔ adjust pH to 7.4

11. Normal Goat Serum	
NGS (10 %)	1 mL
BSA (1 %)	0.1 g
PBST (0.1 %)	9 mL

3.5.5. Western blot

- Acrylamide/Bis Solution 37.5:1 (30% w/v, 2.6% C) Serva
- Ammonium Persulfate (APS, w/v = 10%, electr.grade, 98%) Sigma Aldrich
- Bovine Serum Albumin Carl-Roth GmbH & Co. KG
- Bromphenol Blue Sigma Aldrich
- Forskolin Sigma Aldrich
- Glycerol Carl-Roth GmbH & Co. KG
- Glycin Carl-Roth GmbH & Co. KG
- Hydrochloric Acid 32% p.a. (HCl) Merck KGaA
- Isopropanol Honeywell
- β-Mercaptoethanol Sigma Aldrich
- Methanol Honeywell
- Milk powder, Blotting grade, dry, non-fat Carl-Roth GmbH & Co. KG
- N,N,N',N'-tetramethylethylene-diamine (TEMED) Merck KGaA
- PageRuler™ Prestained Protein Ladder (170 kDa) Thermo Fisher Scientific
- Pierce™ ECL plus Western Blotting Substrate Thermo Fisher Scientific
- Sodium Chloride (NaCl) Merck KGaA
- Sodiumdodecylsulfate SDS (dust-free pellets >98%) Sigma Aldrich
- Tris(hydroxymethyl) Aminomethane Sigma Aldrich
- Tween®20 Sigma Aldrich

12. Lämmli Buffer (5x)	
Tris-HCl Buffer (ph 6.8)	8.33 mL
SDS solution (20 %)	12.5 mL
Glycerol	25 mL
β-Mercaptoethanol	1.75 mL

Bromphenol Blue	0.25 g
H_2O Milli-Q	ad 50 mL

13. Running Buffer (10x)	
Glycin	750 g
Tris	150 g
SDS	50 g
H_2O Milli-Q	5 L

➔ dilute 10x Running Buffer 1:10 with Millipore water

14. Western Buffer (10x)	
Glycin	144.13 g
Tris	30.29 g
H_2O Milli-Q	1 L

15. Western Buffer (1x)	
Western Buffer (10x)	100 mL
Methanol	200 mL
dH_2O	700 mL

16. Tris-HCl Buffer (ph 6.8/8.8)	
Tris	90.9 g
dH_2O	500 mL

➔ dissolve and adjust pH to 6.8 or 8.8 with HCl

17. SDS solution (10 %/20 %)	
SDS	50/100 g
H_2O Milli-Q	500 mL

18. Blocking Buffer	
Milk/BSA	5 g
1x TBST	100 mL

➔ homogenize

19. TBS (10x)	
Tris	180 g
NaCl	440 g
H_2O Milli-Q	ad 5 L

➔ adjust pH to 7.4 with HCl

20. TBST (1x)	
TBS Buffer (10x)	100 mL
Tween® 20	1 mL
ddH_2O	1 L

21. ECLplus	
Solution A	0.975 µL
Solution B	25 µL

➔ mix shortly

3.5.6. Proteomics

- 1,4-Dithiothreitol (DTT) — Merck KGaA
- 2-Iodacetamide (IAA) — Merck KGaA
- Acetonitrile (ACN; Chromasolve® LC-MS) — Sigma-Aldrich
- Ammonium bicarbonate (ABC) — Sigma-Aldrich
- Anti-FLAG® M2 Agarose Beads — Sigma-Aldrich
- Bradford Protein Assay (5x) — Bio-Rad Laboratories GmbH
- Chloroform (for analysis) — Merck KGaA
- FLAG-Peptide — Sigma-Aldrich
- Glacial Acetic Acid, p.a. — Merck KGaA
- HPLC water — VWR
- Methanol (hypergrade for LC/MS) — Merck KGaA
- Nonidet P40 (NP40) — Roche Holding AG
- Phosphatase Inhibitor Cocktail 2 (PI2) — Sigma-Aldrich
- Phosphatase Inhibitor Cocktail 3 (PI3) — Sigma-Aldrich
- Polyethylenimine (PEI) — PolySciences, Inc.
- Protease Inhibitor Complex Complete (PIC) — Roche Holding AG
- RapiGest™ SF Surfactant — Waters Corportation
- Sodium Chloride (NaCl) — Merck KGaA
- StrepTactin Elution Buffer (10x) — iba
- StrepTactin Superflow Beads — iba

• Trifluoracetic Acid (TFA, 100 %)	Fluka
• Trypsin NB Sequencing Grade, modified from porcine pancreas	Serva Electrophoresis

22. Sodium Chloride Solution

NaCl	8.77 g
H_2O Milli-Q	1 L

➔ adjust pH to 5.5 with HCl

23. PEI solution

PEI	100 mg
NaCl solution (pH 5.5)	1 L

➔ adjust pH to 7.8 with HCl; stir overnight
➔ sterilize via filtering through a sterile filter

24. Lysis Buffer

Nonidet P40	0.5 mL
TBS (10x)	10 mL
HPLC water	86 mL
PIC	2 mL
PI2	1 mL
PI3	1 mL

➔ inhibitors added before use

25. Washing Buffer

Nonidet P40	0.1 mL
TBS (10x)	10 mL
HPLC water	88 mL
PI2	1 mL
PI3	1 mL

➔ inhibitors added before use

26. FLAG Elution Buffer (stock)	
FLAG-Peptide	4 mg
TBS (1x)	0.8 mL

➔ 20 µL stock buffer mixed with 480 µL TBS (1x)

27. Strep Elution Buffer	
Strep Elution Buffer (10x)	1 mL
HPLC water	9 mL

28. BSA Buffer (10x; 10 mg/mL; stock)	
BSA	100 mg
HPLC water	10 mL

➔ 20 µL stock buffer mixed with 180 µL HPLC water

29. ABC solution	
ABC	19.8 mg
HPLC water	5 mL

➔ freshly prepared before use

30. DTT solution	
DTT	15.4 mg
HPLC water	5 mL

➔ freshly prepared before use

31. IAA solution	
IAA	55.5 mg
HPLC water	5 mL

➔ freshly prepared before use

32. RapiGest™ solution	
RapiGest	1 mg
HPLC water	50 µL

33. Acetic acid dilution (HAc; 50 mM)	
Glacial acetic acid, p.a.	100 µL
HPLC water	19 mL

34. Trypsin Solution (0.5 µg/µL)	
HAc (50 mM)	50 µL
HPLC water	25 µg

➔ freshly prepared before use

35. 0/5 solution	
TFA (100 %)	50 µL
HPLC water	950 µL

➔ freshly prepared before use

36. 50/5 solution	
TFA (100 %)	50 µL
ACN (50 %)	950 µL

➔ freshly prepared before use

37. 80/5 solution	
TFA (100 %)	50 µL
ACN (80 %)	950 µL

➔ freshly prepared before use

3.6. Bacteria

- *E. coli* - Library Efficiency® DH5α Competent Cells — Thermo Fisher Scientific
- *E. coli* - One Shot® *ccd*B Survival™ 2 T1® Competent Cells — Thermo Fisher Scientific

3.7. Human cell lines

- ARPE19 – retinal pigmented epithelial cells spontaneously arising and amelanotic (CRL-2302) — American Type Culture Collection
- HEK293T – human embryonic kidney cells expressing large T antigen of SV40 (CRL-3216) — American Type Culture Collection
- hTERT-RPE1 – retinal pigmented epithelial cells immortalized with human telomerase reverse transcriptase (CRL-4000) — American Type Culture Collection

3.8. Plasmids

- pSpCas9(BB)-2A-Puro (PX459) V2.0 (AmpR, PuroR) (gift from Feng Zhang) — Addgene
- pDONR201 (KanR) — Invitrogen
- pDEST (pcDNA 3.0 backbone; AmpR) modified with C- or N-terminal Strep/FLAG tag — Invitrogen modified by CJ Gloeckner; [108]
- pEGFP-mSmo (KanR) — Addgene
- pPtc1-YFP (KanR) — Addgene

3.9. Genes

Table 1 – Genes	Transcript ID from ensembl.org
TTC30A	ENST00000355689.6
TTC30B	ENST00000408939.4
LCA5	ENST00000369846.9
SSNA1	ENST00000322310.10

3.10. sgRNAs

Table 2 – TTC30A/B sgRNAs	
TTC30A #1 sense	TAGCGCGGTAAACTCCCCGT
TTC30A #1 antisense	ACGGGGAGTTTACCGCGCTA
TTC30A #2 sense	AGTTTACCGCGCTAGTGTAC
TTC30A #2 antisense	GTACACTAGCGCGGTAAACT
TTC30B #1 sense	CGGGGATCTGCGCGCCGCTC
TTC30B #1 antisense	GAGCGGCGCGCAGATCCCCG
TTC30B #2 sense	CGTAGCGTGCATTGCGGATG
TTC30B #2 antisense	CATCCGCAATGCACGCTACG
HDR construct	TTGCTCTGTTGCCATAGTAACCGCACCCATA ACAGCCGTGGTGGTTATGGATTATAAAGAT GATGATGATAAAGCTGGCCTTAGCGGTCGC AGATCCCCGACGGGGAGTTCACCGCGGT

Table 3 – LCA5 sgRNAs	
LCA5 exon 3 sense	AAGAACTGACCAGCGATGAT
LCA5 exon 3 antisense	ATCATCGCTGGTCAGTTCTT
LCA5 exon 6 sense	TCTTTATTTGGAGAGGACTT
LCA5 exon 6 antisense	AAGTCCTCTCCAAATAAAGA

Table 4 – SSNA1 sgRNAs	
SSNA1 exon 1 sense	GCAGAACTACAACAACGAGC
SSNA1 exon 1 antisense	GCTCGTTGTTGTAGTTCTGC
SSNA1 exon 3 sense	CTTTGCTCAGCGTTCTCAAG
SSNA1 exon 3 antisense	CTTGAGAACGCTGAGCAAAG

3.11. Primer

Table 5 – TTC30A/B Primer	
TTC30A forward	CGTCTTTCCCCTTCTGACTGCC
TTC30A reverse	GCAGATCGCCCTCGCTATACTTG
TTC30B forward	GTAGTCTTTCCCCTCCTGAATG
TTC30B reverse	ATTGCGGATGAGGCGGTACAC
TTC30A/B SDM forward	CTGAAGAGGTTTTCATTAAG
TTC30A/B SDM reverse	AATGAAAACCTCTTCAGGAG

Table 6 – LCA5 Primer	
LCA5 exon 3 forward	TCTGGATGCCAATGTGAATTGTGG
LCA5 exon 3 reverse	TCTTCTAGGTCCACCAGACTCTTT
LCA5 exon 6 forward	AGCTGAACCAGGTAACTTTCAATATG
LCA5 exon 6 reverse	CCTTCCCTTCCATTTCAGAATTATTGTA

Table 7 – SSNA1 Primer	
SSNA1 exon 1 forward	GCGATGACGCGCTAGTT
SSNA1 exon 1 reverse	TTGCGTGCCAGGTTCTC
SSNA1 exon 3 forward	GGCTTAGGACCTTACCAACAG
SSNA1 exon 3 reverse	TGCTGCCGTGAAGAACAA

Table 8 – General Primer	
FLAG-tag forward	ATGGATTATAAAGATGATGATGATAAA
CMV forward	CGCAAATGGGCGGTAGGCGTG
U6 forward	GAGGCCCTATTTCCCATGATTCC
pcDNA reverse	GGCAACTAGAAGGCACAGTC

Table 9 – SDM Primer	
TTC30A/B SDM forward	CTGAAGAGGTTTTCATTAAG
TTC30A/B SDM reverse	AATGAAAACCTCTTCAGGAG

3.12. Antibodies

3.12.1. Primary antibodies

Table 10 – Primary antibody list

Name	Biological source	Dilution (IFS/WB)	Company
Acetylated Tubulin	mouse	1:250/1:2000	Abcam
ARL13B	mouse	1:200	UC Davis/NIH Neuromab
ARL13B	rabbit	1:200	ProteinTech Group Inc.
β-Actin	mouse	1:5000	Cell Signaling Technology
γ-Tubulin	rabbit	1:1000	Novus Biologicals
GAPDH	rabbit	1:10,000	Cell Signaling Technology
Gli2	mouse	1:100	SantaCruz Biotechnology
GT335	mouse	1:1500	AdipoGen Life Sciences
IFT57	rabbit	1:200/1:1000	ProteinTech Group Inc.
IFT88	rabbit	1:200/1:1000	ProteinTech Group Inc.

IFT140	rabbit	1:200	ProteinTech Group Inc.
LCA5	rabbit	1:200/1:1000	ProteinTech Group Inc.
PKAcat	mouse	1:1000	SantaCruz Biotechnology
P-PKA substrate	rabbit	1:1000	Cell Signaling Technology
Rootletin (CROCC)	mouse	1:100	SantaCruz Biotechnology
Smo	mouse	1:100	SantaCruz Biotechnology
SSNA1	mouse	1:50/1:200	Novus Biologicals
TTC30	mouse	1:100	SantaCruz Biotechnology

3.12.2. Secondary antibodies

Table 11 – Secondary antibody list

Host	Spectrum	Dilution	Product	Company
goat anti-mouse	488 nm (green)	1:350	Alexa Fluor	Thermo Fisher Scientific
goat anti-mouse	568 nm (red)	1:350	Alexa Fluor	Thermo Fisher Scientific
goat anti-mouse	647 nm (far-red)	1:350	Alexa Fluor	Thermo Fisher Scientific
goat anti-rabbit	488 nm (green)	1:350	Alexa Fluor	Thermo Fisher Scientific
goat anti-rabbit	568 nm (red)	1:350	Alexa Fluor	Thermo Fisher Scientific
goat anti-rabbit	647 nm (far-red)	1:350	Alexa Fluor	Thermo Fisher Scientific
goat anti-mouse	488 nm (green)	1:100	STAR	Abberior
goat anti-rabbit	568 nm (red)	1:100	ATTO	Sigma Aldrich
goat anti-rabbit	633 nm (far-red)	1:100	ATTO	Sigma Aldrich
goat anti-mouse	HRP	1:10,000		Jackson ImmunoResearch
goat anti-rabbit	HRP	1:10,000		Jackson ImmunoResearch

3.13. Kits

- Bio-Rad Protein Assay Kit — Bio-Rad Laboratories GmbH
- Pierce™ ECL Plus Western Blotting Substrate — Thermo Fisher Scientific
- Gateway® BP ClonaseTM II Enzyme Mix — Thermo Fisher Scientific
- Gateway® LR ClonaseTM II Enzyme Mix — Thermo Fisher Scientific
- Lipofectamine™ 3000 Transfection Kit — Thermo Fisher Scientific
- PeqGold Cycle - Pure Kit — VWR
- PureYield™ Plasmid Midiprep System — Promega GmbH

4. Methods

4.1. Cloning

4.1.1. Phosphorylation and annealing of sgRNA

The CRISPR/Cas9 target online prediction tool (CCTop) [109] was used for designing single strand oligonucleotides. Settings included a target site length of 20 nucleotides and a core length of 12 nucleotides. A total maximum of four mismatches and two core mismatches was set. The protospacer adjacent motif (PAM) was NGG and selected species was *homo sapiens* (GRCh38/hg38). The predicted sgRNAs were chosen according to their efficiency, their possible off-target effects and their gene location [110]. Chosen oligonucleotides were then ordered and produced by IDT. Complementary 5'-3' (sense) and 3'-5' (antisense) sgRNA strands were mixed with polynucleotide kinase (PNK) buffer and T4 PNK (Table 12). This reaction mixture was incubated for 30 min at 37 °C enabling the T4 kinase to phosphorylate the 5'-OH group of the oligonucleotides. Afterwards, single strands were annealed to a double strand by a short incubation at 95 °C for 5 min. This was followed by a slow reduction of 5 °C per minute to a minimum of 25 °C.

Table 12 – Phosphorylation and annealing of oligonucleotides

sgRNA 5'-3' strand (sense)	1 µL
sgRNA 3'-5' strand (antisense)	1 µL
PNK Buffer (10x)	1 µL
T4 PNK	1 µL
ddH_2O	6 µL

➔ 37 °C for 30 min; 95 °C for 5 min
➔ Ramp down to 25 °C with 5 °C per minute

4.1.2. Restriction digest and ligation

The previously annealed oligonucleotides were diluted and then cloned into pSpCas9 vector. Therefore, DTT was added for linearization by cleaving disulfide bonds of the targeted dsDNA. Additionally, FastDigest BbsI and FastDigest Buffer were added (Table 13). This restriction

enzyme cut the vector and as result blunt and/or sticky ends were formed. Lastly, ATP-dependent T4 DNA-Ligase was used for insertion of the previously phosphorylated and annealed sgRNA into the now linearized pSpCas9 vector utilizing the newly formed blunt/sticky ends. Therefore, the reaction mix was incubated at 37 °C for 5 min followed by 21 °C for 5 min. These two steps were repeated five times.

Table 13 – Cloning the oligonucleotides into pSpCas9 vector

pSpCas9-vector (100 ng)	1 µL
Oligonucleotides (1:200)	2 µL
FastDigest Buffer	2 µL
DTT (10 mM)	1 µL
ATP (10 mM)	1 µL
FastDigest BbsI	1 µL
T4 DNA-Ligase	0.5 µL
ddH_2O	11.5 µL

➔ 37 °C for 5 min; 21 °C for 5 min; repeat 5 times

For digestion of residual linearized (not ligated) DNA, PlasmidSafe-Exonuclease and corresponding buffer were added to the mix (Table 14). This reaction was conducted for 30 min at 37 °C followed by 30 min at 70 °C. A total of 5 µL solution were then used for transformation.

Table 14 – PlasmidSafe exonuclease reaction

Ligation reaction	11 µL
PlasmidSafe Buffer (10x)	1.5 µL
ATP (10 mM)	1.5 µL
PlasmidSafe ATP-dependent DNase	1 µL

➔ 37 °C for 30 min; 70 °C for 30 min

4.1.3. Gateway cloning

Gateway cloning system allows simple transfer of DNA fragments between different plasmids. The initial step of introducing flanking attB sites was already performed and hence the required entry clone was available for BP reaction. During the BP reaction the inserted DNA of

interest (cassette) of the entry clone is transferred to the donor vector. Therefore, entry clone, donor vector and BP Clonase II were mixed and incubated 4 h at 25 °C (Table 15).

Table 15 – BP reaction

Donor vector (100 ng/µL)	1 µL
Insert (100 ng/µL)	3 µL
BP Clonase II	1 µL

➔ 25 °C overnight

After transformation, amplification and purification of the donor vector, subsequently a LR reaction was performed bringing the DNA fragment into a destination vector. According to protocol donor vector, destination vector and LR Clonase II were mixed and again incubated 4 h at 25 °C (Table 16). The destination vector was then the expression vector containing necessary promotors, tags and the gene of interest which could be transformed into *E. coli* and later be sequenced.

Table 16 – LR reaction

Destination vector (100 ng/µL)	1 µL
Template (Entry vector; 100 ng/µL)	1 µL
ddH_2O	2 µL
LR Clonase II	1 µL

➔ 25 °C overnight

4.1.4. Site directed mutagenesis (SDM)

SDM was used to introduce a specific mutation at a desired position in a dsDNA plasmid. Therefore, oligonucleotides were custom designed for the target region and were already harboring the correct mutation. Additionally, the primer one in 5'-3' (sense) and the other in 3'-5' (antisense) direction were overlapping.

The first step was a PCR for denaturation of the dsDNA plasmid, SDM primer annealing and the amplification of the mutated plasmid. Therefore, PCR reaction mixture needed a buffer for GC-rich vector regions (backbone) and a Phusion high fidelity polymerase with a low error rate due to its proof-reading function. Elongation time was adjusted to the size of the plasmid (~2000 bp per min; Table 17).

Table 17 – SDM vector amplification (PCR)	
GC Buffer (5x)	4 µL
Phusion (high fidelity) polymerase	0.3 µL
dNTP Mix (10 mM)	0.2 µL
SDM primer forward	1 µL
SDM primer reverse	1 µL
Template vector (100 ng/µL)	1 µL
ddH_2O	12.5 µL

- ➔ 100 °C for 3 min
- ➔ 98 °C for 30 sec; 67 °C for 40 sec; 72 °C for 4 min; repeat 19 times
- ➔ 72 °C for 5 min

The second step was the digestion of the template vector without desired mutation (Table 18). DpnI restriction enzyme only cuts methylated bacterial DNA (from transformation in *E. coli*). Hence, non-methylated but mutated DNA was not cut.

Table 18 – SDM template vector digest	
SDM PCR reaction mix	20 µL
GC Buffer (5x)	4 µL
DpnI restriction enzyme	1 µL

- ➔ 37 °C for 1 h

An agarose gel electrophoresis was performed to prove a successful digest of template DNA (Table 19). Finally, the SDM plasmids were transformed into *E. coli* for amplification and subsequent sequencing.

Table 19 – SDM agarose gel loading	
SDM digest reaction mix	10 µL
DNA loading dye (6x)	1 µL

- ➔ 1 % agarose gel; 90 V for 30 min

4.1.5. Transformation of chemically competent *E. coli*

To amplify plasmid DNA after cloning, chemically competent *E. coli* were used. DH5α strains were used for vectors harboring target DNA sequences and ccdB survival strains for empty

vectors. Therefore, bacteria were slowly thawed on ice and subsequently 50 µL of competent *E. coli* were mixed with 1-5 µL plasmid DNA. After incubation of 45 min on ice a heat shock was performed for 45 sec at 42 °C to transform the DNA into the cells. For recovery 250 µL S.O.C medium was added and incubated at 37 °C for 60 min in a shaking incubator (160 rpm). The mixture (50-150 µL) was plated onto selective LB agar plates overnight at 37 °C. Thereby, the antibiotics added to the plates was correlating to the resistance gene of the vector. The next day, single colonies were picked and transferred to fresh selective LB medium. Again, followed by an incubation at 160 rpm and 37 °C in a shaking incubator overnight.

4.1.6. Glycerol stock

After transformation 500 µL *E. coli* cell suspension were added into 500 µL glycerol (80 %). This mixture was thoroughly homogenized and transferred to PP cryo tubes. This glycerol stock could then be kept for long-term storage at -80 °C.

4.1.7. Purification of plasmid DNA

The isolation of amplified DNA in *E. coli* (DH5α or *ccd*B Survival) the PureYield™ Plasmid Midiprep system was used according to manufacturer's protocol. The bacteria strains were pelleted (10 min; 4,500 g) and the supernatant discarded. The pellet was suspended (3 mL resuspension solution) and lysed in 3 mL alkaline buffer, followed by neutralization with the 5 mL of acidic buffer. Next, plasmid DNA was separated from proteins, bacterial membranes and genomic DNA by centrifugation at 15,000 g for 15 min. The plasmid DNA containing supernatant was poured onto a silicate membrane, where it was bound. After endotoxin removal and several washing steps, the membrane was vacuum-dried to get rid of residual EtOH. The purified DNA was eluted with 0.5 mL nuclease free deionized water.

4.2. Nucleic acid methods

4.2.1. Photometric determination of DNA concentration

The concentration of DNA was measured with a NanoDrop spectrophotometer. Nuclease-free water was used as blank. Therefore, 2 µL of a sample were transferred to the NanoDrop. The optical density at 260 nm for DNA determined DNA concentration. Additionally, via $OD_{260/280}$ the purity could be calculated.

4.2.2. Polymerase chain reaction

Polymerase chain reaction (PCR) was used to amplify specific DNA fragments. Therefore, a mixture was generated containing template DNA, specific forward and reverse primer, a thermostable polymerase and dNTPs for elongation as well as PCR buffer (Table 20). The initial PCR step was a denaturation at 95 °C of double stranded DNA in single stranded DNA. After denaturation primer were able to bind their complementary sequence at 50-65 °C. The elongation of bound primer occurred at 72 °C. These steps were repeated up to 40 times on a thermocycler.

Table 20 – PCR

Green Buffer (10x)	2 µL
dNTP Mix (10 mM)	0.4 µL
DreamTaq Polymerase	0.2 µL
Primer forward (1:10)	1 µL
Primer reverse (1:10)	1 µL
DMSO (1 %)	0.2 µL
Template DNA	1 µL
Aqua bidest.	14.2 µL

- ➔ 95 °C for 5 min
- ➔ 95 °C for 30 sec; 50-65 °C for 40 sec; 72 °C for 2 min; repeat 39 times
- ➔ 72 °C for 5 min

4.2.3. Gel electrophoresis

Amplified PCR product was separated by their length using agarose gel electrophoresis. Therefore, 1 g of agarose gel was suspended in 100 mL 1x TBE. While boiling the agarose dissolved and upon cooling the solution slowly turned solid. Before hardening 4 µL ethidium bromide were added. The viscous solution was poured into the gel chamber and a comb produced the sample pockets. Afterwards, 5 µL DNA ladder and 10 µL of the samples were loaded. A voltage of 100 V was applied for up to 40 min. DNA fragments were separated according to their size and were visualized using a gel documentation system.

4.2.4. PCR product purification

PCR products were purified according to the manufacturer's protocol of Cycle Pure Kit. The same amount of CP buffer (10 µL) was added to the amplified PCR mix and shortly vortexed before pouring it on a PerfectBind® DNA Column. The columns were centrifuged for 1 min at 10,000 g and the buffer discarded. The bound DNA was washed twice with washing buffer (contains ethanol) and subsequently centrifugated, for 2 min at 10,000 g, to get rid of residual EtOH. Finally, the purified PCR product was eluted with 40 µL deionized water.

4.2.5. Sequencing

Lastly, after extraction, amplification and purification, the targeted DNA fragment or plasmid was sequenced. Therefore, 3 µL Primer (10 µM) and 9 µL DNA (100 ng/µL) were mixed and sent in for sequencing.

4.3. Cell culture

4.3.1. Thawing cells

Cryo tubes with either frozen HEK293T, hTERT-RPE1 or ARPE19 cells were quickly transferred from liquid nitrogen storage into a water bath (37 °C). Under a sterile laminar air flow bench, 9 mL DMEM were added, supplemented with 10% fetal bovine serum (FBS) and 0.5% penicillin/streptomycin (P/S). To quickly get rid of cell toxic DMSO, the cell suspension was shortly centrifuged (3 min at 500 g). The supernatant was discarded and the cell pellet resuspended with 10 mL supplemented DMEM. The suspension was poured onto a 10 cm petri dish and put into the incubator. Incubator settings were 37 °C, 90 % humidity and 5 % CO_2.

4.3.2. Splitting cells

Under a sterile laminar air flow bench the medium of confluent cells (~90%) was discarded. To get rid of excess FBS, cells were washed with 5 mL DPBS. For detaching cells from the petri dish, 2 mL 0.05 % Trypsin-EDTA were added and shortly incubated. Supplemented DMEM was re-added to stop trypsinization. After homogenization, cells were transferred to a new petri dish and diluted (e.g., 1:5 or 1:10).

4.3.3. Freezing cells

Under sterile conditions the medium of a 10 cm dish was discarded, the cells were washed (DPBS), trypsinized and homogenized in supplemented DMEM. After transfer into a tube and a short centrifugation step (3 min; 500 g), the supernatant was again discarded, and the cell pellet resuspended with cryo-medium (4 mL FBS containing 10 % DMSO). The cell suspension was transferred into PP CryoTubes and subsequently freezed at 4 °C for 10 min, followed by -20 °C for 45min and -80 °C overnight. Lastly the frozen cells were long term stored in liquid nitrogen at -196 °C.

4.3.4. Lipofectamine™ transfection

Lipofectamine™ transfection was performed according to the manufacturer's protocol and used for transfecting sgRNAs (CRISPR/Cas9) and for generating stable transfected cell lines. Initially, cells were counted and 150,000 cells/mL (HEK293T; hTERT-RPE1) to 200,000 cells/mL (ARPE19) were seeded per well (6-well plate). Transfection started 6 h later with the dilution of 5 µl Lipofectamine 3000™ reagent in 250 µl DMEM (not supplemented). Furthermore, 4 µl P3000™ reagent and 2000 ng DNA were also diluted in 250 µL DMEM (not supplemented). Both dilutions were combined, thoroughly mixed and incubated for 10 min at RT (Table 21). This incubation was necessary for lipid formation which then contain the DNA for transfection. This mixture was added dropwise onto the seeded cells and incubated for 72 h.

Table 21 – Lipofectamine™ 3000 transfection kit

A) DMEM	250 µL
Lipofectamine™ 3000 reagent	5 µL
➔ gently homogenize	
B) DMEM	250 µL
P3000™ reagent	4 µL
DNA	2000 ng
➔ gently homogenize	

➔ mix A and B (1+1) and incubate 10 min at RT; add dropwise onto cells

4.3.5. Puromycin treatment

The px459 vector used for CRISPR/Cas9 experiments harbors a puromycin resistance gene. Therefore, to select for successfully transfected cells, puromycin (2 µg/µL) was added and incubated for three days (HEK293T; ARPE19). hTERT-RPE1 cells have an intrinsic puromycin resistance, hence the antibiotic concentration was increased to 40 µg/µL. After three days HEK293T and ARPE19 cells received fresh supplemented DMEM without puromycin. RPE1 cells were trypsinized and were incubated two more days with antibiotic.

4.3.6. Single clone selection

Following puromycin treatment, surviving cells were single clone selected to obtain a cell line derived from one single cell, thus containing a homozygous genome. Therefore, under sterile laminar air flow bench cells were trypsinized, suspended, homogenized and counted. This cell suspension was then diluted and ~1000 (HEK293T; hTERT-RPE1) to 3000 cells (ARPE19) were added onto a 14 cm petri dish. After three days of incubation, cells were washed (DPBS) and slowly detached with Trypsin (0.05 %) in DPBS (1:20). Separated colonies derived from one single cell were selected with a microscope and subsequently transferred to a 24-well plate. After several days of incubation single clone selected cell lines (SCS) were expanded to 6-well plates and further to 10 cm dishes. Followed by DNA extraction, amplification and sequencing.

4.3.7. Stable cell line generation

Cells that were transiently transfected (Lipofectamine™ 3000) with a vector containing a neomycin resistance gene (NeoR), were treated with 0.4 mg/mL geneticidinsulfate (G418). G418 is an antibiotic also affected by NeoR. To ensure a stable insertion of the transfected DNA into the genome a treatment of at least four weeks was necessary. Stable transfected cell lines could then be used for phenotypical characterization.

4.3.8. Quick genomic DNA extraction

To extract genomic DNA 200 µL cell suspension was centrifuged for 3 min at 1000 g. The supernatant was discarded and the pellet resuspended in 100 µL QuickExtract™ solution. The

suspension was incubated in a thermocycler first for 15 min at 65 °C, second for 15 min at 68 °C and lastly for 10 min at 98 °C. This genomic DNA extract could be stored at -20 °C.

4.4. Localization studies

4.4.1. Fluorescence microscopy

Under sterile conditions cells were trypsinized, suspended, homogenized and counted. Then 125,000 cells/mL were seeded onto coverslips in a 12-well plate and incubated overnight (37 °C, 90 % humidity and 5 % CO_2). The next day medium was changed to DMEM without supplements to induce ciliary formation. When investigating Shh pathway, 1-24 hrs prior to fixation to activate the signaling pathway, 52,65 µL smoothened agonist (SAG; 1:1000) was added to 1 mL DMEM to get a final concentration of 100 nM. After three days the medium was discarded and the cells were fixed (4 % para-formaldehyde (PFA) for 15min at RT and/or ice-cold methanol for 5 min). Fixation was followed by three washing steps (ice-cold DPBS for 10 min). For the last washing step, the coverslips were put upside down onto 50 µl drops of PBS in a humidity chamber covered with parafilm above water-soaked tissue. Furthermore, fixed cells were permeabilized with 50 µL 0.3 % Triton X-100 in DPBS for 5 min. Next, cells were blocked for one hour with 50 µL normal goat serum (10 % NGS, 1 % bovine serum albumin (BSA), 0.1 % Triton X-100 in DPBS) at RT. Primary antibodies were diluted in blocking buffer and 50 µL were added onto cells for 1h at RT. Afterwards, cells were washed with DPBS three times for 10 min each at RT followed by secondary antibody incubation for 1 h in the dark (50 µL, RT). Secondary antibodies were diluted in DPBS. Cells were again washed three times for 10 min each at RT with DPBS. Nuclei were stained with 30 µL diamidino-phenylindole (DAPI) (1:10,000), followed by two more DPBS washing steps for 10 min at RT. Finally, the coverslips were shortly rinsed with distilled water and transferred onto a microscope slide with 15 µL of Fluoromount-G®. The slides can be stored in the dark at 4 °C. Images were captured using a Zeiss Axio Imager Z1 ApoTome microscope. The setup includes an AxioCam MRm camera as well as 40× (NA 1.3) and 63× (NA 1.4) oil immersion objective lenses. Images were acquired as Z-stacks and processed using Zeiss ZEN 3.0 Blue Edition [8].

4.4.2. Ciliary length and intensity measurements

The process of quantifying ciliary length was accomplished by using the NeuronJ plugin [111] for FIJI software [112]. Therefore, the ciliary channel of ApoTome RAW convert files was optimized for analysis by excluding background signal, identifying true cilia fluorescence signal, and increasing software recognition of cilia [8]. Intensity measurements were also conducted with FIJI software. For this purpose, initial Z-stacks were acquired with identical exposure times, grey values and γ-settings. Additionally, the tubulin intensity was also optimized by calculating the corrected total cell fluorescence [8]. Statistical analysis (unpaired Student *t*-Test) was performed and graphs were created with GraphPad Prism version 5.0.1 for Windows, GraphPad Software [8].

4.4.3. Super resolution microscopy

Preparing the samples was almost identical to the sample preparation for fluorescence microscopy experiments. Differences were the used high precision microscope cover glasses and the TDE mounting medium which proved to be more suitable for super resolution microscopy. Additionally, samples needed to be sealed with nail polish and more importantly different secondary antibodies (STAR, ATTO) were used since they were not prone to bleaching effects. Images were captured using a Leica TCS SP8 scanning microscope. The setup includes 488 nm, 532 nm and 635 nm pulsed excitation lasers as well as 592 nm and 775 nm depletion lasers, 100x oil immersion objective lens (NA 1.4) and a hybrid detector (HyD) [34]. Nyquist calculation determined optimal pixel size of 20 × 20 nm in XY as well as z-steps not exceeding 120 nm, when acquiring a stack. Laser intensity was adjusted accordingly for each sample and images were recorded with 6x zoom and 3x frame averaging[34]. Acquired images were processed with LasX, deconvoluted with Huygens Professional and edited by FIJI software. A Classical Maximum Likelihood Estimation (CMLE) algorithm under experimentally defined settings was used for deconvolution. The background level was estimated by the software, with quality threshold at 0.001. The number of iterations was 40 and signal-to-noise ratio was set to 7 (confocal) or 20 (STED). All images were brightness-corrected for the purpose of presentation [34].

4.5. Immunoblotting

Confluent cells were serum deprived overnight (HEK293T) or for three days (hTERT-RPE1; ARPE19) to induce ciliary assembly. When investigating Shh pathway, to inhibit the signaling pathway, 0.5-2 µL/mL Forskolin (4 µg/µL) were added 1 h prior to lysis. The final concentration was 5-20 µM. Afterwards, cells were treated with lysis buffer and scraped of the dishes. This cell suspension incubated in buffer for 30 min on an end-over-end shaker at 4 °C, followed by centrifugation (10,000 g for 10 min at 4 °C). The supernatants were transferred into a new tube and their protein concentration was measured by Bradford assay. The total amount of protein was adjusted for all lysates. Stacking and separation gels were prepared (Table 23 and 23). Furthermore, proteins were denaturized by adding Lämmli buffer and heating the samples at 96 °C for 2 min. Lysates and protein ladder were loaded onto the SDS gel and a current (90V for 15min followed by 120V for ~45min) was applied. Following the SDS-PAGE, the size separated proteins were blotted onto a PVDF membrane using a full-wet tank (90 V for 90 min at 4 °C). After western blot, blocking buffer with 5 % fat-free dry milk or 5 % BSA in 1x TBST was applied for 45 min at RT. The PVDF membrane was then incubated overnight at 4°C with primary antibodies, diluted in blocking buffer. The next day the membrane was washed three times for 10 min in 1x TBST, followed by secondary antibody (diluted in 1x TBST) incubation for 1 h at RT. Afterwards, the membrane was again washed three times for 10 min with 1x TBST and incubated for 2 min with ECLplus western blotting solution in the dark. Images were captured using a Chemi Imager Fusion FX and processed with ImageJ.

Table 22 – Separation gel (10 %)

Millipore water	4.0 mL
Tris-HCl Buffer (ph 8.8)	2.5 mL
Arylamide (30 %)	3.3 mL
SDS (10 %)	100 µL
TEMED	20 µL
APS (10 %)	50 µL

➔ APS added at last; add 1 mL isopropanol to remove bubbles and smoothen the gel border

Table 23 – Stacking gel (5 %)	
Millipore water	3.5 mL
Tris-HCl Buffer (ph 6.8)	0.7 mL
Acrylamide (30 %)	0.7 mL
SDS (10 %)	50 µL
TEMED	20 µL
APS (10 %)	50 µL

➔ APS added at last; before pouring into casting chamber remove excess isopropanol

For western blot analysis the lane of interest was selected and a profile plot created which represents the densities of the bands. The area of these bands was then measured and correlated to the loading control. These calculated relative densities of one blot could then be used to compare band intensities in different samples.

4.6. Proteomics

4.6.1. Immunoprecipitation

For interactome identification of TTC30A and TTC30B on endogenous level, HEK293T control and FLAG-tagged TTC30A or TTC30B cells were seeded on 14 cm petri dishes [8]. Six biological replicates were prepared for each condition. At ~90 % confluency, cells were serum starved for 16 h inducing ciliary assembly [8]. The next day cells were lysed and all steps were performed on ice to prevent protein degradation. For lysis non-supplemented DMEM was discarded, 1 mL lysis buffer was added and cells were scraped off. The lysate was homogenized and incubated on an end-over-end shaker for 30 min. After centrifugation for 10 min at 10,000 g the supernatant was transferred to a new reaction tube followed by measuring protein concentration by Bradford Assay.

Anti-FLAG-M2-agarose beads (25 µL packed beads per sample) were washed with 1x TBS, lysis and washing buffer. To not lose too many beads, they were shortly centrifuged after each washing step for 1 min at 5,000 g. Afterwards, the beads were mixed with washing buffer and equally divided to the number of samples.

Identical amounts of protein for each sample were incubated with FLAG-bead suspension for 1 h, followed by three washing steps (washing buffer) in spin columns [8]. For elution of

bound protein, 100 µL FLAG-peptide solution was added and incubated for 10 min at 25°C and 1200 rpm on a thermo shaker. Finally, the spin columns were centrifuged for 60 sec at 1,000 g and the eluates were collected.

4.6.2. Affinity purification

For Lebercilin interactome analysis by Strep based affinity purification, Strep/FLAG tagged overexpression constructs were transiently transfected into TTC30B KO, TTC30A/B KO and Cas9 control cells [8]. Therefore, cells were transfected at ~60 % confluency. 1 ml PEI solution and 8000 ng DNA per 14 cm petri dishes were incubated 10 min at RT. This transfection mix was added dropwise to the cells which were then incubated for at least 48 hrs. As control Strep/FLAG-tagged RAF1 was used [8].

Cell lysis, Bradford assay, preparing Beads, Bead incubation and purification were similar to a FLAG-Immunoprecipitation. Differences were Strep-Tactin Superflow (25 µL packed) beads and 100 µL Strep elution buffer.

4.6.3. Bradford assay

To measure the protein concentration of cell lysates Bradford assay was performed. Therefore, different BSA concentrations were mixed with 5.5 µL lysis buffer and used for calibration (Table 24). Triplicates of each BSA dilution (5 µL) and lysates (1 µL; 1:5 dilution) were pipetted into a 96-well plate. To start the reaction 250 µL Bradford (1x) were added into each well and after a short incubation (5 min) the OD (595 nm) was measured using Tecan Luminescence Reader.

Table 24 – Bradford assay

BSA dilution [mg/mL]	BSA stock [µL]	HPLC H_2O [µL]	Lysis buffer [µL]
0	0	50	5.5
0.2	10	40	5.5
0.4	20	30	5.5
0.6	30	20	5.5
0.8	40	10	5.5
1.0	50	0	5.5

4.6.4. Protein precipitation

Following a FLAG-Immunoprecipitation or Strep based affinity purification, a methanol–chloroform-based protein extraction was performed. Therefore, eluates were treated with 800 µL hypergrade LC/MS-methanol, shortly vortexed and centrifuged for 60 sec at 9,000 g. For precipitation, 200 µL chloroform (for analysis) were added, again vortexed and centrifuged (60 sec; 9,000 g), followed by 600 µL HPLC water, vortexing and centrifugation (2 min; 16,000 g). After this step, the upper phase was discarded. Lastly, 600 µL hypergrade LC/MS-methanol were added, vortexed and centrifuged (4 min; 16,000 g). The supernatant was again discarded and the pellet dried for 5 min under a laminar air flow bench.

4.6.5. Protein digest (in solution)

The precipitated protein was resuspended in a mixture of 30 µL ABC, 4 µL RapiGest™ and 1 µL DTT and incubated for 10 min at 60 °C on a thermoblock. After the suspension was cooled down 1 µL IAA was added an incubated in the dark for 30 min at RT. To start the digestion 1 µL Trypsin was added (0.5 µg/µL) and incubated overnight at 37 °C.

The next day enzymatic digestion was stopped by mixing 1.7 µL TFA to each sample. The acidified solution transferred into a PP insert, incubated for 10 min at RT and centrifuged for 15 min at 16,000 g. The clear solution was then desalted using StageTips. The C18 matrix of the tips needed to be activated with 20 µL 80/5 (80 % ACN/5 % TFA) solution, followed by a rinsing step with 20 µL 0/5 (H_2O/5 % TFA) solution. Then the complete sample was added and again washed with 20 µL 0/5 solution. Elution was done in two steps with 20 µL 50/5 (50 % ACN/5 % TFA) and 80/5 solution. Finally, the purified eluate was reduced to ~5 µL by a SpeedVac. To prepare the samples for MS analysis 10 µL of 0.5 % TFA were added.

4.6.6. Mass spectrometry LC-MS/MS analysis

An Ultimate3000 RSLCnano was coupled with a nano spray ion source to the Orbitrap Fusion Tribrid mass spectrometer. The tryptic peptide mixtures were loaded onto a µPAC trapping column (C18 trapping column with pillar diameter 5 µm, inter pillar distance 2.5 µm pillar length/bed depth 18 µm, external porosity of 9 %, bed channel width of 2 mm and a length of 10 mm, porous shell thickness of 300 nm and pore size of 100-200 Å). Injection was conducted with a flow rate of 10 µL/min in 100 % of loading buffer (0.1% FA in HPLC-grade

water) [8]. After 3 min, peptides were eluted and separated on an analytical 50 cm µPAC C18 nano column (pillar diameter 5 µm, inter pillar distance 2.5 µm pillar length/bed depth 18 µm, external porosity of 59 %, bed channel width of 315 µm and a length of 50 cm, porous shell thickness of 300 nm and pore size of 100-200 Å) at a flow rate of 300 nL/min with a linear gradient from 2 % up to 30 % of buffer B (80 % ACN, 0.08 % formic acid in HPLC-grade water) in buffer A (2 % ACN, 0.1 % formic acid) for 82 min after an initial step of 3 min at 2 % buffer B. Remaining peptides were eluted with a step gradient (30 % to 95 % in 5 min) followed by 5 min at constant 95 % of buffer B before the gradient was decreased rapidly in 5 min to 2 % of solvent B for the final 20 min [8]. In the data-dependent analysis, full-scan MS spectra were measured on the Fusion in a mass-charge range from m/z 335–1500 with a resolution of 120,000 [8]. The ten most abundant precursor ions (cycle time of 3 s between master scans) were selected with a quadrupole mass filter, if they exceeded an intensity threshold range of 5.0 e3 to 1.0 e20 and were at least doubly charged (2-7), for further fragmentation using higher-energy collisional dissociation (HCD) followed by mass analysis of the fragments in the iontrap. The selected ions were excluded for further fragmentation the following 60 s [8].

MaxQuant software [113] was used to analyze the received MS/MS data. Trypsin/P was set as digesting enzyme with a maximum of two missed cleavages. Methionine oxidation and N-terminal protein acetylation were selected for variable modifications. For fixed modifications, Cysteine carbamidomethylation was set. The data was analyzed by label-free quantification (LFQ) with the minimum ratio count of two. Re-quantification was not performed in LFQ. First Search was enabled. The current SwissProt database (2019) was selected for peptide and protein identification. The contaminants were excluded by MaxQuant contaminant search. A minimum peptide number of 1 and a minimum peptide length of 7 was tolerated. For quantification, minimum unique and razor peptides were set to 1. More detailed settings are listed in the appendix (Appendix 2).

Protein identification was followed by statistical analysis using Perseus [114]. The initial data set was filtered for proteins only identified by site, reversed peptide sequences and potential contaminants [8]. Proteins were only statistically analyzed when they were detected in at least four out of six biological replicates, belonging to same condition. Missing values were replaced by a constant, followed by an unpaired two-sample Student *t*-test (permutation-based FDR < 0.05) [8]. Groups were averaged and result stability over the replicates was

tested with an outlier test (significance A, Benjamini–Hochberg FDR < 0.05). Finally, proteins meeting the significance criteria were considered as being significantly enriched [8].

5. Results

5.1. Experimental approach

The approach for investigating protein function and revealing their involvement in cilia related processes was a combination of mainly two different procedures. Therefore, the feature of the CRISPR/Cas9 system was used to delete or insert nucleotides at almost any desired position in the DNA sequence. Hereby, single cell derived isoform specific knockout clones were created and their phenotypical appearance was characterized. Furthermore, mass spectrometric analysis of protein complexes from likewise created endogenously tagged cells was conducted and their possible interacting proteins were identified. This combination serves to connect an observed phenotype with potential interacting proteins to dissect the underlying mechanism and to exclude coincidental findings (**Figure 10**).

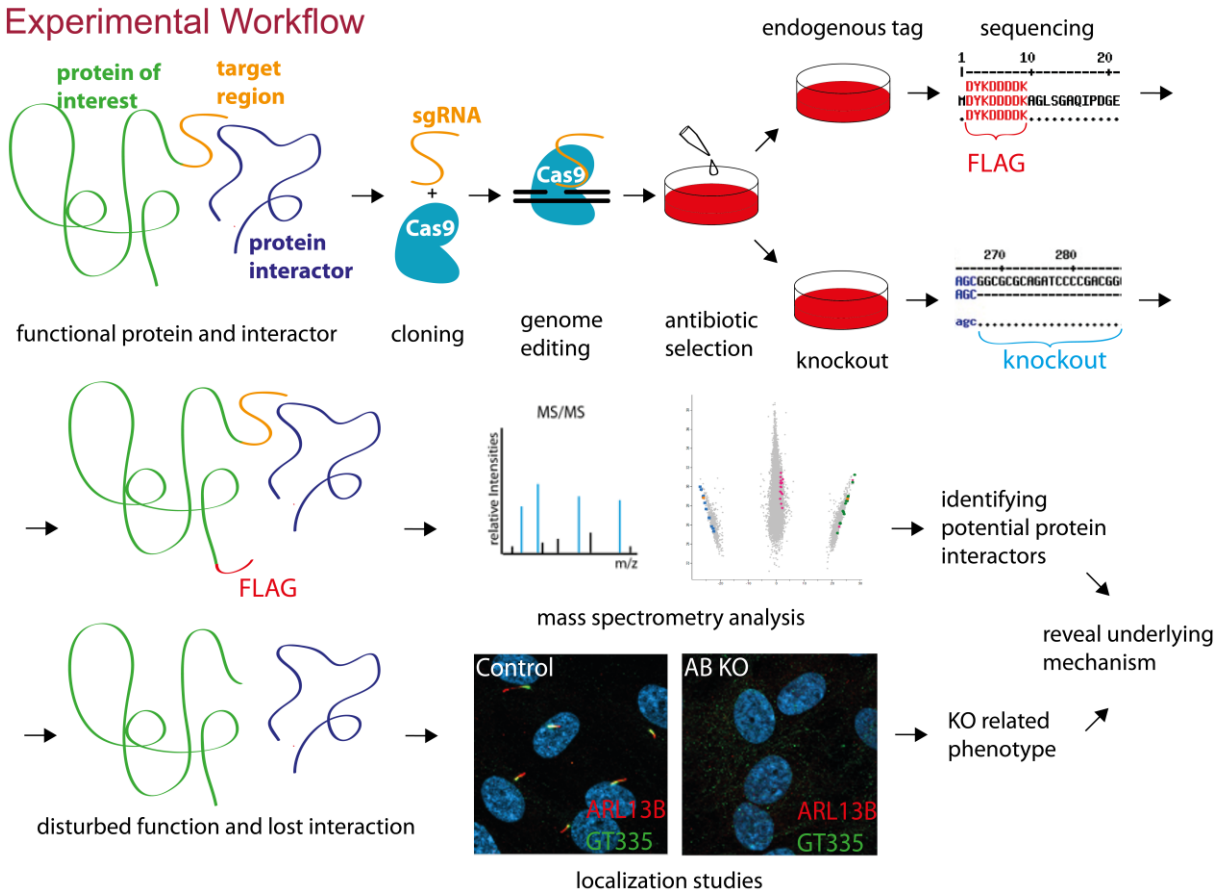

Figure 10 – Experimental workflow – The overview is depicting the experimental workflow. Cells were transfected with a sgRNA (orange) containing Cas9 expression vector (blue). The sgRNA is targeting the protein of interest (green) at a specific region (orange) and in combination with Cas9 a specific knockout can be generated. Furthermore, a combination of sgRNA and repair construct leads to an insertion of a desired sequence (e.g., FLAG-tag) on endogenous level. Afterwards, cells were selected with antibiotics for successful transfection and sequenced. Cells with knock-in of a protein tag were

used for MS analysis and identification of potential protein interactors. Additionally, in localization studies knockout cell lines were analyzed for their phenotype. By combining potential interactors with an observed phenotype an unknown protein function can be hypothesized and further investigated.

5.2. TTC30

5.2.1. Generation of TTC30A/B knockout cell lines

The investigation of a paralogue-specific function of TTC30A and B in ciliogenesis required the generation of retinal-pigmented epithelial knockout cells (hTERT-RPE1 KO) using CRISPR/Cas9. The transfection of hTERT-RPE1 cells with TTC30A- or B-targeting sgRNAs was followed by single clone selection and DNA extraction [8]. To specifically target TTC30A or B and to generate double KO cells, deletions by combining two sgRNAs were induced [8]. Using Sanger sequencing, deletions followed by an open-reading frameshift and predicted early stop codon were identified (**Figure 11, 12 and 13**). Furthermore, sequencing verified the successful generation of homozygous TTC30A and TTC30B single KO as well as a TTC30A/B double KO [8].

CRISPR/Cas9 mediated specific TTC30A KO generation in hTERT-RPE1 cells was successful (**Figure 11**). Close to the start codon of TTC30A exon 1, two PAM sequences were utilized. One is located on the sense strand in 5’ to 3’ direction, 25 bp from the starting codon. The second PAM can be found on the anti-sense strand in 3’ to 5’ direction, 26 bp after the first PAM sequence. The deletion of 20 bp led to an early stop codon which was located 143 bp after the second sgRNA target region. This p.G12VfsX50 mutation in the following referred to as TTC30A KO resulted in a deletion of 89.83 % of TTC30A.

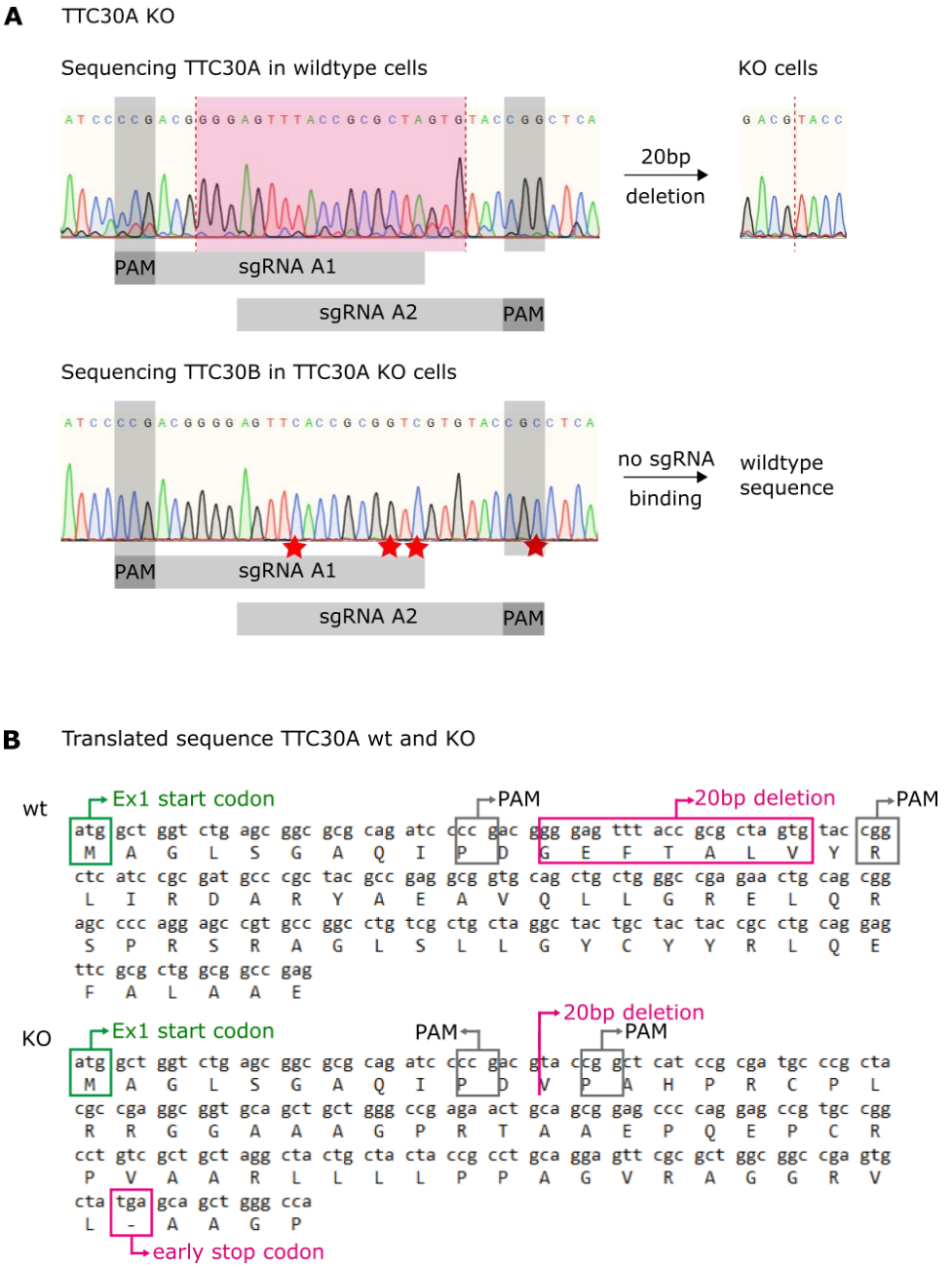

Figure 11 – Sequencing results for TTC30A wildtype and knockout – (**A**) Shown are fragments of wildtype TTC30A/B genes along with PAM sequences (dark grey), sgRNA binding sites (light grey) and deleted base pairs (magenta). Sequencing results after CRISPR/Cas9-mediated KO generation depict a homozygous 20 bp deletion. Specific TTC30A sgRNAs do not bind in the TTC30B gene, resulting in a specific KO. Sequence mismatches of sgRNAs are highlighted with red stars. (**B**) Translation of nucleotide sequence fragments in wt and KO cells reveals a frameshift caused by CRISPR/Cas9-mediated deletion that led to a premature stop codon. Modified after [8]

Furthermore, sequencing revealed the TTC30B gene was not affected by the CRISPR/Cas9 system, because only one of the two PAM sequences is shared between TTC30A and B. The respective sgRNA showed three mismatches within the target sequence, so the binding of this sgRNA was unlikely. Hence, these small differences in the nucleotide sequence were sufficient

to introduce TTC30A specific genomic changes. Possible off-targets were identified in exonic, intronic or inter genomic regions, but with a minimal probability of binding (Appendix 3.1 and 3.2).

Also, CRISPR/Cas9 mediated specific TTC30B KO generation in hTERT-RPE1 cells was successful (Figure 12). Close to the start codon of TTC30B exon 1, two PAM sequences were identified.

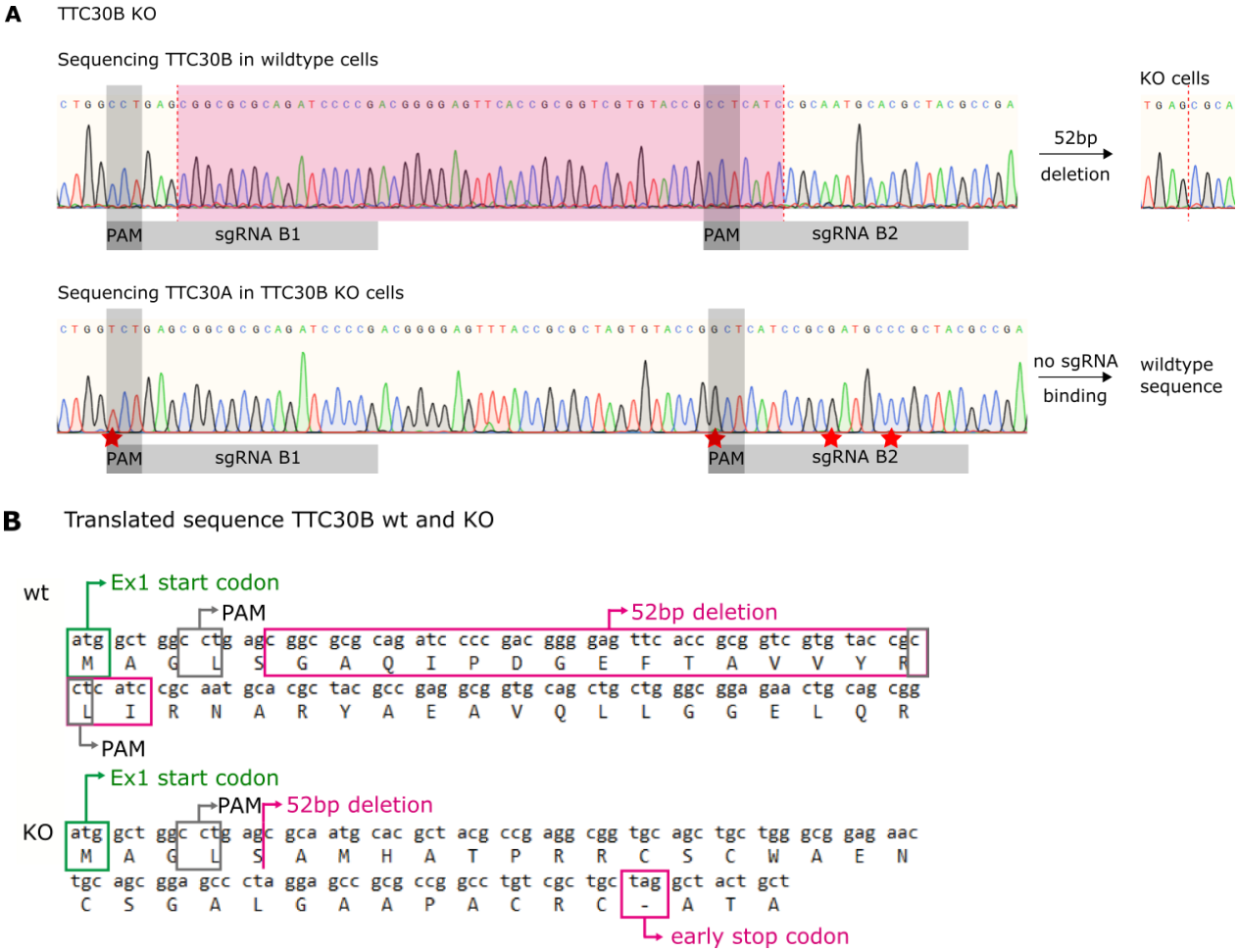

Figure 12 – Sequencing results for TTC30B wildtype and knockout – (**A**) Shown are fragments of wildtype TTC30A/B genes along with PAM sequences (dark grey), sgRNA binding sites (light grey) and deleted base pairs (magenta). Sequencing results after CRISPR/Cas9-mediated KO generation depict a homozygous 52 bp deletion. Specific TTC30B sgRNAs do not bind in the TTC30A gene, resulting in a specific KO. Sequence mismatches of sgRNAs are highlighted with red stars. (**B**) Translation of nucleotide sequence fragments in wt and KO cells reveals a frameshift caused by CRISPR/Cas9-mediated deletion that led to a premature stop codon. Modified after [8]

Both PAM sequences are located on the anti-sense strand in 3' to 5' direction. The first PAM was 5 bp behind the start codon and the second 48 bp later. The early stop codon was located 85 bp after the second sgRNA target region. This p.G6AfsX28 mutation in the following referred to as TTC30B KO resulted in a deletion of 92.44 % of TTC30B. Accordingly,

sgRNAs were not overlapping and not interfering with each other. Subsequently, they led to a homozygous 52 bp deletion. Sequencing revealed, that the TTC30A gene was not affected, since both PAM sequences are unique for TTC30B. Hence, these small differences in the nucleotide sequence were sufficient to introduce TTC30B specific genomic changes. Possible off-targets were identified in exonic, intronic or inter genomic regions, but with a minimal probability of binding (**Appendix 4.1 and 4.2**).

Finally, CRISPR/Cas9 mediated TTC30A and TTC30B double KO generation in hTERT-RPE1 cells was successful (**Figure 13**). Specific sgRNAs for TTC30A and TTC30B which proved to be efficient in single KO generation were combined. The combination led to a 20 bp deletion in TTC30A and to a 52 bp deletion in TTC30B. The deletion in both paralogues also resulted in an early stop codon in both genes.

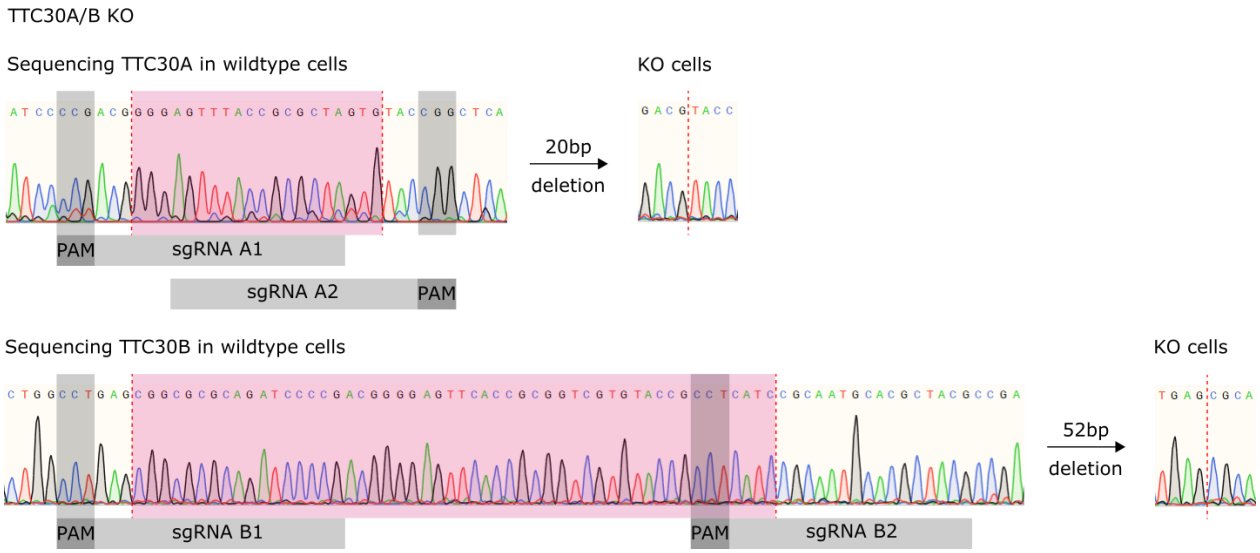

Figure 13 – Sequencing results for TTC30A/B double knockout – Shown are fragments of wildtype TTC30A/B genes along with PAM sequences (dark grey), sgRNA binding sites (light grey) and deleted base pairs (magenta). Sequencing results after CRISPR/Cas9-mediated KO generation depict a homozygous 20 bp deletion in TTC30A gene (**top**) and a 52 bp deletion in TTC30B (**bottom**). Both deletions led to a premature stop codon. Mixing TTC30A and B specific sgRNAs resulted in homozygous TTC30A and B double KO. [8]

5.2.2. Verification of TTC30 knockout cell lines

Initially, TTC30A/B single and double KO cells were lysed, followed by SDS-PAGE and western blot to investigate their total protein level and to verify differences in protein abundance in wildtype (wt) versus mutant cell lines. Unfortunately, there is no antibody available to distinguish between TTC30A and TTC30B due to the amino acid sequence similarity [8]. Still, a

clear reduction in TTC30 signal intensity can be seen in single KO compared to control cells. In the double KO, no signal could be detected [8]. Additionally, the protein level of acetylated tubulin and GAPDH (loading control) were investigated and they were evenly distributed in all samples (Figure 14).

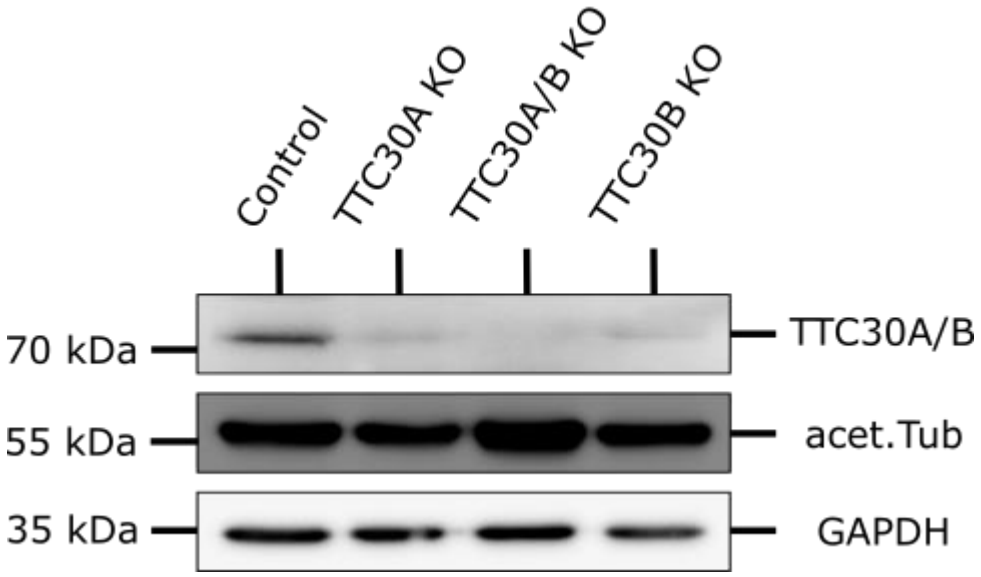

Figure 14 – Protein level of TTC30A/B and acetylated tubulin in TTC30A/B wildtype and knockout cells – In hTERT-RPE1 control, TTC30A/B single and double knockout cells, protein level of TTC30A/B, acetylated tubulin and GAPDH as loading control were checked by western blot. [8]

To further verify the CRISPR/Cas9 mediated KO, immunofluorescence (IF) microscopy of homozygous and specific hTERT-RPE1 TTC30A, TTC30B single and TTC30A/B double KO cells was performed [8]. To visualize the cilium, an antibody against ARL13B was used. This small GTPase, which is involved in ciliogenesis and Sonic hedgehog (Shh) signaling, is associated with the ciliary membrane [115]. For this reason, it is frequently used as ciliary marker. Still the TTC30 antibody could not distinguish between TTC30A and TTC30B, but again a clear reduction in TTC30 signal intensity can be seen in single KO compared to control cells [8]. In TTC30A/B double KO cells the TTC30 signal could not be differentiated from background. In addition, the signal for ciliary marker ARL13B was also not distinguishable. This indicated that a complete loss of TTC30A/B directly leads to inhibited ciliogenesis, possibly due to failed IFT-B complex assembly [31].

Subsequently, rescue cell lines were generated by transfecting TTC30A/B double KO cells with either TTC30A or TTC30B wildtype expression vector, followed by antibiotic mediated selection for stably transfected cells. Regarding these rescue cells both proteins, TTC30 and

ARL13B, were re-localizing to the cilium (**Figure 15**). This proved that the phenotype described in the KO cells was specific for the loss of TTC30 [8].

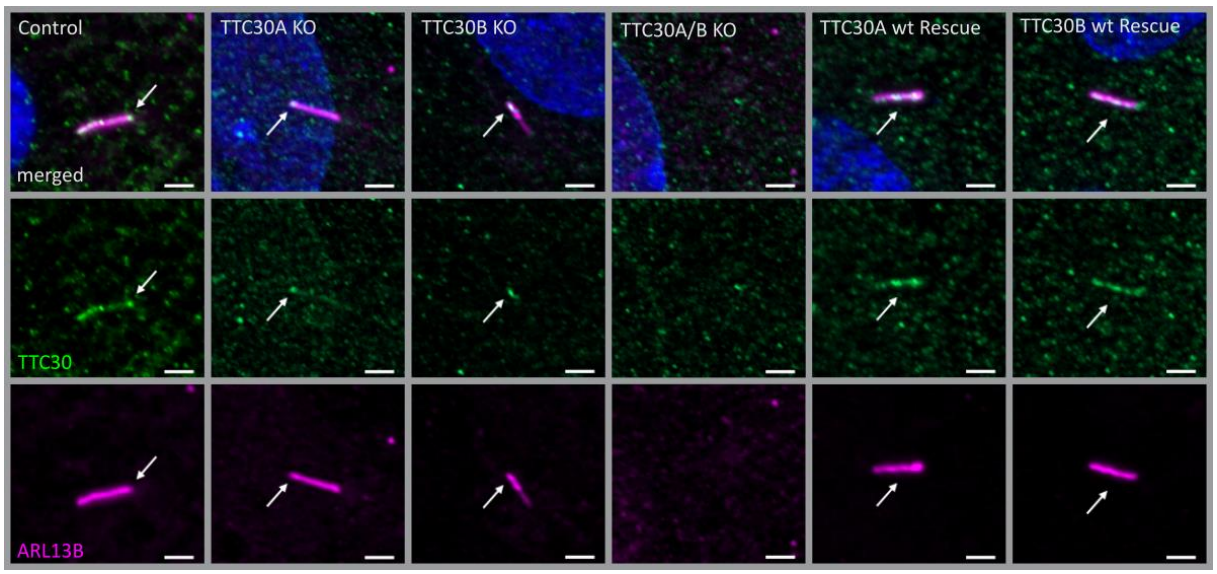

Figure 15 – TTC30A/B knockout verification by immunofluorescence staining – Fluorescent light microscopy pictures of hTERT-RPE1 control, TTC30A, TTC30B and TTC30A/B double KO cells, TTC30A and TTC30B rescue (from left to right) are shown. The cells were stained for ARL13B (magenta) and TTC30 (green), DNA is marked in dark blue and co-localization shown in white. The scale bar measures 2 µm. [8]

The combination of reduced signal in single KO cells, no signal in double KO cells and reappearing signal in rescue cells confirms the successful TTC30A/B single and double KO generation. According to KO verification by IF, the western blot results also confirmed the successful generation of TTC30A/B single and double KO cells. Acetylated tubulin, as one of the main components in the ciliary axoneme, was thought to be affected because of the suggested impact of TTC30 on ciliogenesis with no ciliary assembly, but no difference in intensity was visible. This indicated that total protein level of acetylated tubulin is not influenced by TTC30A/B (**Figure 14**).

5.2.3. Localization of TTC30A/B homogenously along the cilium

First IF studies depicted a quite random localization of TTC30 along the cilium. Hence, the localization needed to be further investigated. Therefore, a confocal laser scanning microscopy (LSM) excitation laser was combined with a stimulated emission depletion (STED) laser. This method, super resolution microscopy, narrows the point spread function (PSF) and increases the resolution to achieve a more detailed picture. TTC30 was again co-stained with

ARL13B in hTERT-RPE1 control cells and both signals were detected all along the cilium with no visible hotspots (**Figure 16**).

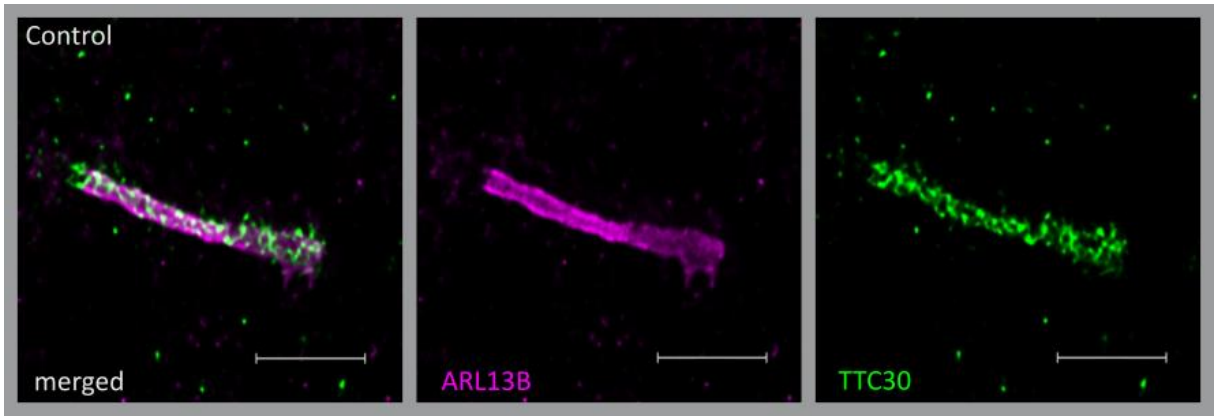

Figure 16 – TTC30A/B localization by STED super resolution microscopy – STED super resolution microscopy pictures of hTERT-RPE1 control are shown, depicting TTC30 localization in the cilium. The cells were stained for ARL13B (magenta) and TTC30 (green). Co-localization is shown in white. The scale bar measures 2 µm.

TTC30 as a component of the IFT-B complex was expected to be equally distributed since the intraflagellar transport is permanently active in ciliated cells. IFT-B is essential for carrying cargo (e.g., tubulins) from the ciliary base to the tip and is therefore vital for ciliary assembly, maintenance and function. This anterograde transport is followed by retrograde transport of IFT-B back to the ciliary base (**Figure 3**) [1, 9, 10]. This leads to a localization of TTC30 along the axoneme. Similarly, ARL13B was evenly distributed along the cilium.

5.2.4. Single TTC30A or TTC30B knockout affects ciliogenesis

Cilia number and length were investigated using again the ciliary protein ARL13B, which can be used as a marker for these measurements (**Figure 15, 16 and 17**) [8]. Furthermore, GT335 labeling polyglutamylated tubulin at the proximal compartment of the cilium under ciliated conditions was used to analyze ciliation (**Figure 17**) [8, 116, 117]. In previous studies, polyglutamylation was shown to be influenced by a complete loss of TTC30/IFT70 [8, 32]. Interestingly, ciliary length and the level of polyglutamylated tubulin in TTC30A or TTC30B KO cell lines were mildly but significantly reduced compared to control cells [8]. The average ciliary length in control cells was 4.097 µm ± 0.055 µm; in TTC30AKO cells 3.363 µm ± 0.048 µm; and in TTC30B KO cells 3.122 µm ± 0.041 µm ($n_{control}$ = 308; $n_{TTC30AKO}$ = 224; $n_{TTC30BKO}$ = 245). On average, cilia in KO cells were approximately 1 µm shorter compared to control cells (TTC30A KO: 21.04%; TTC30B KO: 29.22% reduction) [8]. GT335 intensity in KO cells was even

more strongly affected. The average intensity dropped from 1.053 relative intensity units (IU) ± 0.026 IU in control cells to 0.6590 IU ± 0.026 IU (62.58% in TTC30A KO) and 0.617 IU ± 0.034 IU (58.56% in TTC30B KO) (**Figure 17**) [8]. These effects were even more severe in TTC30A/B double KO cells, where ciliary and tubulin marker cannot be distinguished from the background, showing that cilia formation was absent [8].

Importantly, the loss of cilia formation in TTC30A/B double KO cells was rescued by either TTC30A or TTC30B (**Figure 15 and 17**) [8]. Therefore, these cells were either transfected with TTC30A or TTC30B wildtype expression vectors and subsequently treated with G418 (NeoR) to generate stably transfected rescue cells. The ciliary length of stable TTC30A rescue cells was 3.449 µm ± 0.113 µm and 3.680 µm ± 0.131 µm in stable TTC30B rescue cells ($n_{control}$ = 308; $n_{TTC30ARescue}$ = 41; $n_{TTC30BRescue}$ = 32). The average GT335 intensity was 0.6610 IU ± 0.04015 IU (in TTC30A wt rescue cells) and 0.5829 IU ± 0.0418 IU (in TTC30B wt rescue cells). Thus, ciliary length and intensities for polyglutamylated tubulin are comparable to those of TTC30A and TTC30B single KO cells [8]. Strikingly, this stable cell line overexpression of one paralogue does not significantly increase ciliary length or GT335 intensity. These properties were only significantly exceeding single KO values when both paralogues were present.

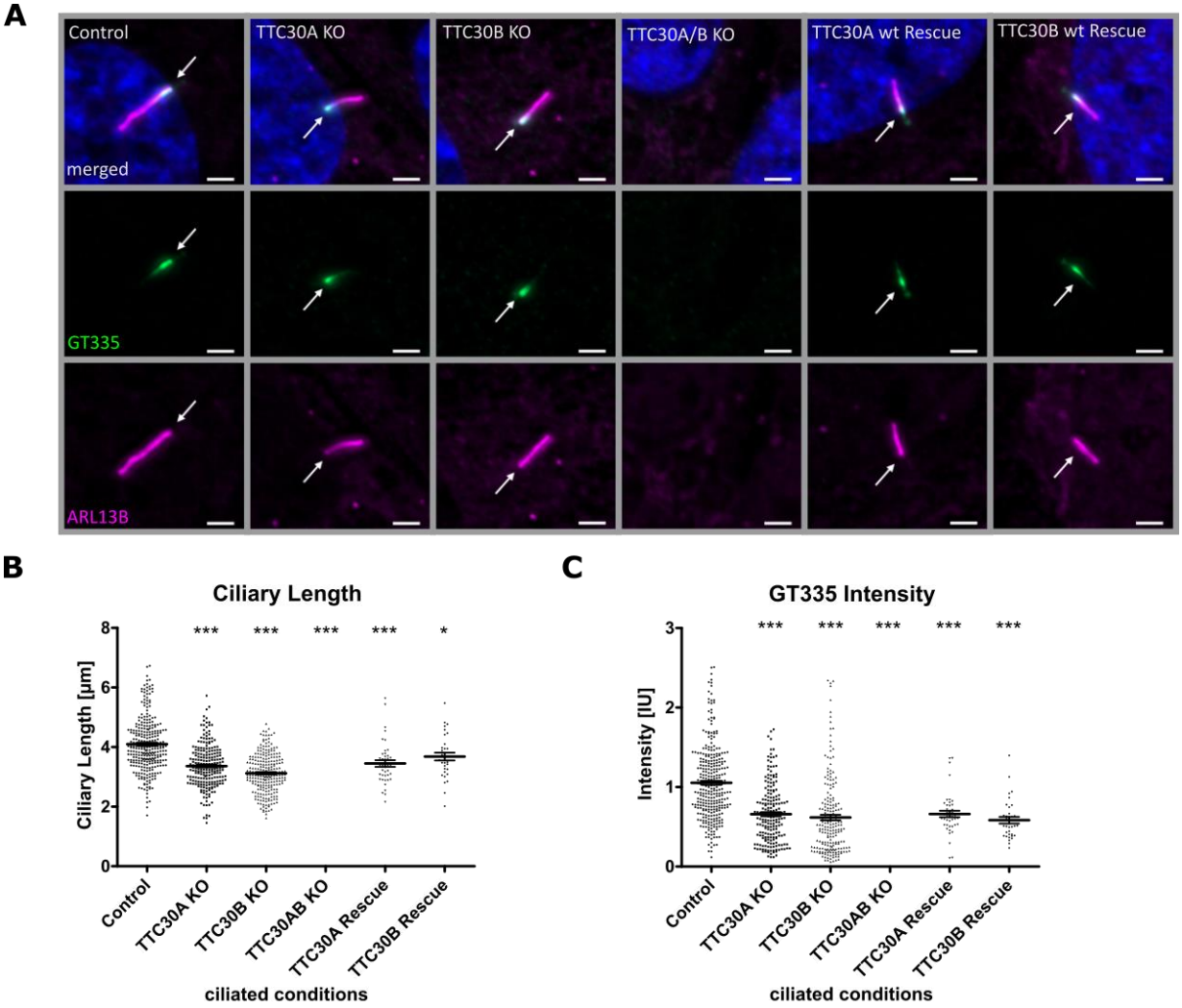

Figure 17 – Ciliary length and GT335 intensity measurements in TTC30A/B wildtype, knockout and rescue cells – (**A**) Fluorescent light microscopy images of hTERT-RPE1 control, TTC30A, TTC30B, TTC30A/B double KO cells, TTC30A and TTC30B rescue (from left to right) are shown. The cells were stained for ARL13B (magenta) and polyglutamylated tubulin (GT335, green), DNA is marked in dark blue and co-localization is shown in white. The scale bar measures 2 µm. In TTC30A/B control, single and double KO as well as rescue cells, ciliary length (**B**) was measured using ARL13B as an indicator for ciliary length. Measurements of fluorescent intensity of polyglutamylated tubulin staining is shown in (**C**). In the scatter dot plots, results gained in two independent experiments are shown with each dot representing one cilium. For statistical analysis, the mean was calculated. *p* values below 0.05 are represented by * and below 0.001 by ***. Error bars represent the s.e.m. [8]

These data clearly indicate an influence of TTC30 on ciliary length and consequently ciliogenesis. To check if also ciliation is altered in TTC30 KO cells, the total numbers of cells and ciliated cells needed to be investigated. Therefore, nuclei were stained by DAPI and cilia once more with ARL13B. Whereby, each nucleus was representing one cell. Cilia were then counted and normalized to the total amount of nuclei. The ratios of hTERT-RPE1 control, TTC30A and TTC30B single KO cells were comparable (~80%). Only the number of ciliated cells

in TTC30A/B double KO could not be measured, since the ARL13B signal could not be distinguished from the background (Figure 18).

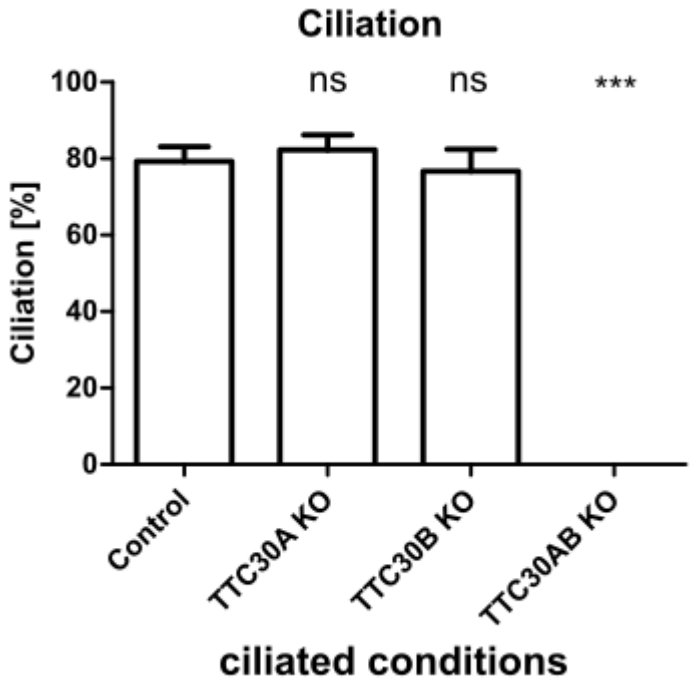

Figure 18 – Ciliation of TTC30A/B wildtype and knockout cells – In hTERT-RPE1 TTC30A/B single and double knockout cells the number of cilia was counted and divided by the number nuclei obtaining the level of ciliation. *p* values below 0.001 are represented by ***. p values above 0.05 are determined not significant (ns). Error bars represent the s.e.m. [8]

TTC30 single KO leads to a disturbed ciliary assembly resulting in shorter cilia but the total amount of ciliated cells remains unchanged.

5.2.5. Single TTC30A or TTC30B have no effect on IFT complex A or B component localization

Further, it was evaluated whether a loss of TTC30 affected the ciliary localization of IFT complexes. The total protein levels of IFT-B protein IFT88 and IFT-A protein IFT140 were investigated by western blot [8]. IFT88 and IFT140 overall intensities were slightly variable, therefore intensities were measured and normalized to GAPDH as loading control (Figure 19).

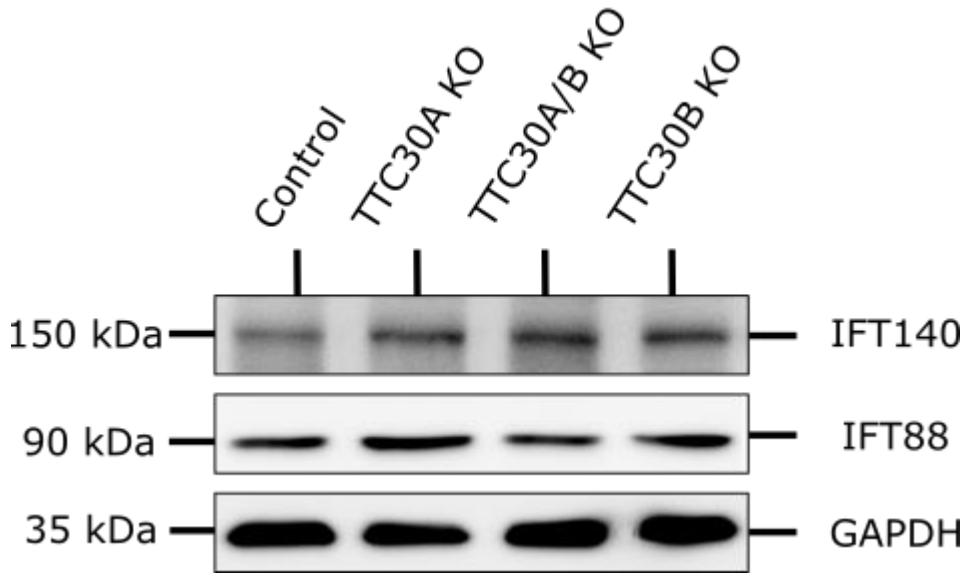

Figure 19 – Protein level of IFT88 and IFT140 in TTC30A/B wildtype and knockout cells – In hTERT-RPE1 control, TTC30A/B single and double knockout cells, protein level of IFT140, IFT88 and GAPDH as loading control were checked by western blot. [8]

The resulting ratios (IFT88: n = 4; IFT140: n = 5) appeared similar in TTC30A/B single and double KO cells compared to control cells (**Figure 20**), showing that overall TTC30A/B single or double KO does not influence the expression of IFT88 or IFT140 [8].

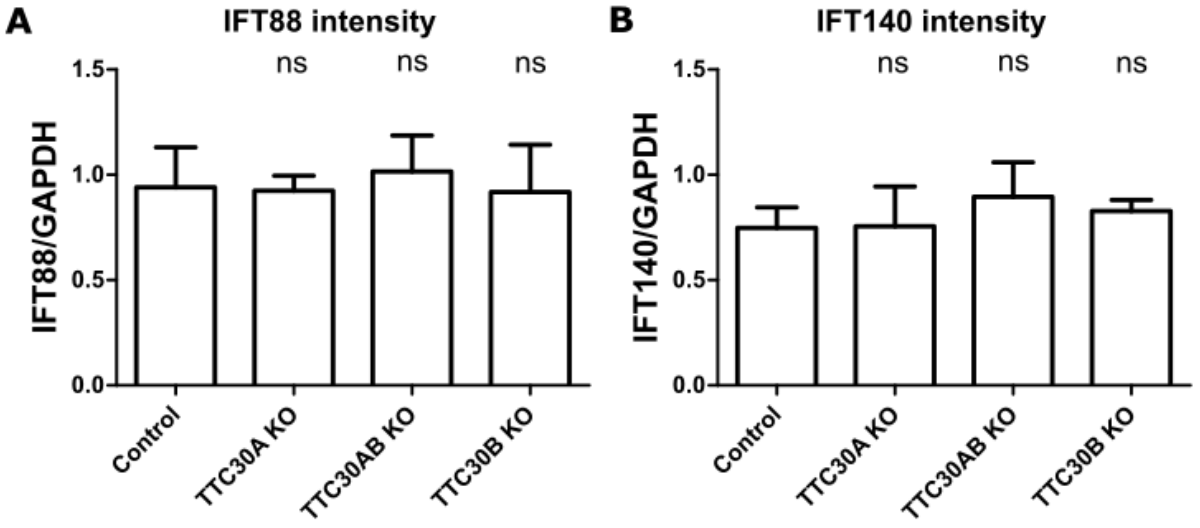

Figure 20 – Protein level intensity measurements of IFT88 and IFT140 in TTC30A/B wildtype and knockout cells – In hTERT-RPE1 TTC30A/B single and double knockout cells the protein level of IFT88 (**A**) and IFT140 (**B**) were quantified by measuring their intensity. These values were normalized to the loading control (GAPDH). The resulting ratios of IFT88 (n = 4) as well as IFT140 (n = 5) for TTC30A, TTC30AB and TTC30B KO cells were comparable to those of control cells. For statistical analysis the mean was calculated. *p* values above 0.05 are deemed not significant (ns). Error bars represent the s.e.m. [8]

Additionally, IFT88 and IFT140 were investigated in TTC30 single and double KO cells, as well as rescue cells, with immunofluorescence staining. All cells were stained for ARL13B and either IFT88 or IFT140 [8]. Interestingly, IFT88 and IFT140 localization was unaffected in both TTC30A and B single KO cell lines. Once more, in double KO cells the signal could not be distinguished from the background. In TTC30A/B rescue cells, IFT88 and IFT140 were re-localizing to the cilium (Figure 21) [8].

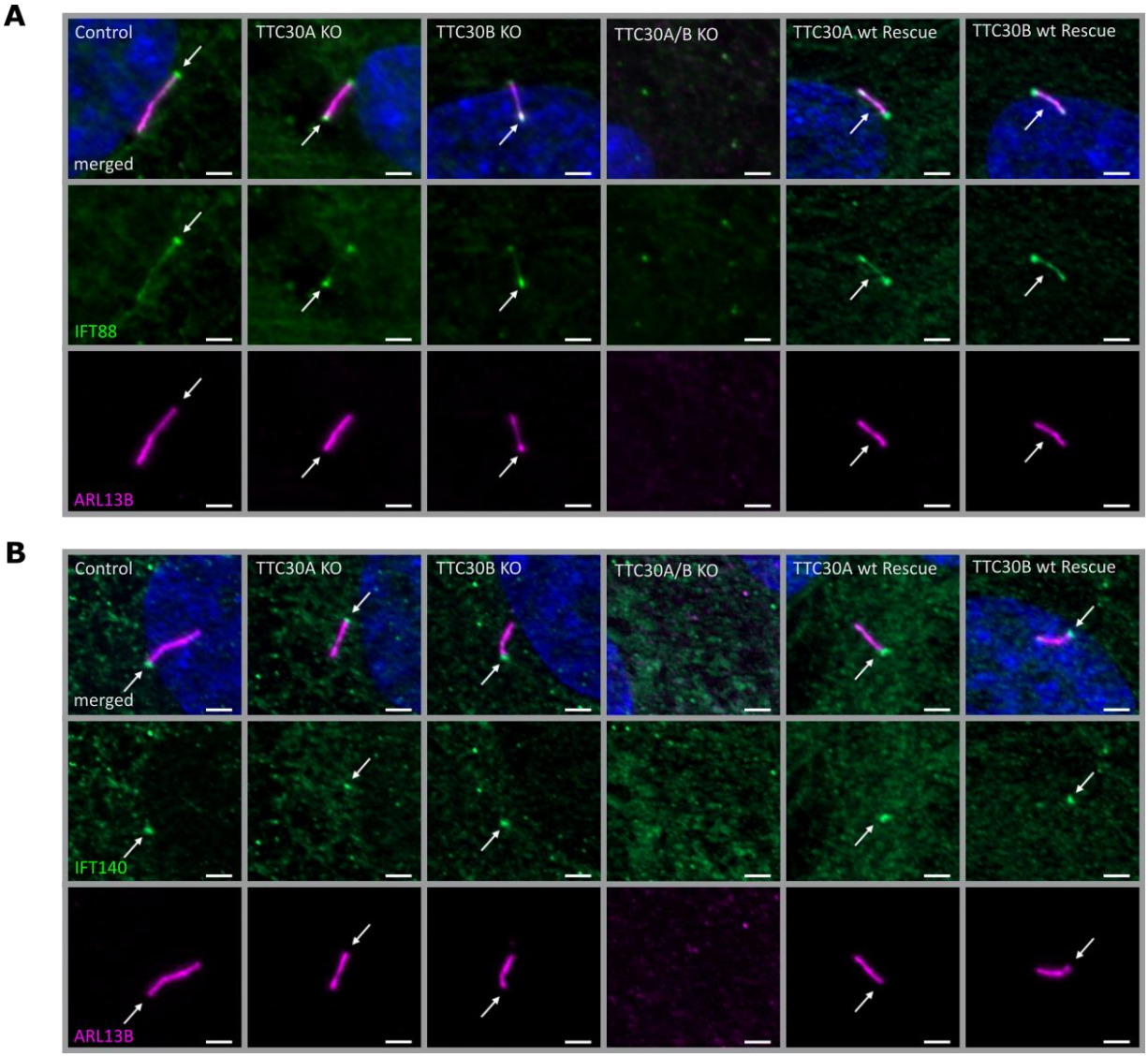

Figure 21 – Localization of IFT88 and IFT140 in TTC30A/B wildtype, knockout and rescue cells – Fluorescent light microscopy images of hTERT-RPE1 control, TTC30A, TTC30B, TTC30A/B double KO cells, TTC30A and TTC30B rescue (from left to right) are shown. The cells were stained for ARL13B (magenta), DNA is marked in dark blue and co-localization shown in white. The green channel depicts IFT88 (**A**) or IFT140 (**B**). The scale bar measures 2 µm. [8]

To investigate if the localization of IFT complex A and B proteins to the basal body is disturbed due to TTC30A/B knockout, IFT88/IFT140 co-staining with γ-tubulin in hTERT-RPE1 control, TTC30A KO, TTC30B KO and TTC30A/B double KO cells was performed [8].

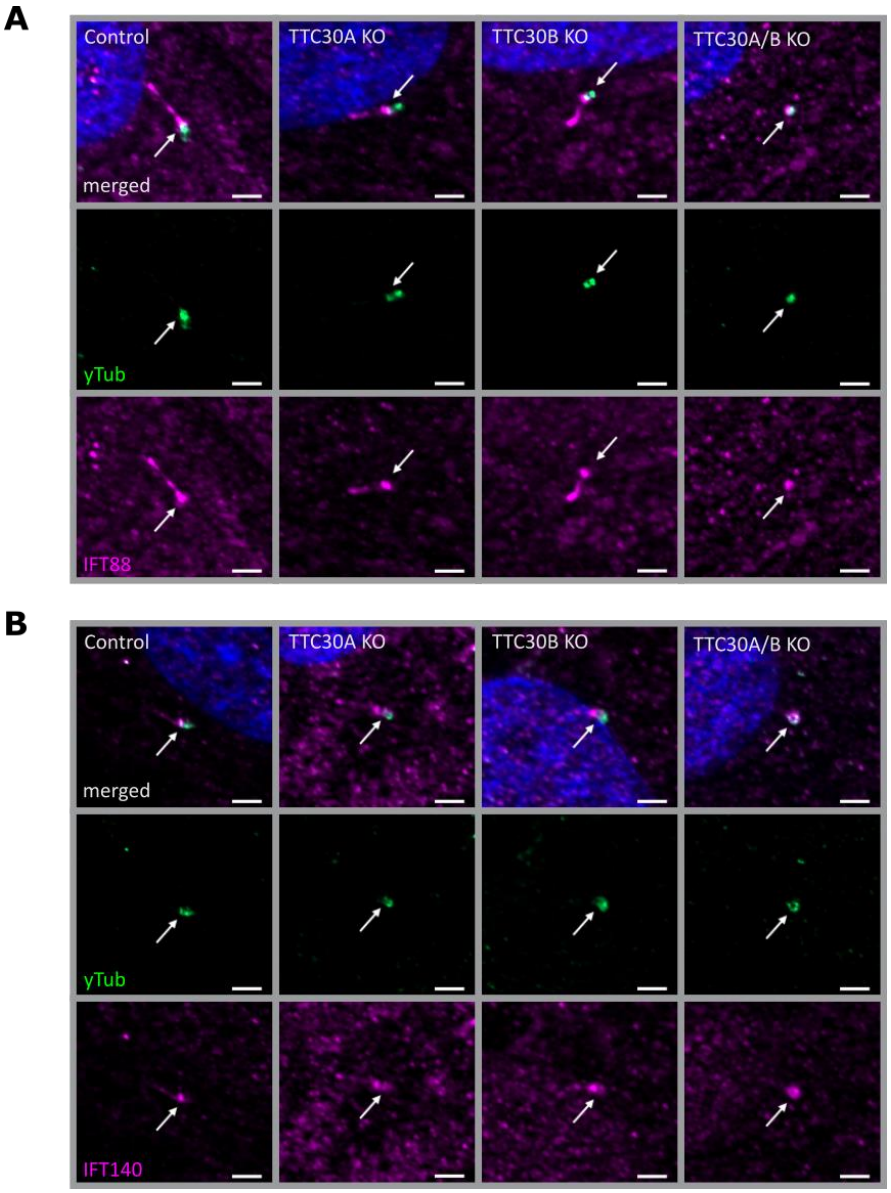

Figure 22 – Co-localization of γ-tubulin with IFT88 or IFT140 in TTC30A/B wildtype and knockout cells – Fluorescent light microscopy pictures of hTERT-RPE1 control, TTC30A, TTC30B and TTC30A/B double KO cells (from left to right) are shown. The cells were stained for γ-tubulin (green), DNA is marked in dark blue and co-localization is shown in white. The magenta channel depicts IFT88 (**A**) or IFT140 (**B**). The scale bar measures 2 µm. [8]

Both IFT proteins could be detected along the cilium and at the basal body in control and single KO cells, whereas γ-tubulin was only located at the base. In TTC30A/B double KO cells no cilia were assembled, but IFT proteins still co-localize with γ-tubulin at the basal body

(Figure 22) [8]. This concludes, that in general IFT complex A and B were still expressed and localizing to the ciliary base.

5.2.6. TTC30A and TTC30B paralogues are separately detected by mass spectrometry

Following proper KO generation, verification and phenotype characterization, the interactome was analyzed revealing new potential interacting proteins and additional functions of TTC30 paralogues. For this comparative analysis of the paralogues TTC30A and B, endogenously FLAG-tagged HEK293T cells were generated using CRISPR/Cas9. Preceding the analysis of TTC30A and B complexes, we aimed at verifying successful, paralogue-specific tagging [8]. DNA of these cells was extracted, amplified and sent in for Sanger sequencing. Unfortunately, results were always inconclusive. Consequently, mass spectrometry was used to validate specifically FLAG-tagged TTC30A and TTC30B HEK293T cells. Six biological replicates of both conditions were prepared for cell lysis, immunoprecipitation, protein digest, purification and MS analysis. Received MS/MS data sets were analyzed with MaxQuant. For peptide identification an enhanced SwissProt database was used. TTC30A and TTC30B peptide sequences were extended by the FLAG-tag amino acid (aa) sequence (DYKDDDDK) on the N-terminus after starting codon (ATG; M) in 5'-3' direction. The identified peptides were then filtered with Perseus. Peptides only identified by site, reversed peptide sequences, or potential contaminants were removed and only peptides detected in at least four out of six replicates were used for statistical analysis [8].

Comparative mass spectrometry revealed several peptides with an equal distribution in both samples (Figure 23) [8]. These protein fragments were assigned to both paralogues and were therefore not suitable for differentiation (22 peptides). However, specific peptides could be detected in either A (14 unique peptides) or B samples (11 unique peptides). The peptides unique for one or the other paralogue were significantly enriched in the corresponding samples (*t*-test, permutation-based FDR < 0.05, significance A, Benjamini–Hochberg FDR < 0.05; Appendix 5) [8]. These results demonstrate the successful and specific insertion of the FLAG-tag at the endogenous level for both paralogues, enabling a paralogue-specific interactome study (Figure 23) [8].

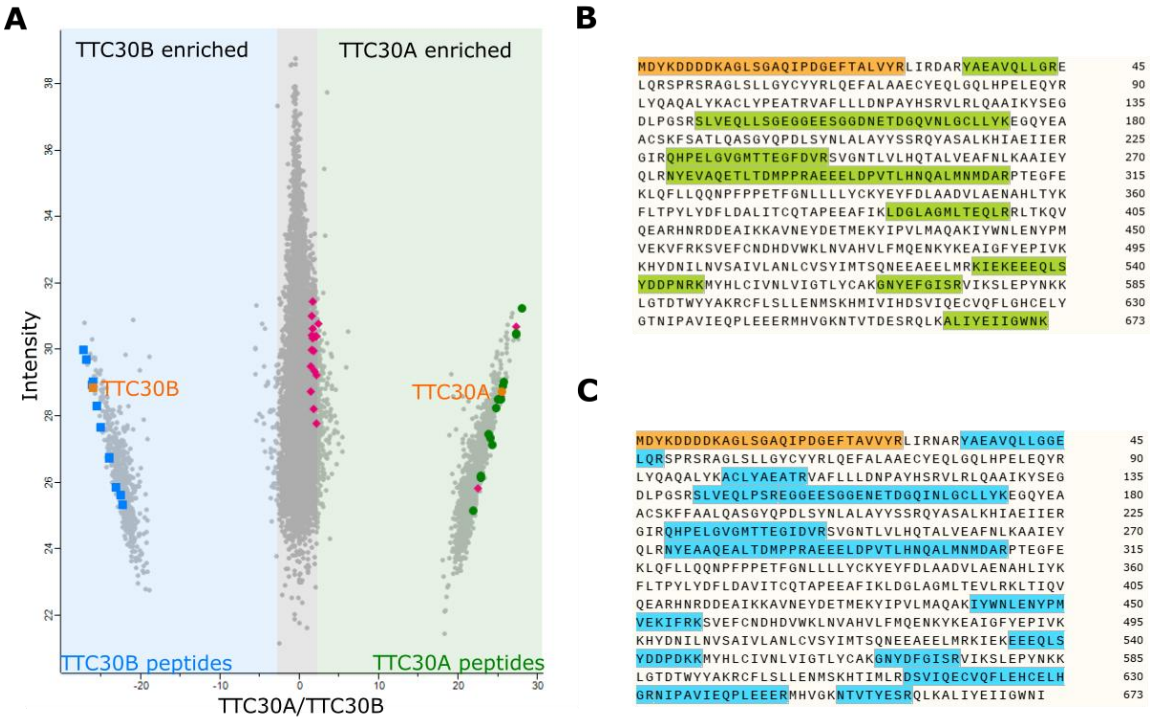

Figure 23 – Detection of unique TTC30A or TTC30B peptides by mass spectrometry analysis – The scatter plot (**A**) depicts the distribution of all peptides detected. The x-axis depicts the $\log_2$ ratios of identified peptides and the y-axis the $\log_2$ of their respective intensities. Peptides occurring with higher abundance in TTC30A samples can be found on the right (green), whereas peptides with higher abundance in TTC30B samples on the left (blue). Peptides, which are equally abundant, can be found in the middle (grey). Specific and significantly enriched unique peptides are marked in green (TTC30A) and blue (TTC30B), and FLAG-tagged peptides in orange. Non-significant TTC30 peptides are marked in magenta. The amino acid sequences illustrate the specifically detected fragments of TTC30A ((**B**); green) and TTC30B ((**C**); blue) along with their FLAG-tagged peptides (orange) and the corresponding position in the protein sequence. [8]

5.2.7. TTC30A and TTC30B immunoprecipitation on endogenous level reveal unknown and paralogue specific protein interactors

Immunoprecipitation and a subsequent protein complex analysis were conducted by utilizing the same endogenously FLAG-tagged TTC30A and TTC30B HEK293T cells as used for the peptide specific validation approach above [8]. A CRISPR/Cas9 empty vector treated and therefore untagged single clone was used as control. In total, six biological replicates for each condition were seeded. Cells were then lysed and an immunoprecipitation was performed. Protein digest, purification and MS analysis were followed by identification and quantification using MaxQuant as well as statistical analysis using Perseus [8]. The proteomics data were filtered to remove proteins only identified by site, reversed peptide sequences, or potential contaminants. Within the conditions, only proteins quantified in at least four out of six replicates were used for statistical analysis. An unpaired two-sample Student *t*-test

(permutation-based FDR < 0.05), to test result stability over the replicates, and an outlier test (significance A, Benjamini–Hochberg FDR < 0.05) were applied. Proteins meeting the significance criteria were considered as being significantly enriched [8]. For both TTC30A and B, all 16 IFT-B proteins were detected, proving the capability of each paralogue to bind to the IFT-B complex (**Figure 24**) [8].

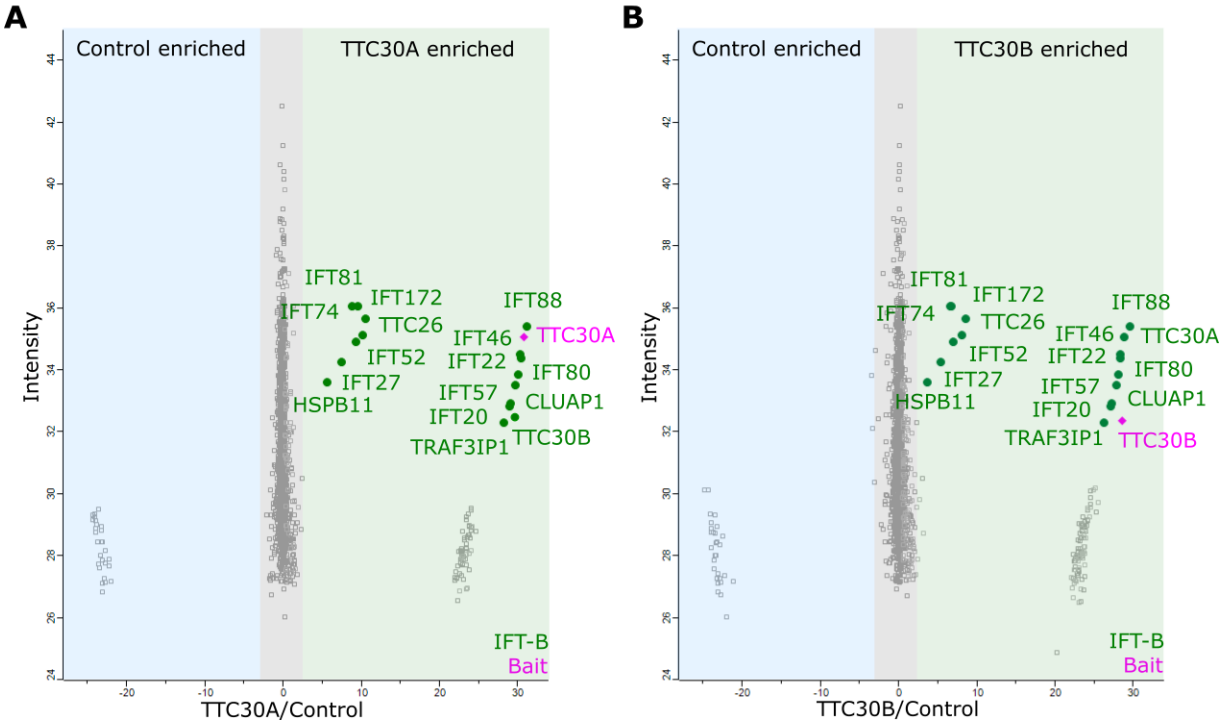

Figure 24 – Detection of IFT-B components for TTC30A/B by mass spectrometry analysis – The scatter plots show the distribution of all proteins identified for TTC30A (**A**) as well as TTC30B (**B**). The x-axis depicts the $\log_2$ ratios and the y-axis shows the $\log_2$ of their respective intensities. The bait proteins TTC30A and B are shown in magenta and IFT complex B proteins in green. Proteins showing an increased binding to TTC30A/B are on the right compared to the control on the left. [8]

Interestingly, mass spectrometry analysis did not only show the possibility to clearly distinguish between TTC30A and TTC30B, despite being almost identical, and the capability of each paralogue to bind the whole IFT-B complex. Beyond that, not yet known interacting proteins were identified (**Figure 25**) [8].

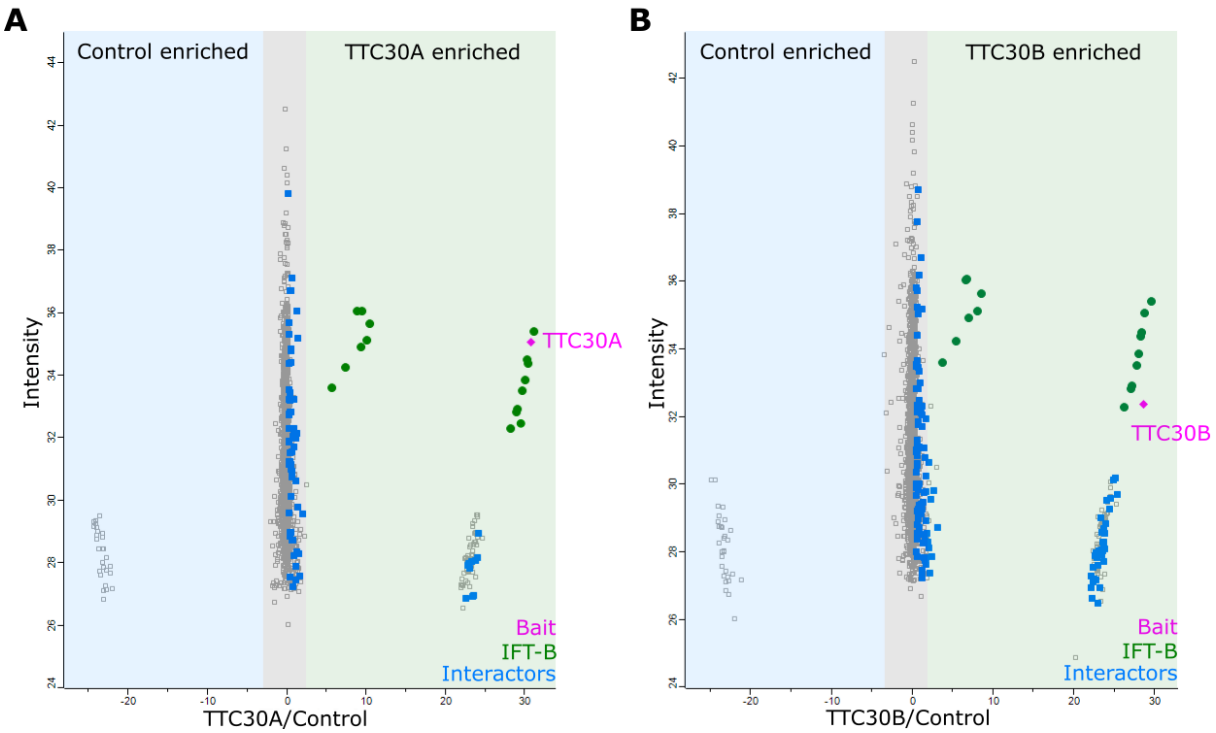

Figure 25 – Detection of new TTC30A/B potential protein interactors by mass spectrometry analysis – The scatter plots show the distribution of all proteins identified for TTC30A (**A**) as well as TTC30B (**B**) on endogenous level. The x-axis depicts the $\log_2$ ratios and the y-axis shows the $\log_2$ of their respective intensities. The bait proteins TTC30A and B are shown in magenta and IFT complex B proteins in green. Proteins showing an increased binding to TTC30A/B are on the right compared to the control on the left. Possible protein interactors are shown in blue and were significantly enriched when compared to the control (significance A < 0.05; permutation-based FDR < 0.05).

Besides IFT-B1 and IFT-B2, 71 proteins for TTC30A and 129 proteins for TTC30B were identified, with 24 being present in both datasets. However, 47 proteins only being detected with TTC30A (**Table 25**) and 105 proteins significantly enriched with TTC30B (**Table 26**) hint towards non-overlapping and specific molecular functions for each paralogue individually [8]. All interactors were sorted according to the cellular process, they are most likely involved in, with the GetGo enrichment analysis tool (**Appendix 6 and 7**) [26]. A subset of the most interesting so far unknown potential interactors for TTC30A and TTC30B is listed with their most likely relevant function in a ciliary background (**Table 27**).

Table 25 – Novel TTC30A interactors – An immunoprecipitation was performed with endogenously FLAG-tagged TTC30A HEK293T cells and Cas9 control cells. The table depicts the gene names of identified interactors with their -$\log_2$ median *p*-values of six biological replicates. IFT-B1 (green) and IFT-B2 (blue) complex proteins as well as novel protein interactors (white) are listed according to their *p*-value. Some of the most interesting proteins are highlighted (red). All proteins shown were significantly enriched when compared to Cas9 control (significance A < 0.05; permutation-based FDR < 0.05).

Genes	TTC30A
IFT88	37,01
TTC30B	24,05
TTC30A Bait	12,55
IFT22	12,42
IFT46	6,66
TTC26	5,20
IFT52	4,66
IFT81	4,60
IFT74	4,35
IFT27	3,78
HSPB11	3,71
IFT20	38,18
TRAF3IP1	37,51
IFT57	12,14
CLUAP1	11,67
IFT80	9,56
IFT172	5,74

Genes	TTC30A
LIAT1	10,02
FLNA	8,18
ODR4	7,53
MCM3	7,48
MCM5	5,71
IGF2BP3	5,36
FTSJ3	5,32
SKA1	5,06
LTBP1	4,61
RNF219	4,27
MCM6	4,15
CRKL	4,08
SF3A2	4,03
PRKACA	3,98
BOLA2	3,98
TAF4	3,94
CUL4B	3,91
EIF2AK3	3,50
MCM4	3,45
SNAP29	3,35
MCM7	3,16
SF3A3	3,11
PTBP2	2,90
SNRPD3	2,89
CXorf57	2,88
ZC3HAV1L	2,47
SNRPB2	2,40
CEP350	2,38
PTPN1	2,31
AAMDC	2,22
RAD50	2,17
SNRPA1	2,16
RBM10	2,15
LLGL1	2,12
FOXRED2	2,01
GLOD4	1,99

Genes	TTC30A
SUN2	1,97
PHF6	1,97
LRCH2	1,96
SUB1	1,93
RNASEH2A	1,92
RADIL	1,91
EEF1A2	1,91
HSPA6	1,86
PPM1A	1,86
LIN28B	1,85
NUDT19	1,79
NUP88	1,73
ZNF639	1,72
CCDC88A	1,70
MTPN	1,70
MYCBP	1,69
FLNC	1,67
MYO5B	1,62
WDR12	1,55
SART3	1,55
MRE11A	1,55
SRRM2	1,53
SF3B4	1,48
SYNE1	1,47
PYCR1	1,46
SF3B5	1,40
PWP1	1,38
NIPSNAP1	1,35
ARL6IP4	1,35
MCM2	1,33
SLC4A1AP	1,32
ZNF638	1,31
CDC40	1,31
APOBEC3C	1,31
MBD3	1,31

Table 26 – Novel TTC30B interactors – An immunoprecipitation was performed with endogenously FLAG-tagged TTC30B HEK293T cells and Cas9 control cells. The table depicts the gene names of identified interactors with their -$\log_2$ median *p*-values of six biological replicates. IFT-B1 (green) and IFT-B2 (blue) complex proteins as well as novel protein interactors (white) are listed according to their *p*-value. Some of the most interesting proteins are highlighted (red). All proteins shown were significantly enriched when compared to Cas9 control (significance A < 0.05; permutation-based FDR < 0.05).

Genes	TTC30B
IFT88	35,33
TTC30B Bait	33,18
TTC30A	11,93
IFT22	11,76
IFT46	6,09
TTC26	4,57
IFT52	3,89
IFT81	3,83
IFT74	3,70
HSPB11	3,19
IFT27	3,16
IFT20	45,48
TRAF3IP1	39,80
IFT57	11,55
CLUAP1	11,07
IFT80	8,92
IFT172	4,66

Genes	TTC30B
MCM3	10,42
MCM5	10,16
CAMSAP3	7,71
SNRPD3	7,61
MRPS17	7,49
DHX30	7,30
PRPF31	6,93
MRPS23	6,83
IGF2BP3	6,60
LARP1	6,58
MCM6	6,54
MRPS25	6,06
MCM2	5,99
GAR1	5,95
MCM4	5,52
TRIM28	5,34
PWP1	5,26
U2SURP	5,07
SRRM2	4,85
MCM7	4,75
PSPC1	4,75
HIST1H4A	4,61
CHERP	4,56
ARHGEF10	4,55
USP39	4,51
PURA	4,38
RBM17	3,93
MRTO4	3,82
CXorf57	3,79
SF3B4	3,33
OGT	3,31
CT45A10	3,29
APOBEC3C	3,06
VWA8	3,05
PHRF1	3,04
FOXRED2	3,00
PROSER1	2,98
SKI	2,91

Genes	TTC30B
NUP210	2,07
TXNDC16	2,04
PHF6	2,03
MTMR14	2,01
ZC3H14	2,00
SRSF6	1,97
MRPS9	1,97
AHNAK	1,96
PTCD3	1,95
SNRPC	1,94
CAPN1	1,94
BOP1	1,94
MPHOSPH6	1,91
TXNDC12	1,90
MYO5B	1,89
CDC40	1,88
PTRH2	1,87
CSNK2A1	1,86
SDCBP	1,85
UBA52	1,84
HSPA6	1,84
CROCC	1,80
DDX42	1,80
SETMAR	1,80
NUP85	1,79
CORO2A	1,78
NOL6	1,77
ASNA1	1,75
PPP1R14B	1,73
NUP88	1,73
HSPB1	1,73
ATP2B1	1,72
UBE2V1	1,72
MRPS2	1,71
GRB2	1,70
FAM98B	1,70
NUP62	1,68
NUP50	1,68

RDX	2,90	APEH	1,68
DGCR8	2,88	KEAP1	1,67
PPAN	2,87	NUP214	1,64
EEF1A2	2,83	HIST2H3A	1,64
ZNF638	2,80	ZFR	1,63
TET2	2,66	TET1	1,63
SPIN2B	2,54	MRPS5	1,61
NAT10	2,49	NAA10	1,61
HP1BP3	2,48	H1FX	1,60
PURB	2,46	WDR12	1,60
ZC3H13	2,46	NDFIP1	1,59
PES1	2,45	FASTKD2	1,58
UBL5	2,43	PIN1	1,57
ERAL1	2,42	RADIL	1,57
GRHPR	2,37	AKAP8	1,56
COPS8	2,31	MRPS26	1,55
DDX18	2,30	PCK2	1,55
SMCHD1	2,30	DKC1	1,55
FARP2	2,25	ZBED5	1,49
PTBP2	2,25	FEN1	1,44
CLPP	2,23	PRMT1	1,44
STAT1	2,23	OS9	1,39
MRPS12	2,22	TBL3	1,38
DDX27	2,21	RRP7A	1,37
UBE2O	2,16	AGPS	1,34
FMR1	2,15	SNX2	1,33
GTPBP10	2,10		

Table 27 – Most relevant TTC30A/B interactors and their function in ciliary context – The tables depict a subset of the most relevant interactors found after specific TTC30A/B interactome analysis. The possible interactors of TTC30A (left) and TTC30B (right) are listed along with their function in cilia.

TTC30A Interactor	Function
ODR4	GPCR trafficking
PRKACA	Sonic hedgehog signaling
SNAP29	cilium biogenesis and degradation
CEP350	mediating ciliation
SUN2	centrosome localization
CCDC88A	AKT-mTOR signaling, ciliogenesis and cilium morphology
SYNE1	centrosome migration

TTC30B Interactor	Function
CAMSAP3	microtubule organization, BB positioning
SKI	TGF-β signaling, Wnt signaling
RDX	actin binding to the plasma membrane, linked to hearing loss
STAT1	JAK-STAT signaling
CSNK2A1	Wnt signaling
CROCC	Centrosome cohesion, cilia stability, ciliary rootlet component
OS9	Hh ligand biogenesis

5.2.8. TTC30A and TTC30B redundancy protects IFT complex B integrity

To better understand the strong phenotype observed in double KO compared to single KO cells, the IFT-B complex composition was analyzed in TTC30B single and TTC30A and TTC30B double KO HEK293T cells [8]. Successful CRISPR/Cas9-based KO generation was validated by Sanger sequencing (**Appendix 8**). For the purification of the IFT-B complex Lebercilin was used as bait. Lebercilin is known to interact with IFT-B as well as IFT-A complex proteins without being an integral part of the complex [8, 80, 118].

For affinity purification, Strep/FLAG-tag-containing constructs for LCA5 and RAF1 as control were transiently transfected and therefore expressed in TTC30B single, TTC30A/B double KO and Cas9 empty HEK293T control cells [8, 108]. Strep-based affinity purification was followed by quantitative mass spectrometry. The results of four biological replicates were filtered for a minimum of three valid values. Significantly enriched proteins comparing LCA5 to RAF1 control in each cell line (significance B < 0.05, paired *t*-test, permutation-based FDR corrected < 0.05) were considered as specific interactors [8]. These were comparatively analyzed in KO versus Cas9 control cells (**Table 28**). As expected, TTC30B was not detected in TTC30A/B and

TTC30B KO cells, but significantly enriched in Cas9 control cells with LCA5. TTC30A was highly enriched in TTC30B KO and Cas9 control cells. In TTC30A/B KO cells, a signal comparable to RAF1 with LCA5 was seen, which is most likely due to carry-over during sample preparation or mass spectrometry measurement [8].

With Lebercilin as bait, a significant decrease in IFT-B1 complex binding was observed when comparing protein–protein interactions detected in double KO and Cas9 control cells, while IFT-B2 was mostly stable and showed no loss in binding [8]. This might indicate instability in the link of IFT-B1-B2 due to the loss of TTC30. Interestingly, no change was detected in TTC30B single KO cells, which is in line with the fact that a single KO is not sufficient to impede ciliogenesis completely [8].

Table 28 – IFT-B1 protein binding was impaired in TTC30A/B double KO cells – Strep-based affinity purification of overexpressed LCA5 or RAF1 as control was performed in TTC30A/B KO, TTC30B KO and Cas9 control cells, respectively. Here, the calculated ratios of the $\log_2$ median values of four biological replicates for all 16 IFT-B proteins and LCA5 (red) are shown. All proteins shown were significantly enriched when compared to RAF1 except HSPB11 and TTC26, which did not pass the *t*-test, but are included for completeness (significance B < 0.05, permutation-based FDR < 0.05). IFT-B1 proteins are depicted in green and IFT-B2 proteins in blue. Values ranging between -1 and -30 are highlighted in red. Modified after [8]

Bait	LCA5		RAF1			LCA5		
Genes	TTC30A/B KO vs. Control	TTC30B KO vs. Control	TTC30A/B KO	TTC30B KO	Cas control	TTC30A/B KO	TTC30B KO	Cas control
TTC30B	-28.42	-28.42	0.00	0.00	0.00	0.00	0.00	28.42
TTC30A	-10.88	0.42	0.00	0.00	22.36	19.87	31.17	30.75
IFT52	-1.13	0.32	0.00	0.00	20.46	29.69	31.14	30.82
IFT46	-1.04	0.45	21.56	21.85	23.18	29.37	30.87	30.42
IFT81	-1.44	0.14	20.64	23.03	22.58	30.79	32.37	32.24
IFT74	-1.32	0.14	24.04	24.01	24.30	30.86	32.32	32.18
IFT88	-1.27	0.57	19.93	0.00	23.55	30.16	32.00	31.43
TTC26	-1.24	0.21	23.99	23.94	24.05	29.66	31.12	30.91
IFT27	-1.03	0.17	25.32	25.19	25.27	29.51	30.71	30.54
IFT22	-1.02	0.26	0.00	23.17	22.89	29.69	30.97	30.71
HSPB11	-0.94	0.26	24.00	23.97	24.24	28.20	29.40	29.13
TRAF3IP1	-0.34	0.88	23.45	22.69	21.40	29.91	31.13	30.24
CLUAP1	-0.33	0.43	0.00	0.00	18.33	31.27	32.03	31.60
IFT57	-0.27	0.46	21.63	21.16	20.58	31.54	32.27	31.81
IFT80	-0.20	0.53	18.97	0.00	0.00	31.96	32.70	32.16
IFT172	-0.18	0.46	24.82	24.41	24.62	34.01	34.64	34.18
IFT20	-0.06	0.60	0.00	0.00	0.00	30.93	31.60	31.00
LCA5	0.47	0.42	24.86	24.98	24.46	37.55	37.50	37.08

5.2.9. TTC30B knockout has no effect on novel protein interactor CROCC

One of the most prominent potential and so far unknown TTC30B interactor investigated was Rootletin (ciliary rootlet coiled-coil; CROCC; **Table 26 and 27**), an important component of the ciliary rootlet, required for centrosome cohesion and cilia stability [119-121]. Therefore, an immunofluorescence staining was conducted with ARL13B for cilia and CROCC for rootlet staining. In the TTC30A/B single and double KO the signal intensity of Rootletin was comparable to the control (**Figure 26**). This suggests that CROCC is an upstream interactor, which is not influenced by TTC30. This result matches to the previous finding of unaffected basal body and leads to the conclusion that TTC30A and B do not affect the ciliary rootlet.

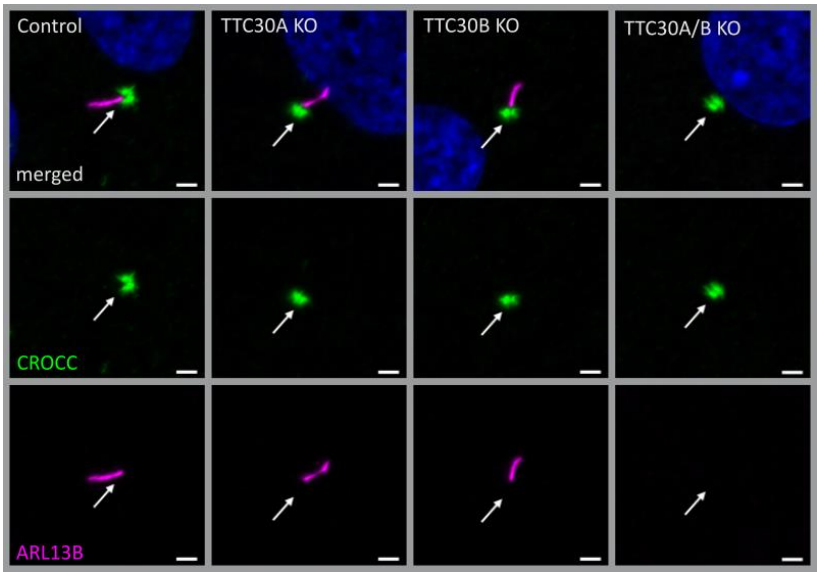

Figure 26 – Localization of Rootletin in TTC30A/B wildtype and knockout cells – Fluorescent light microscopy pictures of hTERT-RPE1 control, TTC30A, TTC30B and TTC30A/B double KO cells (from left to right) are shown. The cells were stained for Rootletin (CROCC; green), ARL13B (magenta), DNA is marked in dark blue and co-localization shown in white. The scale bar measures 2 µm. [8]

5.2.10. PKA mediated down regulation of Sonic hedgehog signaling pathway is dependent on TTC30A

Another potential and most promising TTC30A protein interactor investigated was the protein kinase A catalytic subunit α (PRKACA; **Table 25 and 27**). PKA is a cAMP-dependent protein kinase A and has several functions in glycogen, sugar and lipid metabolism [122]. Moreover, this kinase is part of the cilia specific Sonic hedgehog signaling pathway (Shh) [90, 94, 100]. To investigate TTC30 related function hTERT-RPE1 Cas9 control, TTC30A KO and TTC30B KO cells were treated with DMSO or Forskolin (5 µM). Forskolin inhibits Shh pathway by increasing

ciliary cAMP level and subsequently the level of phosphorylated PKA (pPKA) resulting in increased phosphorylation of PKA substrates [123]. Forskolin is dissolved in DMSO and therefore DMSO treatment was a necessary control because of its possible cell toxic effects.

After cell lysis of TTC30A/B single KO and Cas9 empty control hTERT-RPE1 cells, SDS-PAGE and western blot were performed to visualize differences of protein level in non-phosphorylated PKA catalytic subunits and of phosphorylated PKA substrate. The applied antibody against PKAcat targeted all three different subunits α, β and γ. The phospho-site specific antibody targeted PKA substrates containing a phospho-Ser/Thr residue with arginine at the -3 and -2 positions [124]. Acetylated tubulin was used as loading control since it was not influenced by TTC30 KO (Figure 14) and because the mass of GAPDH (37 kDa) was too close to PKAcat (40 kDa). Protein level of non-phosporylated PKAcat were comparable in all samples. Strikingly, in Forskolin treated TTC30A KO cells the signal intensity of phosphorylated PKA substrates was stronger compared to control and TTC30B KO cells. The signals of control and TTC30B KO cells were comparable (Figure 27).

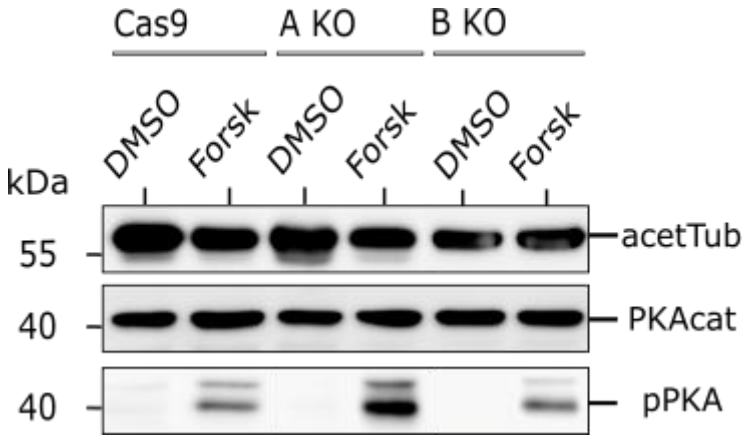

Figure 27 – Protein level of PKAcat and pPKA substrates in Forskolin treated TTC30A/B control and knockout cells – The protein level of PKA catalytic subunit phosphorylated PKA and acetylated tubulin as loading control were checked by western blot. hTERT-RPE1 control and TTC30A/B single knockout cells were treated with DMSO or Forskolin (Forsk; 5 µM) prior to cell lysis.

This result clearly showed the activating effect of Forskolin on protein kinase A. But more importantly it demonstrated that the specific interaction of TTC30A with PRKACA is necessary for physiological Shh activation. Whereas a loss of interaction leads to enhanced Shh inhibition. In TTC30B KO cells, where only TTC30A was still expressed, Forskolin had no effect on the phosphorylation of PKA substrates and most likely no effect on Shh signaling. Mass spectrometry data suggested that TTC30A and TTC30B have, despite being paralogues,

additional unique interactors and are involved in further ciliary functions which is exemplified here for PRKACA.

5.2.11. TTC30A knockout inhibits Sonic hedgehog signaling pathway

Based on the interactome analysis and the western blot results Sonic hedgehog signaling was affected in TTC30A knockout cells. Additionally, in previous studies in a chinese pedigree a rare missense mutation in TTC30B was discovered and this A375V point mutation could already be linked to Shh signaling [33].

Smoothened (Smo) is an early-stage key element of Shh signaling pathway. Upon activation of Shh pathway, Smo enters the cilium to trigger downstream effectors which ultimately exit the cilium and activate target genes in the nucleus regulating cellular and cilia related processes [93, 97]. Hence, TTC30A or TTC30B single KO, TTC30A/B double KO as well as control hTERT-RPE1 cell lines were transiently transfected with a GFP-labeled Smo expression vector. Transient transfection was followed by antibiotic treatment and selection for stably transfected cells. Using fluorescence microscopy, Smo-GFP was observed to localize to the cilium in control and TTC30B KO cells, co-stained with ARL13B. However, this localization was not detected in TTC30A single knockout and in TTC30A/B double knockout cells. The lost Smo-GFP localization in TTC30A single KO cells and TTC30A/B double KO cells was restored by transiently transfecting TTC30A wildtype DNA. Smo-GFP was then again localizing to the cilium. To investigate TTC30 mutation A375V, site directed mutagenesis was used to insert the mutation into Strep/FLAG-tag TTC30A or B wildtype overexpression constructs, respectively. The rescue seen with wildtype construct could not be achieved by transfecting mutated TTC30A (A375V) expression vector into TTC30A/B double knockout cells (Figure 28).

Furthermore, the rescue of TTC30A/B double KO cells with TTC30A/B wildtype and A375V constructs was repeated under treatment with Smoothened agonist (SAG). SAG initiates the activation of the Shh pathway and subsequently more Smo-GFP should accumulate at the cilium [125]. The results show the increased intensity of Smo-GFP in SAG treated control cells to non-treated cells. This increase was also visible in rescue TTC30B wt or mutant cells and in rescue TTC30A wt cells. Strikingly, in Smo-GFP stable TTC30A/B double KO cells transfected

with mutated TTC30A rescue construct and treated with SAG no localization of Smo to the cilium was visible (Figure 28).

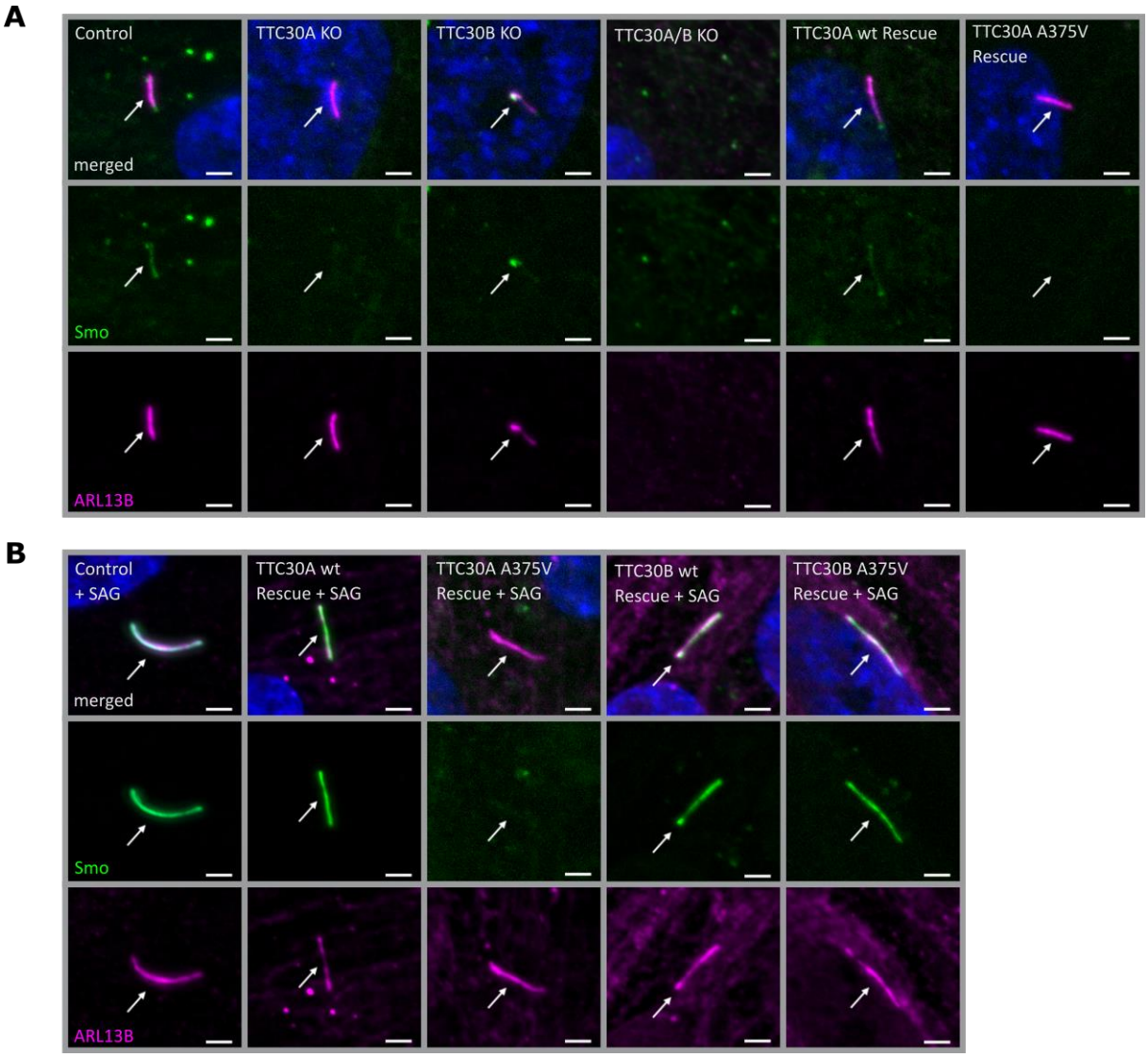

Figure 28 – Localization of Smoothened in TTC30A/B wildtype, knockout and rescue cells with or without Sonic hedgehog activation – Fluorescent light microscopy images of hTERT-RPE1 control, TTC30A, TTC30B, TTC30A/B double KO cells, TTC30A wt and TTC30A A375V rescue cells (from left to right) are shown (**A**). Additionally, hTERT-RPE1 control, TTC30A wt, TTC30A A375V, TTC30B wt and TTC30B A375V rescue cells are depicted (**B**), which were treated with SAG. The cells were stained for ARL13B (magenta), smoothened (Smo; green), DNA is marked in dark blue and co-localization shown in white. The scale bar measures 2 µm.

This finding verified the previous result, that TTC30A is indeed involved in Shh pathway (Figure 27). The loss of Smo localizing to the cilium could only be rescued by transfection of TTC30A wt DNA. Transfection with TTC30A A375V or SAG mediated activation of Shh pathway did not recover this severe phenotype. Furthermore, the discovered mutation by Du *et al.* introduced in TTC30A could be directly linked to a loss of ciliary accumulation of Smo. But the

same A375V point mutation introduced in TTC30B rescue construct did not show this phenotype.

Thus, indicating again that TTC30A and TTC30B have not only a common task ensuring intraflagellar transport but also have specific protein interactions and respective functions. While TTC30B shows several interactions with transmembrane proteins [26], TTC30A clearly seems to be involved in Shh signaling.

5.2.12. TTC30A KO mediated downregulation of Sonic hedgehog is independent of Patched1

The initial step of Shh signaling, Hh ligand binds Patched1 (Ptch1), which then exits the cilium. Subsequently, Ptch1 relieves its inhibition of Smo, which then in return enters the cilium and can affect downstream targets [88]. Hence, the observed strong phenotype in TT30A KO cells, Smo not migrating to the cilium, could be a result of Ptch1 not leaving the cilium and therefore still inhibiting Smo.

To investigate an influence of TTC30A/B on Ptch1, TTC30A or TTC30B single KO as well as Cas9 control hTERT-RPE1 cell lines were transiently transfected with a YFP-labeled Ptch1 expression vector. Transient transfection was followed by antibiotic treatment and selection for stably transfected cells. In IF experiments, Ptch1-YFP could be observed to localize to the cilium in control and TTC30A/B KO cells co-stained with ARL13B. This localization was not detected in TTC30A/B single knockout and control cells upon Shh activation with SAG (**Figure 29**) [125].

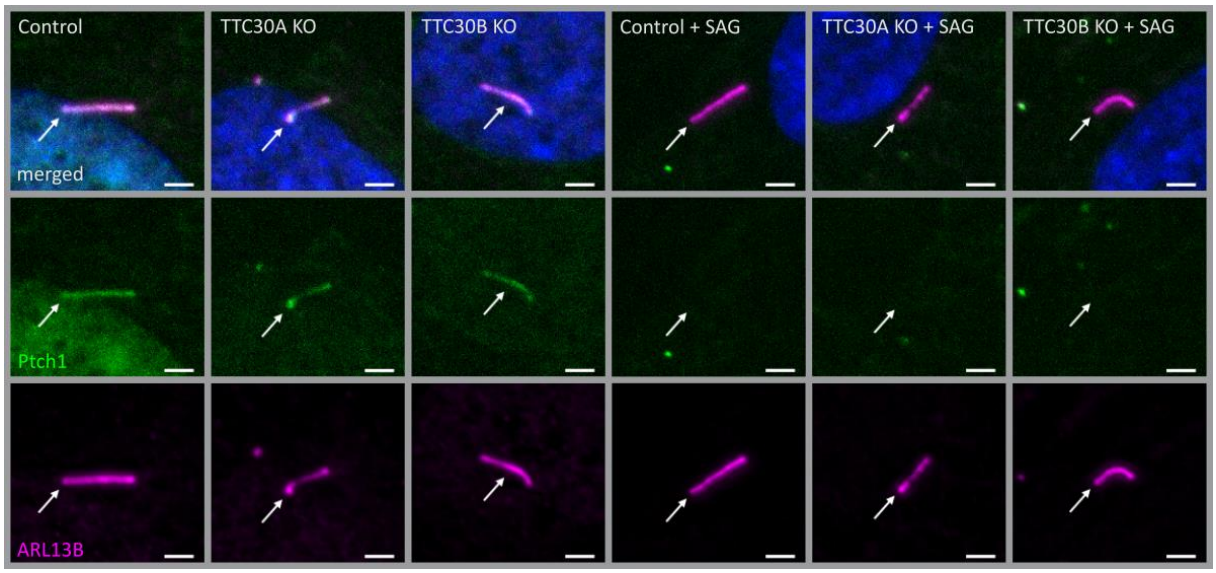

Figure 29 – Localization of Patched1 in TTC30A/B wildtype and knockout with or without Sonic hedgehog activation – Fluorescent light microscopy images of hTERT-RPE1 control, TTC30A, TTC30B, (from left to right) are shown. Cells were either not treated (**left**) or treated with SAG (**right**). The cells were stained for ARL13B (magenta), Patched1 (Ptch1; green), DNA is marked in dark blue and co-localization shown in white. The scale bar measures 2 µm.

In Shh off-state Ptch1 was localizing to the cilium in all cell lines and upon SAG mediated activation Ptch1 exited the cilium. This result determines that Ptch1 is not affected by TTC30A/B and that the inhibition of Smo entering the cilium in TTC30A KO cells is independent of Ptch1.

5.2.13. TTC30A mutation A375V leads to decreased IFT57 interaction

To determine the influence of TTC30 A375V mutation on protein interactions a comparative mass spectrometry analysis was performed. Therefore, HEK293T control cells were transiently transfected with an overexpression vector containing a Strep/FLAG-tag and either TTC30A/B wildtype sequence as control or the mutated A375V variant [33, 108].

First, cells were lysed, followed by a Strep/FLAG-tag-based affinity purification. After protein digest and purification, quantitative mass spectrometry was performed [108]. MaxQuant software was used for identification and quantification of proteins. Statistical analysis was done with Perseus. All identified proteins were filtered removing proteins only identified by site, reversed peptide sequences, or potential contaminants. The results of six biological replicates were filtered for a minimum of four valid values [8]. Intensities of possible protein interactors for mutated TTC30A/B were compared to wildtype TTC30A/B and considered as

specific interactors when they were Student's *t*-test (permutation-based FDR < 0.05) and significance A positive (Benjamini–Hochberg FDR < 0.05) (**Figure 30**). Proteins with significantly increased abundancy in cells transiently transfected with wildtype TTC30A/B, respectively significantly decreased abundancy in cells transiently transfected with mutated TTC30A/B were considered as partner with decreased interaction.

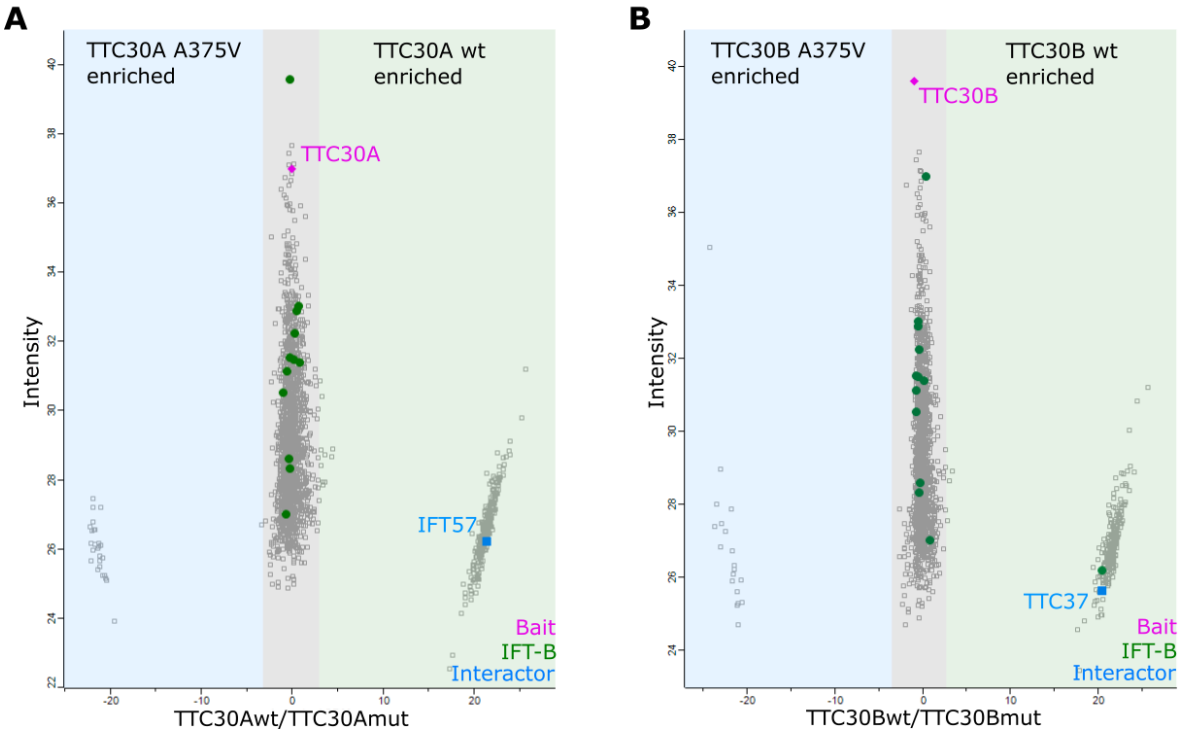

Figure 30 – Detection of decreased protein interaction in mutated TTC30A/B by mass spectrometry analysis – The scatter plots show the distribution of all proteins identified for TTC30A (**A**) as well as TTC30B (**B**). The x-axis depicts the $\log_2$ ratios and the y-axis shows the $\log_2$ of their respective intensities. The bait proteins TTC30A and B are shown in magenta and IFT complex B proteins in green. Proteins showing an increased binding to TTC30A/B wt are on the right compared to TTC30A/B A375V on the left. Possible protein interactors that were significantly enriched for either TTC30A/B wt or TTC30 A375V (significance A < 0.05; permutation-based FDR < 0.05) are shown in blue.

The results showed that the most intense signal with comparable abundance in TTC30A/B wt and TTC30A/B A375V cell lines were the bait proteins, TTC30A and TTC30B. This was expected and proved that experimental setup and outcome were valid. Furthermore, IFT-B complex components were also equally abundant in wt TTC30B and mutant TTC30B cells. Regarding wt TTC30A and mutated TTC30A cells, most of IFT-B component signals were also comparable to each other. Surprisingly, the signal of IFT57, part of the IFT-B2 subcomplex, was significantly decreased in TTC30A A375V cells. Therefore, this interaction was most likely impaired. In total, 129 protein showed reduced interaction due to A375V missense mutation, 83 proteins

in cells transfected with mutant TTC30A (Table 29) and 46 proteins in cells transfected with mutant TTC30B (Table 30).

Table 29 – Decreased TTC30A protein interactions due to A375V mutation – An immunoprecipitation was performed with Cas9 control cells transiently transfected with either FLAG-tagged TTC30A wt or FLAG-tagged TTC30A A375V. The table depicts the gene names of identified interactors, and TTC30A and TTC30B as reference, with their -$\log_2$ median *p*-values of six biological replicates. Identified protein interactors (white) are listed according to their *p*-value. Some of the most interesting proteins are highlighted (red). All proteins shown were significantly enriched in TTC30A A375V when compared to TTC30A wt (significance A < 0.05, permutation-based FDR < 0.05) and therefore respective interactions are considered reduced.

Genes	TTC30Awt vs TTC30A A375V
TTC30A	0,28
TTC30B	0,04
PAWR	16,69
RAP1GDS1	16,26
ADAR	13,99
RNPS1	3,57
TMX2	3,57
AASDHPPT	3,57
SMAP	3,57
EXOSC3	3,57
MYO1B	3,57
SPNS1	3,57
CNPY2	3,57
ABCD1	3,57
DNAJC9	3,57
RAB21	3,56
SLC35F6	3,56
ACO1	3,55
ATXN2	3,54
DENR	3,44
UBE2V1	2,48
NDUFB11	2,46
CTH	2,32
GINS4	2,32
DTD1	2,30
VPS11	2,30
NCAM1	2,30
THOC3	2,30
HIBCH	2,30
MRPL47	2,30
EPHX1	2,30

Genes	TTC30Awt vs TTC30A A375V
HSD17B11	2,30
TIGAR	2,30
PITRM1	2,30
RPS29	2,29
SMN1	2,29
UBA3	2,29
USMG5	2,29
FAHD2A	2,29
PSMG4	2,29
CCDC22	2,29
SCYL1	2,29
LRP1	2,29
ENSA	2,29
PPM1A	2,29
MMAB	2,29
RRAGC	2,24
ERP29	2,23
PDXDC1	2,18
GRWD1	2,17
GRB2	2,16
COTL1	2,07
CDC27	2,01
SRSF5	2,00
NUCB2	2,00
PPID	1,99
HEATR3	1,99
NIT2	1,98
NTMT1	1,97
SMU1	1,94
IFT57	1,92
RBX1	1,52
SV2A	1,43

PPP1R8	2,30	HMBS	1,38
RBM10	2,30	GEMIN6	1,37
NIFK	2,30	CFDP1	1,35
HNRNPLL	2,30	NOP56	1,34
ZNF638	2,30	STXBP3	1,33
ATG3	2,30	QRICH1	1,33
MRPS14	2,30	ACIN1	1,33
MEPCE	2,30	GMDS	1,32
DNPH1	2,30	MRTO4	1,32
PDXP	2,30	AKR7A2	1,31
HDGFRP2	2,30	ABI2	1,30

Table 30 – Decreased TTC30B protein interactions due to A375V mutation – An immunoprecipitation was performed with Cas9 control cells transiently transfected with either FLAG-tagged TTC30A wt or FLAG-tagged TTC30A A375V. The table depicts the gene names of identified interactors, and TTC30A and TTC30B as reference, with their -$\log_2$ median *p*-values of six biological replicates. Identified protein interactors (white) are listed according to their *p*-value. Some of the most interesting proteins are highlighted (red). All proteins shown were significantly enriched in TTC30A A375V when compared to TTC30A wt (significance A < 0.05, permutation-based FDR < 0.05) and therefore respective interactions are considered reduced.

Genes	TTC30Bwt vs TTC30B A375V	Genes	TTC30Bwt vs TTC30B A375V
TTC30A	0,10	NFS1	2,27
TTC30B	4,18E-05	GRSF1	2,25
		RNPS1	2,23
SBDS	19,45	OSBP	2,23
SMU1	17,03	ADAR	2,19
PDCD4	15,83	HMGN5	2,09
ACO1	14,72	NOP56	2,07
PITRM1	3,57	EIF2AK2	2,06
PPID	3,57	GEMIN4	2,04
SMAP	3,57	SART1	2,03
NIPSNAP1	3,57	GFM1	2,03
AKR1A1	3,56	L3HYPDH	2,02
FAM162A	3,47	NTMT1	2,01
NT5DC1	3,43	ERLIN2	2,00
NIT2	2,33	WBP11	1,37
YRDC	2,29	PDK2	1,35
MPP5	2,29	ZPR1	1,35
SNRNP40	2,29	PIN4	1,34
TTC37	2,29	CMTR1	1,34
SLC9A3R1	2,29	CFDP1	1,34
UBA3	2,29	IRF2BP2	1,34
DNPH1	2,29	NUCB2	1,32
DRG2	2,29	GINS4	1,31

INTS3	2,29	AKR7A2	1,31
RPS29	2,29		

5.2.14. IFT57 localization is unaffected by TTC30 mutation A375V

According to mass spectrometry data it was evaluated whether a reduced TTC30A-IFT57 interaction also affects the ciliary localization of IFT57. Therefore, control, TTC30A/B single knockout and TTC30A/B double knockout hTERT-RPE1 cells were stained for ARL13B and IFT57. Additionally, these antibodies were also used in TTC30A/B double KO cells transfected with either TTC30A/B wt or TTC30A/B A375V. These rescue cells were treated with G418 to generate and select for stably transfected cells. Interestingly, IFT57 localization was unaffected in all cell lines (**Figure 31**), except TTC30A/B double KO cell lines where again no cilia were assembled and IFT57 signal could not be distinguished from the background.

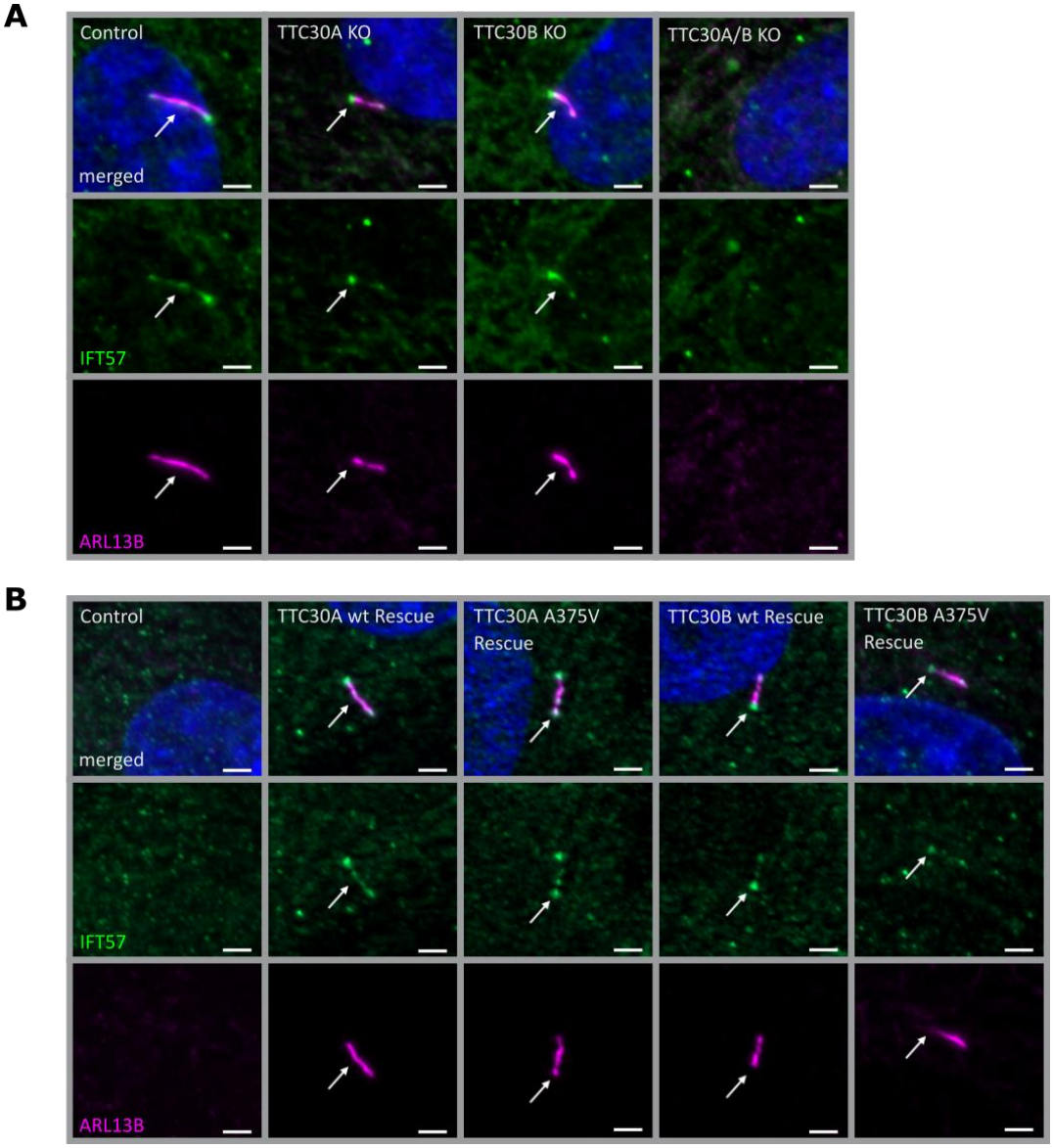

Figure 31 – Localization of IFT57 in TTC30A/B wildtype, knockout and rescue cells – Fluorescent light microscopy images of hTERT-RPE1 control, TTC30A, TTC30B, TTC30A/B double KO cells (from left to right) are shown (**A**). Additionally, hTERT-RPE1 control, TTC30A wt, TTC30A A375V, TTC30B wt and TTC30B A375V rescue cells are depicted (**B**). The cells were stained for ARL13B (magenta), IFT57 (green), DNA is marked in dark blue and co-localization shown in white. The scale bar measures 2 µm.

Nevertheless, IFT57 intensities were measured ($n_{TTC30AwtRescue}$ = 7; $n_{TTC30BwtRescue}$ = 5; $n_{TTC30AwtmutRescue}$ = 10; $n_{TTC30ABwtmutRescue}$ = 5) to determine if IFT57 intensity was reduced. The average intensity was 1.327 IU ± 0.164 IU (in TTC30A wt rescue cells) and 1.249 IU ± 0.113 IU (in TTC30B wt rescue cells). In TTC30A/B double KO cells rescued with mutant TTC30A or TTC30B, average intensity was 1.049 IU ± 0.049 IU (in TTC30A A375V rescue cells) and 0.989 IU ± 0.139 IU (in TTC30B A375V rescue cells). The IFT57 signal intensity in A375V rescue cells was not significantly decreased compared to wt rescue cells. (**Figure 32**).

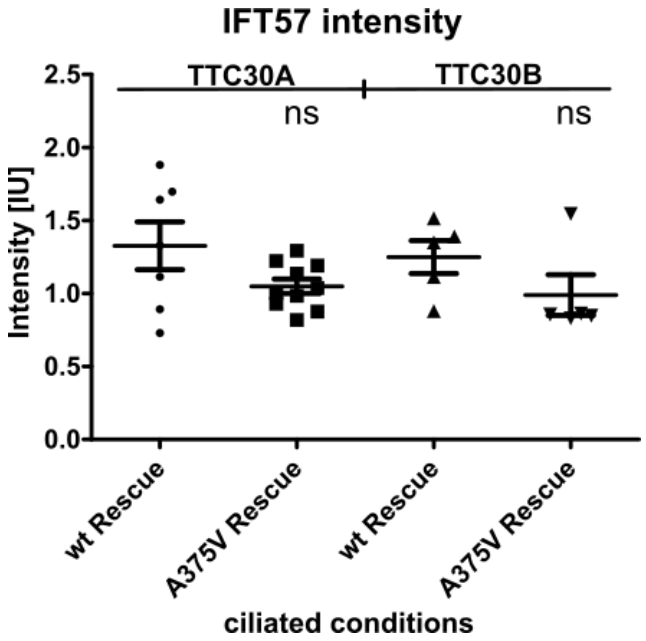

Figure 32 – IFT57 intensity measurements in TTC30A/B wildtype and mutated rescue cells – In TTC30A/B double KO wt and A375V rescue cells, IFT57 fluorescent intensity was measured. The resulting ratios of IFT88 (n = x) as well as IFT140 (n = 5) for TTC30A, TTC30AB and TTC30B KO cells were comparable to those of control cells. For statistical analysis, the mean was calculated. *p* values below 0.05 are represented by * and below 0.001 by ***. Error bars represent the s.e.m.

These results suggest that, even though there were significant changes in binding of IFT57, TTC30A/B KO or A375V mutation did not influence the expression or localization of IFT57.

5.3. Lebercilin

Leber congenital amaurosis (LCA) is a rare hereditary retinal dystrophy which leads to rapid photoreceptor degeneration [22, 23] and mutations in Leber congenital amaurosis 5 (*LCA5*, Lebercilin) gene accounts for about 1%-2% of LCA [23]. Protein network analysis revealed the strong interaction of Lebercilin and SSNA1 [26]. Both proteins were reported to be involved in ciliogenesis and intraflagellar transport [27, 28, 79, 80]. Therefore, the aim was to investigate Lebercilin and SSNA1 function and by that to uncover the nature of their interaction and the underlying mechanism of Leber congenital amaurosis.

5.3.1. Generation of LCA5 knockout cell lines

Initially, to investigate the function of LCA5, hTERT-RPE1 knockout cells were generated. Therefore, the CRISPR/Cas9 system was utilized. To create a viable and useful LCA5 KO, two different sites were picked as targets. For sgRNA design the CCTop tool was used. The first

target site is in exon 3, in the region of the start codon, and the second in exon 6. A successful LCA5 exon 6 KO might lead to a total loss of LCA5 or deletion of exon 7, 8 and 9 which sum up to 54.39 % of the total protein.

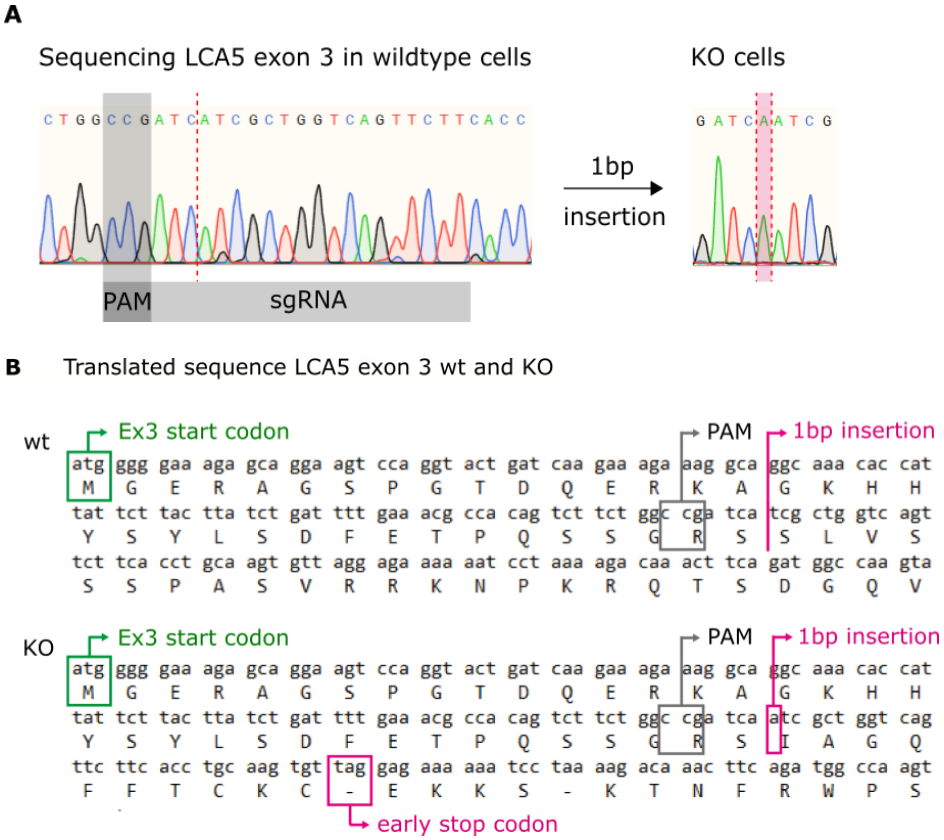

Figure 33 – Sequencing results for LCA5 wildtype and exon 3 knockout – (**A**) Shown is a fragment of hTERT-RPE1 wildtype LCA5 exon 3 gene along with PAM sequence (dark grey), sgRNA binding site (light grey) as well as inserted base pair (magenta). Sequencing results after CRISPR/Cas9-mediated KO generation depict a homozygous 1 bp insertion. (**B**) Translation of nucleotide sequence fragments in wt and KO cells reveals a frameshift caused by CRISPR/Cas9-mediated insertion that led to a premature stop codon.

The transfection of hTERT-RPE1 cells with sgRNAs targeting LCA5 exon 3 and exon 6 was followed by single clone selection and DNA extraction. Sanger sequencing revealed an insertion (exon 3) and a deletion (exon 6) followed by an open-reading frameshift and predicted early stop codon (**Figure 33 and 34**). Furthermore, sequencing verified the successful generation of homozygous LCA5 exon 3 and exon 6 knockouts.

CRISPR/Cas9 mediated LCA5 exon 3 KO generation in hTERT-RPE1 cells was successful (**Figure 33**). A PAM sequence 98 bp after the start codon of LCA5 exon 3 was identified and targeted, leading to a homozygous 1 bp insertion. The insertion caused an early stop codon 13 bp behind the sgRNA target region. This p.S37IfsX10 mutation in the following referred to as LCA5 exon 3 (ex3) KO resulted in a loss of 93,46 % of LCA5 protein. Predicted off-targets are

located in exonic, intronic or inter genomic regions, but with a minimal probability of binding (Appendix 9).

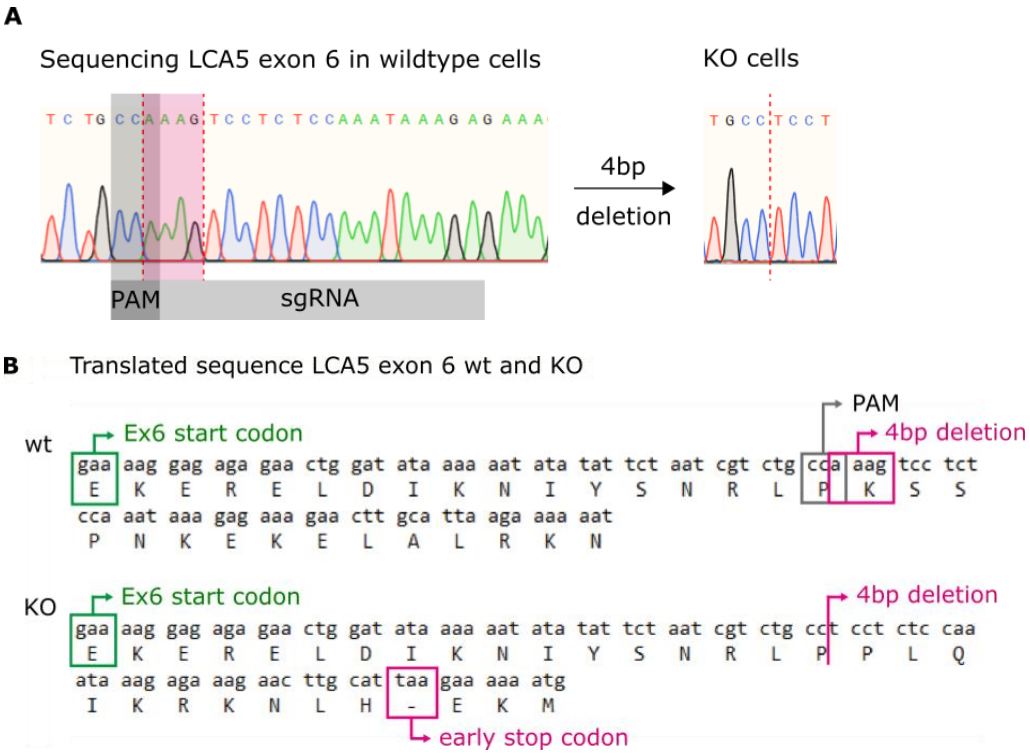

Figure 34 – Sequencing results for LCA5 wildtype and exon 6 knockout – (**A**) Shown is a fragment of hTERT-RPE1 wildtype LCA5 exon 6 gene along with PAM sequence (dark grey), sgRNA binding site (light grey) as well as deleted base pairs (magenta). Sequencing results after CRISPR/Cas9-mediated KO generation depict a homozygous 4 bp deletion. (**B**) Translation of nucleotide sequence fragments in wt and KO cells reveals a frameshift caused by CRISPR/Cas9-mediated deletion that led to a premature stop codon.

CRISPR/Cas9 mediated LCA5 exon 6 KO generation in hTERT-RPE1 cells was successful (**Figure 34**). A PAM sequence was targeted 45 bp after starting codon of LCA5 exon 6, leading to a homozygous 4 bp deletion. This deletion was leading to an early stop codon 14 bp after sgRNA target region. This p.K303PfsX10 mutation in the following referred to as LCA5 exon 6 (ex6) KO resulted in a loss of 54.97 % of LCA5 protein. Predicted off-targets are located in exonic, intronic or inter genomic regions, but with a minimal probability of binding (**Appendix 10**).

5.3.2. Verification of LCA5 knockout cell lines

To verify the CRISPR/Cas9 mediated LCA5 KO cell lines, cells were lysed and their total protein level was investigated by western blot. A clear reduction in LCA5 signal intensity can be seen in LCA5 ex3 and ex6 KO cells compared to control cells (**Figure 35**). GAPDH functioned as

loading control and was evenly distributed in all samples. Western blot data verified the successful generation of LCA5 exon 3/6 KO cells.

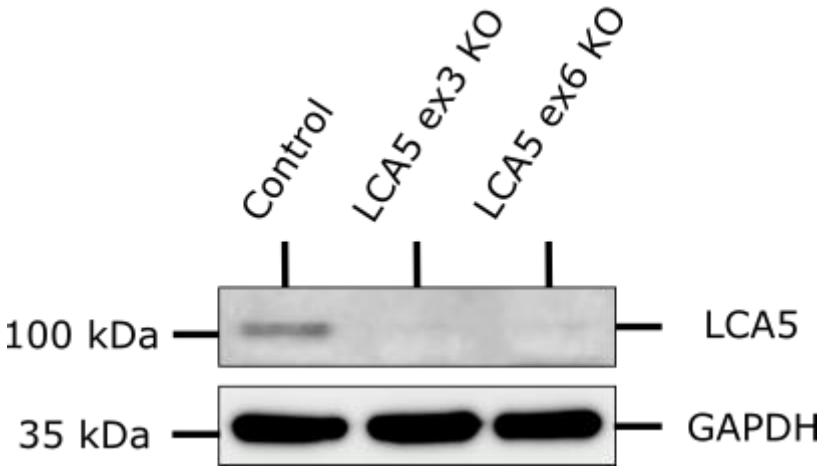

Figure 35 – Protein level of LCA5 in wildtype and exon 3/6 knockout cells – In hTERT-RPE1 control and LCA5 exon 3 and exon 6 knockout cells, protein level of LCA5 and GAPDH as loading control were checked by western blot.

Further, the phenotypical analysis of homozygous LCA5 ex3/ex6 KO cells using immunofluorescence microscopy was performed to verify differences in protein abundance of wildtype versus KO cell lines. RPE1 LCA5 control and LCA5 ex3/ex6 KO cells were stained for LCA5 and ARL13B. A clear loss of LCA5 signal intensity can be seen in both KO cells compared to control cells, confirming the successful KO generation (Figure 36).

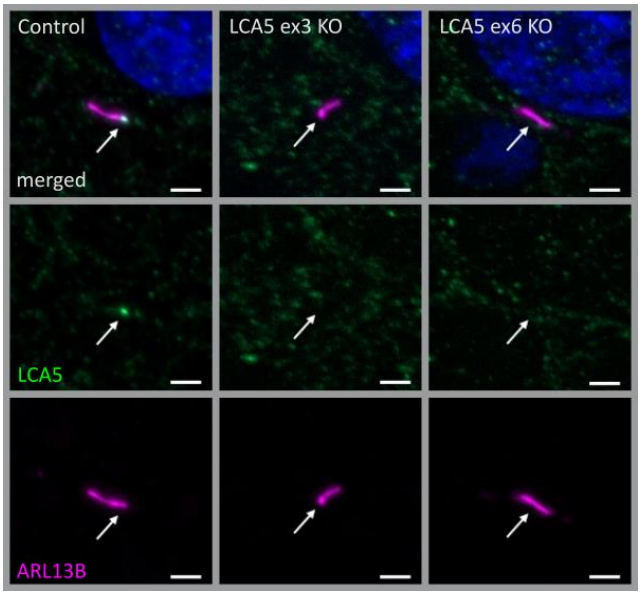

Figure 36 – LCA5 exon 3/6 knockout verification by immunofluorescence staining – Fluorescent light microscopy pictures of hTERT-RPE1 control, LCA5 ex3 and ex6 KO cells (from left to right) are shown. The cells were stained for ARL13B (magenta) and LCA5 (green), DNA is marked in dark blue and co-localization shown in white. The scale bar measures 2 µm.

Additionally, ciliary staining (ARL13B) allowed to observe if a LCA5 KO had an impact on ciliogenesis.

5.3.3. Loss of Lebercilin affects ciliogenesis

Cilia number and length were investigated using the ciliary protein ARL13B, which localizes to the ciliary membrane and can be used as a marker for these measurements (Figure 36) [8]. Interestingly, ciliary length in LCA5 ex3 and ex6 KO cell lines were mildly but significantly reduced compared to control cells. The number of cells harboring cilia was also mildly but significantly reduced (Figure 37). Averaged ciliary length in control cells was 3.547 µm ± 0.034 µm, in LCA5 ex3 KO cells 2.488 µm ± 0.030 µm and in LCA5 ex6 KO cells 2.363 µm ± 0.031 µm ($n_{control}$ = 594; $n_{LCA5ex3KO}$ = 443; $n_{LCA5ex6KO}$ = 384). On average, cilia in KO cells were approximately 1.1 µm (exon 3) respectively 1.2 µm (exon 6) shorter compared to control cells (LCA5 ex3 KO: 29.86 %; LCA5 ex6 KO: 33.32 % reduction). Regarding ciliation, on average 85.43 % ± 1.68 % of the wildtype cells were ciliated. In LCA5 KO cells 67.61 % ± 1.98 % (ex3 KO) and 71.90 % ± 2.37 % (ex6 KO) were ciliated. This was a reduction of 17.82 % (ex3 KO) and 13.53 % (ex6 KO) (Figure 37).

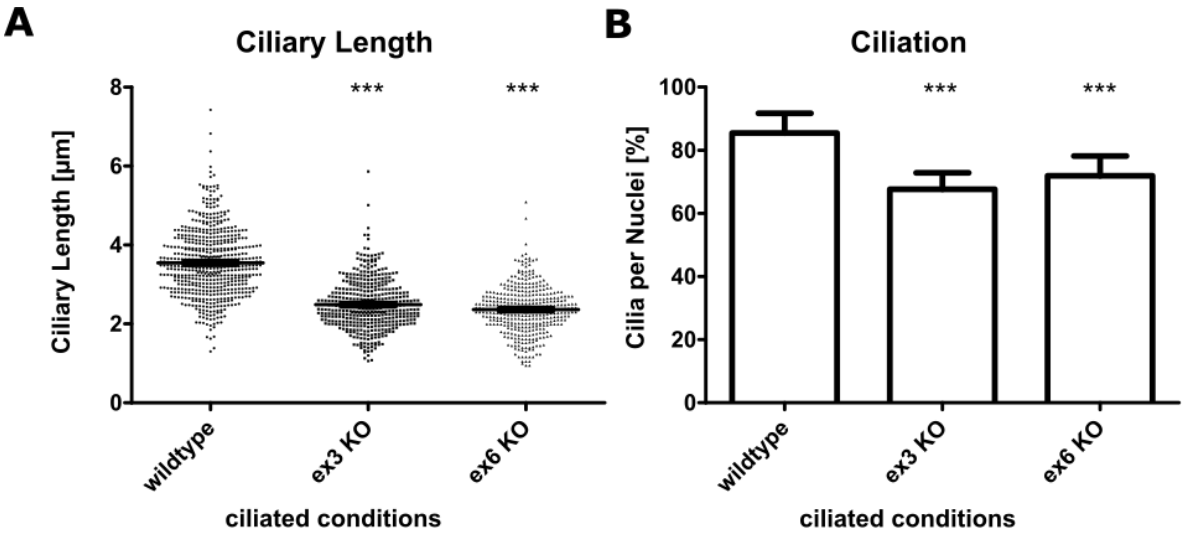

Figure 37 – Ciliary length and ciliation measurements in LCA5 wildtype and exon 3/6 knockout cells – In hTERT-RPE1 LCA5 wt, ex3 and ex6 KO cells ciliary length (**A**) was measured using ARL13B as an indicator for ciliary length. Measurement of ciliation is shown in **B**. In the scatter dot plots, results gained in two independent experiments are shown with each dot representing one cilium. For statistical analysis the mean was calculated. *p* values below 0.001 are represented by ***. Error bars represent the s.e.m.

This data clearly demonstrated an influence of LCA5 on ciliary length and ciliogenesis. In both RPE1 LCA5 knockout cell lines disturbed ciliary assembly resulting in shorter cilia was observed. Additionally, the total amount of ciliated cells was slightly but significantly lowered.

5.4. SSNA1

Lebercilin was reported to strongly interact with SSNA1 [26]. In addition, both proteins are localizing, inter alia, to the basal body and both are involved in ciliogenesis and intraflagellar transport [27, 28, 79, 80]. Furthermore, Lebercilin and SSNA1 seem to be involved in Sonic hedgehog signaling pathway [26]. These findings hint towards a functional relevance of SSNA1 for Lebercilin. Therefore, the investigation of SSNA1 might help to understand Lebercilin misfunction in the context of Leber congenital amaurosis.

5.4.1. Generation of SSNA1 knockout cell lines

For the investigation of SSNA1, its potential interaction with LCA5 and its hypothesized role in Leber congenital amaurosis, the generation of hTERT-RPE1 knockout cells was required. Therefore, the CRISPR/Cas9 system was used to create hTERT-RPE1 SSNA1 KO cells. SSNA1 is a small protein (13.6 kDA) with only three small exons (exon 1 = 52 bp, exon 2 = 200 bp and exon 3 = 108 bp). Overall expected CRISPR efficiency by CCTop was low, therefore all three exons were targeted. After sgRNA transfection of RPE1 cells subsequent single clone selection and DNA extraction were performed. Sanger sequencing revealed an insertion in exon 1 and a deletion in exon 3. Both followed by an open-reading frameshift and predicted early stop codon (**Figure 38 and 39**). Furthermore, sequencing verified the successful generation of homozygous SSNA1 exon 1 and exon 3 knockouts.

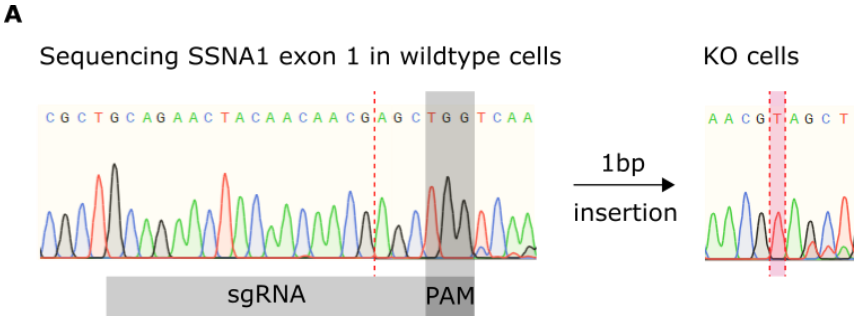

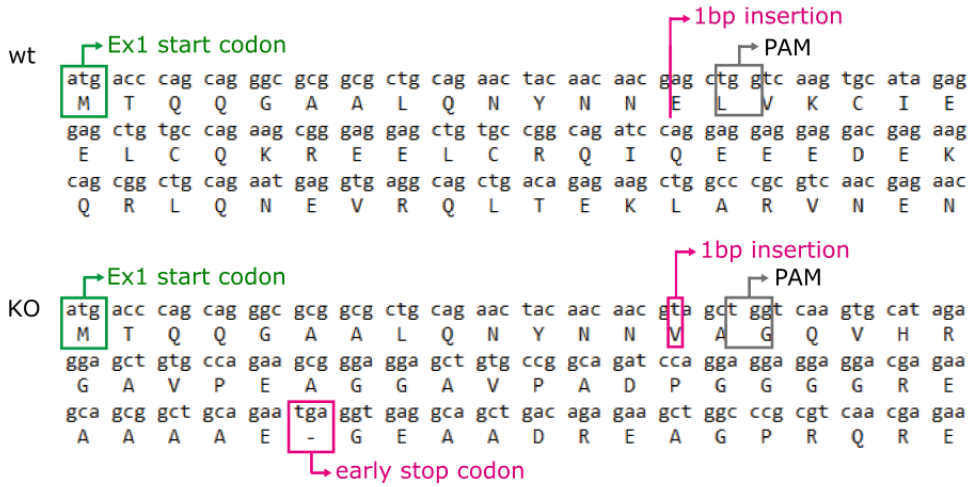

Figure 38 – Sequencing results for SSNA1 wildtype and exon 1 knockout – (**A**) Shown is a fragment of hTERT-RPE1 wildtype SSNA1 ex1 gene along with PAM sequence (dark grey), sgRNA binding site (light grey) as well as inserted base pair (magenta). Sequencing results after CRISPR/Cas9-mediated KO generation depict a homozygous 1 bp insertion. (**B**) Translation of nucleotide sequence fragments in wt and KO cells reveals a frameshift caused by CRISPR/Cas9-mediated insertion that led to a premature stop codon.

CRISPR/Cas9 mediated SSNA1 exon 1 KO generation in hTERT-RPE1 cells was successful (**Figure 38**). A PAM sequence 40 bp behind the start codon of SSNA1 exon 1 was targeted, leading to a homozygous 1 bp insertion. The insertion caused an early stop codon in exon 2, 82 bp after the start codon. This p.E14VfsX32 mutation in the following referred to as SSNA1 exon 1 (ex1) KO resulted in a loss of 62.78 % of SSNA1 protein. Possible off-targets were identified in exonic, intronic or inter genomic regions, but with a minimal probability of binding (**Appendix 11**).

CRISPR/Cas9 mediated SSNA1 exon 3 KO generation in hTERT-RPE1 cells was successful (**Figure 39**). In the middle of SSNA1 exon 3, 36 bp after the start codon, a PAM sequence was targeted, leading to an early stop codon. This stop was located 22 bp before the end of exon 3 and SSNA1 protein. This p.L92QfsX17 mutation in the following referred to as SSNA1 exon 3 (ex3) KO resulted in a loss of only 6.11 % of SSNA1 protein, but the C-terminal untranslated region (452 bp) is affected. Possible off-targets were identified in exonic, intronic or inter genomic regions, but with a minimal probability of binding (**Appendix 12**).

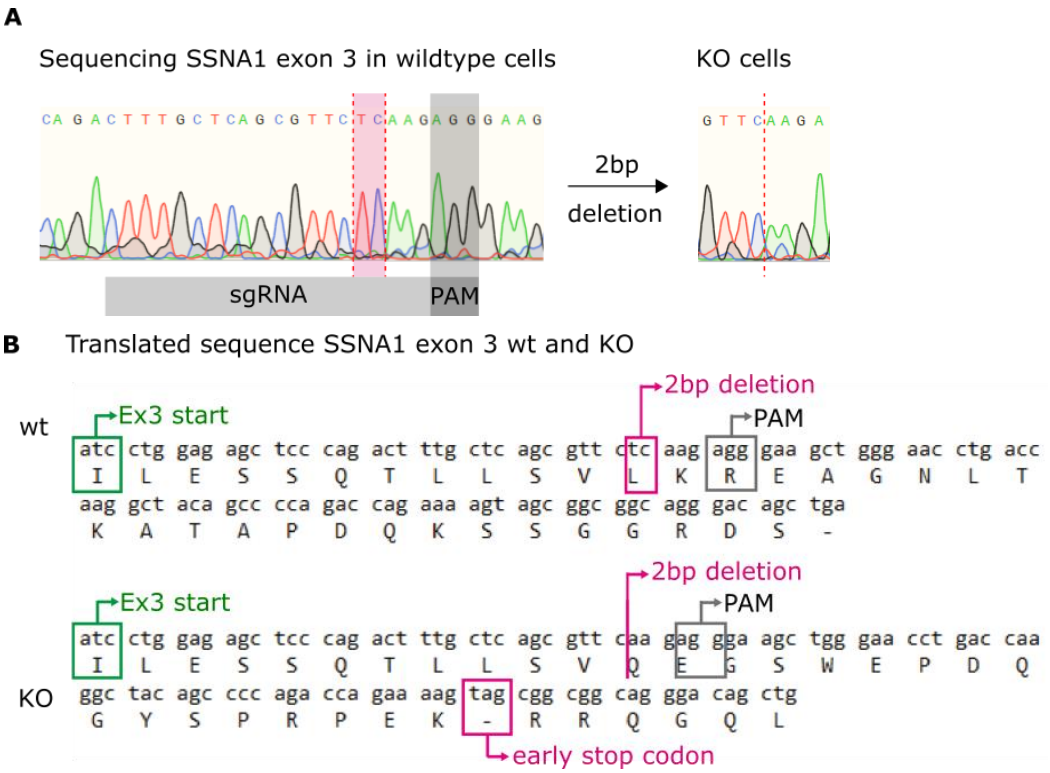

Figure 39 – Sequencing results for SSNA1 wildtype and exon 3 knockout – (**A**) Shown is a fragment of hTERT-RPE1 wildtype SSNA1 ex3 gene along with PAM sequence (dark grey), sgRNA binding site (light grey) as well as deleted base pair (magenta). Sequencing results after CRISPR/Cas9-mediated KO generation depict a homozygous 2 bp deletion. (**B**) Translation of nucleotide sequence fragments in wt and KO cells reveals a frameshift caused by CRISPR/Cas9-mediated insertion that led to a premature stop codon.

5.4.2. Verification of SSNA1 knockout cell lines

The phenotypical analysis of homozygous SSNA1 ex1 and ex3 KO cells using immunofluorescence microscopy was performed to verify differences in protein abundance of wildtype versus KO cell lines. RPE1 SSNA1 control and ex1/3 KO cells were stained for SSNA1 and ARL13B. A decrease in SSNA1 signal intensity can be seen at the basal body of SSNA1 exon 1 KO cells compared to control cells confirming the successful KO generation. Unfortunately, in SSNA1 ex3 KO cells, the antibody signal intensity appeared comparable to the signal intensity of control cells (**Figure 40**). Since, SSNA1 is a small protein, the used antibody targets the whole protein sequence (119 aa). Therefore, it is possible, that truncated protein versions of SSNA1 were detected. The difference in intensity could be explained by the size of truncated SSNA1 and subsequently the probability of antibody binding. Regarding ex1 KO cells 37.22 % of SSNA1 protein and in ex3 KO cells 93.89 % of SSNA1 protein is still left. (**Figure 38 and 39**). Additionally, cells were co-stained with ARL13B, which allowed the investigation of SSNA1 KO and its effect on ciliogenesis.

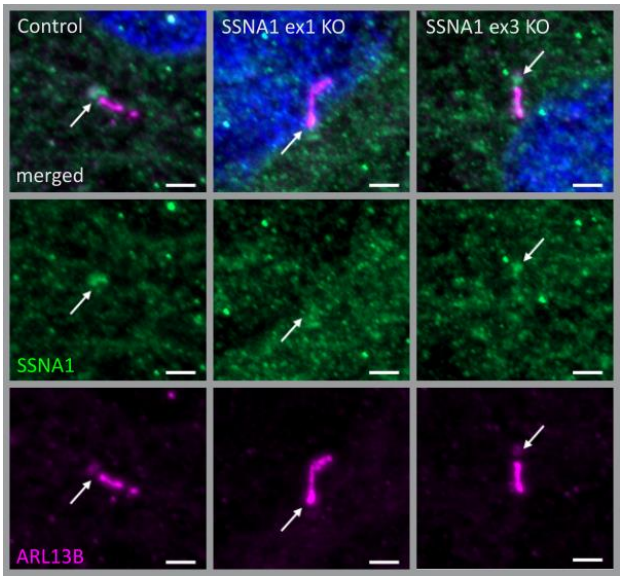

Figure 40 – SSNA1 exon 1/3 knockout verification by immunofluorescence staining – Fluorescent light microscopy pictures of hTERT-RPE1 control, SSNA1 ex1 and ex3 KO cells (from left to right) are shown. The cells were stained for ARL13B (magenta) and SSNA1 (green), DNA is marked in dark blue and co-localization shown in white. The scale bar measures 2 µm.

For further verification of the CRISPR/Cas9 mediated SSNA1 hTERT-RPE1 KO cells were lysed and their total protein level investigated by western blot. Since SSNA1 as microtubule-binding protein is stabilizing dynamic microtubules [34], the protein level of acetylated tubulin and β-actin were also analyzed. But no difference in intensity was visible. Both showed comparable signals in all samples and can therefore be used as loading control. A reduction in SSNA1 signal intensity can be seen in KO compared to control cells (**Figure 41**). For quantification WB signal intensities were measured and normalized to acetylated tubulin as loading control. The signal intensity of 79.84 % ± 0.002 (control cells; n = 2) was decreased to 51.59 % ± 0.11 % (ex1 KO cells; n = 2) and 43.85 % ± 0.02 % (ex3 KO cells; n = 2). This was a reduction of 28.25 % in SSNA1 ex1 KO cells and 35.99 % in SSNA1 ex3 KO cells (**Figure 41**). A reduction in signal intensity for IF and WB experiments could be detected but still a residual signal in both KO cell lines was clearly visible. Verification of SSNA1 ex1 or ex3 KO cells was not finalized and will require further optimization.

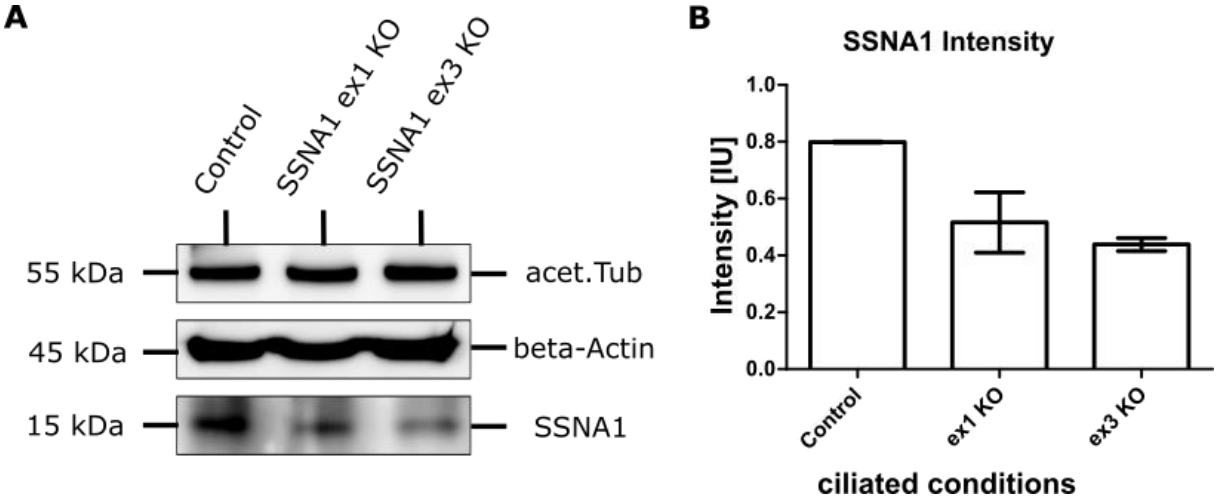

Figure 41 – Protein level of SSNA1 in wildtype and exon 1/3 knockout cells – In hTERT-RPE1 control and SSNA1 ex1 and ex3 knockout cells, protein level of SSNA1, acetylated tubulin and β-actin as loading control were checked by western blot (**A**). Protein level were quantified by measuring their intensity (**B**). These values were normalized to the loading control (acetylated tubulin). The resulting ratios of SSNA1 ex1 (n = 2) and SSNA1 ex3 (n = 2) for SSNA1 KO cells were reduced to those of control cells. For statistical analysis the mean was calculated. *p* values below 0.05 are represented by *, below 0.01 by **. Error bars represent the s.e.m.

5.4.3. SSNA1 exon 1 knockout affects ciliogenesis

Due to involvement of SSNA1 in dynamic microtubule stabilization [34], cilia number and length were investigated using the ciliary protein ARL13B (**Figure 42**) [8]. Sanger sequencing of SSNA1 ex3 suggested, that 93.89 % of SSNA1 protein is still expressed. Additionally, immunofluorescence staining depicted SSNA1 signal intensity comparable to the control. For that reason, SSNA1 ex3 KO cells were not considered for functional tests. Therefore, ciliary length and ciliation were investigated in SSNA1 ex1 KO and control cell lines. Interestingly, ciliary length was in contrast to LCA5 mildly but significantly increased compared to control cells. Whereas ciliation was not affected (**Figure 42**). Averaged ciliary length in control cells was 2.191 µm ± 0.052 µm, in SSNA1 ex1 KO cells 2.903 µm ± 0.065 µm ($n_{control}$ = 358; $n_{SSNA1ex1KO}$ = 316). On average, cilia in KO cells were approximately 0.7 µm longer compared to control cells, an increase of 32.50 %. Regarding ciliation, on average 73.23 % ± 2.53 % of the wildtype cells were ciliated. This was comparable to KO cells, where 69.41 % ± 3.75 % of the SSNA1 ex1 KO were ciliated (**Figure 42**).

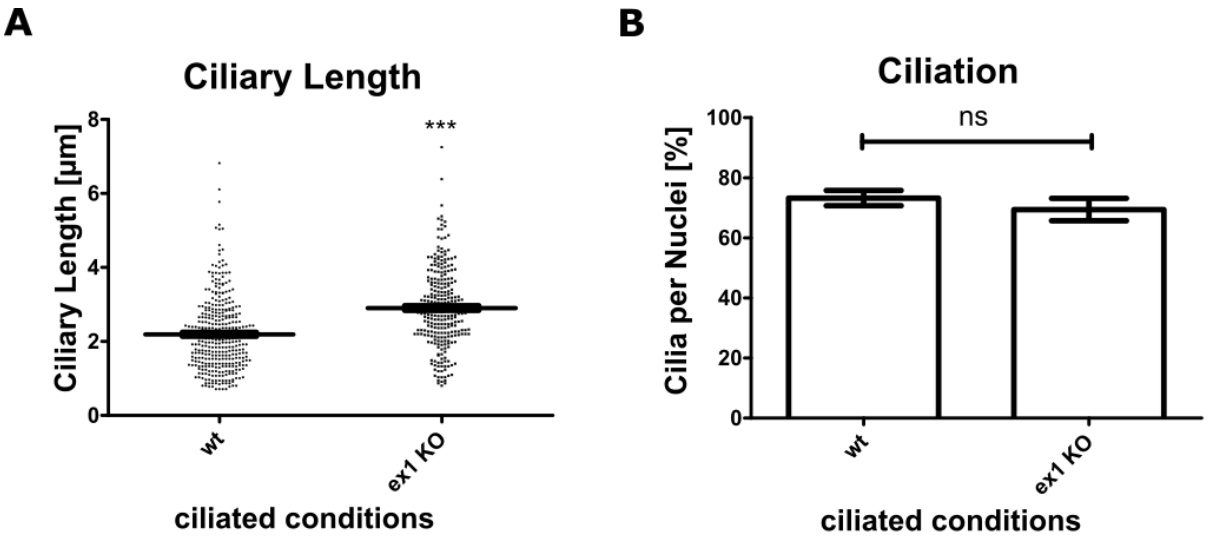

Figure 42 – Ciliary length and ciliation measurements in SSNA1 wildtype and exon 1 knockout cells – In hTERT-RPE1 SSNA1 wt and ex1 KO cells ciliary length (**A**) was measured using ARL13B as an indicator for ciliary length. Measurement of ciliation is shown in **B**. In the scatter dot plots, results gained in two independent experiments are shown with each dot representing one cilium. For statistical analysis the mean was calculated. *p* values below 0.001 are represented by ***. *p* values above 0.05 are deemed not significant (ns). Error bars represent the s.e.m.

These measurements hinted towards an influence of SSNA1 on ciliary length and consequently ciliogenesis. RPE1 SSNA1 ex1 knockout led to enhanced ciliary assembly resulting in elongated cilia. However, total number of cilia per nuclei was unchanged.

5.4.4. SSNA1 knockout inhibits Sonic hedgehog signaling pathway

One of the SSNA1 interaction partners, revealed by Syscilia, was suppressor of fused (SuFu) which is a known regulator of Sonic hedgehog signaling [26]. SuFu is a repressor of Gli proteins, which in their repressed form (GliR) can exit the cilium but do not activate target sequences in the nucleus regulating cellular and cilia related processes. Further, a SSNA1 knockdown resulted in a downregulation of Smo and Gli3 localization to the cilium [28].

Hence, SSNA1 ex1 KO and control cell lines were stained for either Smo or Gli2 and ARL13B. Using fluorescence microscopy, the co-localization of Smo and Gli2 to the cilium was observed in control cells with ARL13B. Strikingly, this localization was reduced in SSNA1 ex1 KO cells for Smo and Gli2 (**Figure 43**). These results indicated an involvement of SSNA1 in Shh signaling pathway, verified the findings of Lai *et al.* and indicated that Gli2 localization to the cilium is also decreased [28].

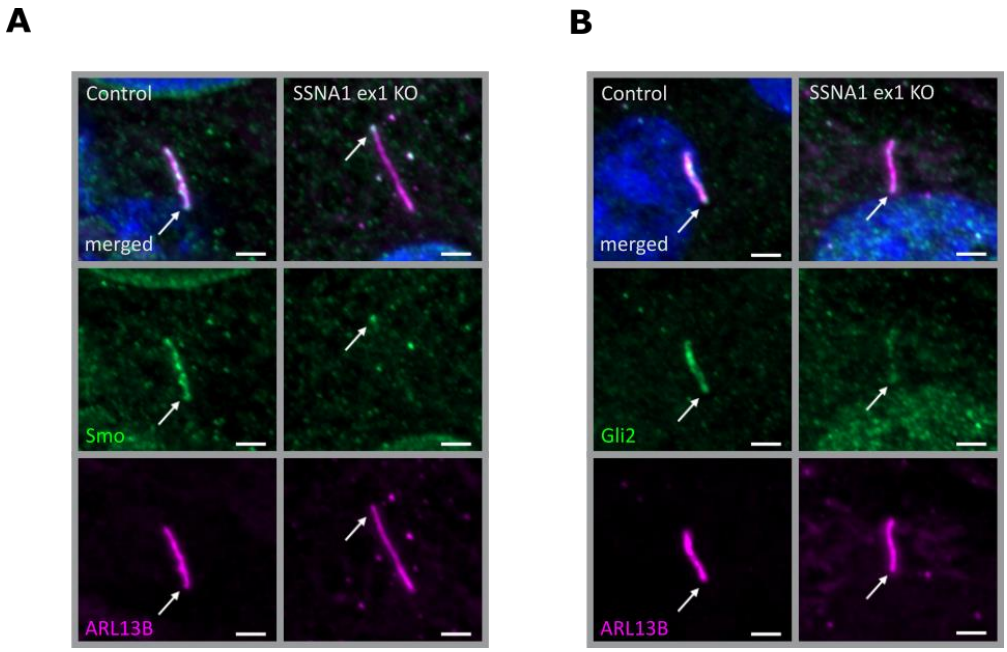

Figure 43 – Localization of Smo and Gli2 in SSNA1 wildtype and exon 1 knockout cells – Fluorescent light microscopy pictures of hTERT-RPE1 control and SSNA1 ex1 KO cells (from left to right) are shown. The cells were stained for ARL13B (magenta) and DNA is marked in dark blue and co-localization shown in white. The green channel depicts Smo (**A**) or Gli2 (**B**). The scale bar measures 2 µm.

5.4.5. SSNA1 knockout leads to ciliary accumulation of Lebercilin after Sonic hedgehog activation

Previous interactome data proposed a potential interaction of SSNA1 and LCA5 [26]. Additionally, potential interactors for Lebercilin (KIF7) and SSNA1 (SuFu) were identified which are involved in Shh [26]. After verification that SSNA1 ex1 KO cells had also an impact on Shh signaling pathway, Lebercilin was investigated to be influenced by Shh. Therefore, hTERT-RPE1 control and SSNA1 ex1 KO cell lines were treated with SAG to stimulate Shh pathway prior to immunofluorescence staining [125]. Cells were then fixed and subsequently stained for LCA5 and ARL13B. Both proteins were shown to co-localize in control and SSNA1 ex1 KO cells. But interestingly, LCA5 signal was increased in SSNA1 ex1 KO cells compared to SSNA1 control cells, suggesting an accumulation of LCA5 in the cilium of Shh pathway activated SSNA1 KO cells (**Figure 44**).

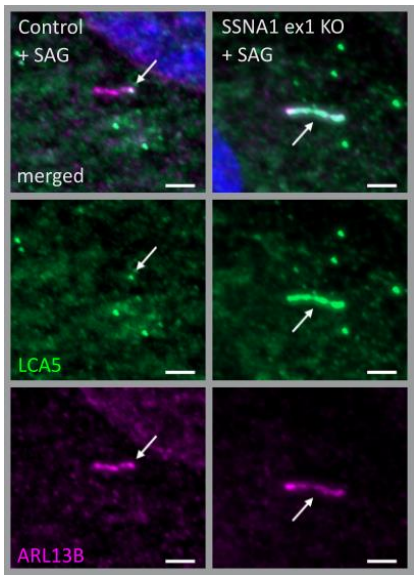

Figure 44 – Localization of LCA5 and ARL13B in SSNA1 wildtype and exon 1 knockout cells under activation of Sonic hedgehog pathway – Fluorescent light microscopy images of hTERT-RPE1 control and SSNA1 ex1 KO cells are shown, which were either treated with SAG. The cells were stained for ARL13B (magenta), LCA5 (green), DNA is marked in dark blue and co-localization shown in white. The scale bar measures 2 µm.

The data gathered here indicates that Lebercilin and SSNA1 have an impact on Shh signaling which is in line with previous findings (**Figure 43**) [28, 34]. It was revealed that SSNA1 influences the localization of Lebercilin (**Figure 44**) and possibly modifies its function. In addition, both proteins had an opposing effect on cilia length (**Figure 42**), which might hint at opposing or complementing functions of Lebercilin and SSNA1. Further investigation is needed to elucidate their function in a ciliary context.

6. Discussion

6.1. TTC30A/B redundancy protects IFT-B complex stability

TTC30A and TTC30B paralogues share a high similarity in their sequence (Appendix 1) [8]. This implies, that these two proteins are most likely redundant in critical molecular processes. Only a small percentage (4.66 % of the sequence) of variation distinguishes TTC30A and B but this disparity might hint towards non-overlapping function which are not yet understood. These minor differences enabled specific targeting of each paralogue. The sgRNA targets were located close to the N-terminus (Figure 11 – 13). Overall, only few off-targets were predicted [109, 110], which could be neglected due to their location in intergenic or intronic sequences with a minimum of three to four mismatches [126]. Finally, both proteins could be specifically addressed due to the accuracy of the CRISPR/Cas9 method (Figure 15 and 15) [8, 127, 128]. In addition, a paralogue specific rescue was restoring cilia assembly and polyglutamylation in the double knockout (KO) background. The level of single KO ciliary length was reached and led to the conclusion that the effect seen in single and double KO cells was specific for TTC30 [8].

The results of the localization and interactome studies indicated that in TTC30A or TTC30B single KO cells, the overall function of intraflagellar transport complexes A and B (IFT-A and IFT-B) is still intact [8]. In contrast, the phenotype of double KO TTC30A/B showed that in absence of TTC30A/B, no ciliogenesis occurred, but IFT140 and IFT88 proteins were still localizing to the basal body (BB; Figure 19 – 22) [8, 31]. This led to the assumption that IFT complex B is destabilized or not assembled and eventually leads to disrupted intraflagellar transport and, subsequently, no ciliary assembly (Figure 15) [8]. This hypothesis is supported by the complex instability seen in TTC30A/B double but not TTC30B single KO cells, with at least the sub-complex IFT-B1 being influenced by the loss of both paralogues simultaneously (Table 28) [8]. However, it is still up for speculation if the instability would result in transport defects. Interestingly, the strong phenotype observed in double KO cells could be partially rescued by expressing TTC30A or TTC30B again (Figure 15) [8]. In conclusion, one TTC30 paralogue, due to redundancy, is enough to restore the integrity of the IFT complex, which is required for the induction of primary cilium assembly. This is in line with the results described by Takei and colleagues in 2018 [8, 31].

Similarly, to the results obtained here, Takei and colleagues generated double KO hTERT-RPE1 cells and were able to rescue cilia when expressing one paralogue only. However, in contrast to the published data, the use of the single KO type revealed a cilia length reduction, which was not shown before and hints towards paralogue-specific functions [8]. In addition, the paralogue-specific rescue restored cilia length to a level comparable to that of single KO cells but not to the level of control cells, which was also true for polyglutamylated tubulin intensity (Figure 17) [8]. The question is if shorter cilia were caused by a lack of TTC30 protein in single KO cells, although they had approximately half of the protein amount left (TTC30A or B). Due to the TTC30 single KO and paralogue redundancy all IFT-B complexes were assembled with either A or B but could not compensate the high amount of protein needed, resulting in reduced ciliary length. However, in TTC30A/B rescue cells, where high protein amounts of either TTC30A or B were available, due to overexpression constructs, cilia resembled only single KO but not wildtype ciliary length. The transfection of TTC30A/B single KO cells with either TTC30A or B wildtype (wt) would reveal if cilia are restored to initial or even increased length.

Interestingly, it was shown that IFT70/TTC30A/B is capable of binding IFT52-IFT88, which is required for ciliogenesis [8, 26, 31, 65, 66]. Takei and colleagues suggested that this binding induces conformational changes in the IFT-B complex which might be a prerequisite for ciliary transport. The mild change in IFT-B complex stability seen here in TTC30A/B double KO cells supports this hypothesis. However, it is still unclear whether the reduction in cilia length is due to (1) less TTC30 protein (2) ciliary tip instability, (3) signaling/transport deceleration, or (4) axoneme instability [8]. In addition, it is not known whether the loss of one paralogue only and a mild cilia length reduction would lead to severe developmental defects or other ciliopathy related symptoms, except synpolydactyly. An involvement of the basal body was not considered, since ciliation was not disturbed in TTC30A/B single KO cells (Figure 18). Therefore, it was of interest to investigate paralogue-specific protein–protein interactions, which might help us to understand the mild effects seen in single KO cells [8].

The aim of TTC30A/B interactome analysis at the endogenous level was to be as close as possible to physiological conditions. Endogenous tagging using the small FLAG-tag, reducing false positive or false negative hits and low interference with protein folding and interaction [129, 130], led to the identification of a specific interactome for each paralogue containing all

IFT-B complex proteins [8]. The most important step was endogenously and specifically FLAG-tagging of TTC30A or B. Otherwise, potential interacting proteins could be matched to the wrong paralogue. By detecting unique peptides for TTC30A or B, which were found to be enriched in corresponding samples, could clearly show that the specific tagging was successful and therefore could assign potential interactors correctly [8]. As a result, all components of IFT complex B could be found to interact with TTC30A as well as TTC30B (Figure 24) [8]. From the identification of the whole complex, a central role in IFT-B for both proteins is suggested, as assumed before [26, 31, 66]. Redundancy might be necessary for correct complex composition and integrity, even if one paralogue is mutated [8]. Interestingly, unique TTC30A or B peptides were found in the related sample, indicating that the paralogues might compete for IFT-B complex binding (Figure 23; Table 28) [8].

These findings underline, in combination with mass spectrometry (MS) data, on the one hand, the need of these two paralogues with similar and non-overlapping functions, and on the other hand the importance of an intact IFT complex B itself [8]. A loss of function in one protein can be compensated to some degree, by the other protein, but not completely. Cells still form a cilium, which is shorter, and that is potentially limited in its functions. A complete loss of both proteins, such as the loss of other IFT proteins, leads to disrupted intraflagellar transport and, subsequently, no cilia formation at all, which is most likely a lethal condition during development [8, 131-133]. Furthermore, these results show that both processes of polyglutamylation and ciliary assembly were affected by isoforms A and B, and therefore are similar to the phenotype found in *zebrafish* (*flr*), *C. elegans* (DYF1) [32] and *C. reinhardtii* [8, 67]. Interestingly, there is no paralogue of TTC30 analogues DYF1/*flr* described that can compensate for phenotypes caused by mutation or complete loss. However, in more complex organisms (frogs, mice), paralogue TTC30 proteins can be found [134, 135]. Therefore, gene duplication resulting in TTC30A and TTC30B might be an evolutionary asset worth conserving [8].

In human cell lines, polyglutamylation, which is influenced by TTC30 orthologues [32], is a major contributor for ciliary signaling and suggests a potential therapeutic strategy by targeting polyglutamylation mechanisms. The aim is to promote the ciliary targeting of signaling machineries and correct signaling defects in ciliopathies [8, 117, 136]. However, the underlying processes of reduced polyglutamylation in cilia or mildly reduced ciliary length in humans remains unclear. The observed hypo-polyglutamylation might also be a result of the

reduced ciliary length maintaining normal ciliary segmentation [8, 137]. The mild reduction in ciliary length might hint towards a transport defect or some influence on ciliary function independent of IFT [8].

6.2. Mass spectrometry analysis reveals TTC30A/B paralogue specific interactors

The TTC30A/B interactome analysis was performed under nearly physiological conditions at endogenous level using the FLAG-tag. This small tag was crucial reducing incorrect protein identifications and had a low impact on protein folding and interaction [129, 130], Localization studies showed that TTC30A and TTC30B could be targeted specifically, despite their similarities, using the CRISPR/Cas9 system. Additionally, MS experiments demonstrated that both paralogues could also be detected separately. Therefore, it was also possible to characterize their interactome individually. Besides the identification of all IFT complex B components interacting with TTC30A as well as TTC30B, 47 proteins were specifically enriched with TTC30A (Table 25) and 105 proteins with TTC30B (Table 26).

So far only few publications hinted at paralogue specific non-redundant functions of TTC30A and TTC30B. In *Xenopus tropicalis*, TTC30A was linked to ciliary chondrodysplasia with polycystic kidney disease [8, 135]. Sonic hedgehog signaling could be linked to a rare TTC30B missense variant [33], leading to synpolydactyly in a chinese pedigree. Intriguingly, synpolydactyly and chondrodysplasia are both skeletal phenotypes [8]. Transmembrane proteins, such as TMEM41B, which show a ciliary effect, were linked to TTC30B [8, 26]. Here, the TTC30A/B specific interactome revealed new presumable protein interactors, hinting at further functions probably influencing cilia related processes.

The most compelling proteins interacting with TTC30A were ODR4, PRKACA, SNAP29, CEP350, SUN2, CCDC88A and SYNE1 (Table 27). SNAP29 has a role in ciliogenesis. As a membrane fusion regulator, it is required for ciliary vesicle assembly which is essential for ciliary growth [138]. Similarly, in mice SYNE1 and SUN2 are also involved in early ciliogenesis where they are required for centrosome migration to the cell surface [139]. Centrosomal protein CEP350 is required for ciliation [140]. In *C. elegans*, ODR4 has a role in seven transmembrane olfactory GPCRs trafficking to the cilium and is therefore crucial for receptor dependent ciliary signaling [141]. CCDC88A is among others interacting with Gα-subunits. It is involved in AKT-mTOR signaling and was also shown to have a role in BB positioning as well as ciliogenesis in *C.*

elegans [142]. Protein kinase A catalytic subunit α (PRKACA) is a key regulator for Sonic hedgehog (Shh) inhibition [92].

For TTC30B CAMSAP3, SKI, RDX, STAT1, CSNK2A1, CROCC and OS9 were the most intriguing interactors. CAMSAP3 is essential for microtubule organization, BB positioning and function of motile cilia in mice [143]. RDX links membrane proteins with actin filaments of the cytoskeleton and mutated RDX results in neurosensory hearing loss [144]. SKI has a role in TGFβ and Wnt signaling [145, 146]. CSNK2A1 is also involved in Wnt signaling [147]. In *S. cerevisiae*, OS9 was shown to be required for hedgehog (Hh) ligand biogenesis [148] and STAT1 is a key player in the JAK-STAT signaling pathway [149]. The first investigated possible TTC30B interactor in this list was CROCC/rootletin, which is described as an essential protein for centrosome cohesion and cilia stability [119, 120]. In photoreceptors, mutant rootletin leads to photoreceptor instability and retinal degeneration [8, 150]. The *C. elegans* ortholog Che-10 is needed to support IFT-related transport and transition zone integrity [8, 151]. However, no effect on rootlet structures was seen (Figure 26), but transport speed or transition zone integrity were not analyzed [8].

In addition to these paralogue-specific interactors, so far unknown shared interactors were also identified. In the interactome of TTC30A and TTC30B the minichromosome maintenance (MCM) proteins 2, 3, 4, 5, 6 and 7 were found. The MCM2-7 complex usually functions as helicase and initiates DNA replication [152] but two of the components (MCM2 and 7) were shown to have an additional ciliary function. A depletion of MCM2 and MCM7 in zebrafish impaired left-right asymmetry and in human fibroblasts centrosome aberrations and shorter cilia could be observed [153].

In conclusion, the described possible protein interactors hint at additional common but also specific functions for TTC30A or TTC30B which suggest an involvement in ciliogenesis or cilia related signaling. These findings further complement the suggested TTC30B specific transmembrane proteins, which were the first hint at a paralogue specific interactome [26]. Newly discovered interactors need to be further elucidated using tissue-specific investigations evaluating their impact on primary cilia function [8]. In this study presented here, another TTC30A specific interactor was investigated in more detail, which ultimately resulted in an altered regulation of Shh signaling.

6.3. Lost interaction of TTC30A and PRKACA results in inhibition of Sonic hedgehog pathway

One promising TTC30A protein interactor investigated was the protein kinase A catalytic subunit α (PRKACA). In the Shh off-state PKA phosphorylates full length Gli2 and Gli3 (GliFL) transcription factors, which are then processed into their repressed forms (GliR). When Shh is activated, GliFL is not processed to GliR, but to its active form GliA. The ratio of GliA/GliR regulates the expression of target genes (e.g., Patched1 and Gli1) [96].

Initially, to determine whether TTC30A has truly an effect on PKA the total protein level was investigated. Treatment of single KO cells with Forskolin did not change the total amount PKA catalytic subunits (PKAcat). However, the amount of phosphorylated protein by PKA was considerably increased in hTERT-RPE1 TTC30A single KO compared TTC30B single KO and control cells (Figure 27) when these cells were treated with Forskolin. This chemical compound increases intraciliary cAMP level [123]. PKA regulatory subunits are phosphorylated by cAMP and then dissociate from PKA catalytic subunits. PKAcat are relieved from inhibition and phosphorylate target protein substrates [92].

To further investigate the effect of TTC30A KO on Shh, other pathway components were examined. Increased phosphorylation mediated by PKA leads to an inhibition of Sonic hedgehog [95]. In this off-state Patched1 (Ptch1) is localized in the ciliary membrane and inhibits Smoothened (Smo) from entering the cilium [88]. Hence, this initial step was considered next for a functional test. Therefore, localization studies with Smo and Ptch1 were performed with and without Smoothened agonist (SAG) stimulation, which activated Shh pathway [125]. Results showed that Smo was not localizing to cilium in TTC30A KO (± SAG). While in the Shh off-state Ptch1 was localizing to the cilium and in the on-state Ptch1 was leaving the ciliary membrane. Meaning that Ptch1 is unaffected, but Smo is affected by TTC30A KO. Again, TTC30B KO did not show this phenotype and was comparable to the control.

This TTC30A specific phenotype of lost ciliary localization of Smo, even when Shh was activated, could be completely rescued by expressing TTC30A wt. The transfection with mutated (A375V) TTC30A was not able to recover this strong phenotype. In contrast, the mutated (A375V) TTC30B rescue construct was able to reverse this phenotype. These results

imply, that the inhibition of ciliary Smo uptake, mediated by PKA, and subsequently the downregulation of Sonic hedgehog signaling is a specific TTC30A dependent function.

For further verification and precise description of the role of TTC30A in Sonic Hedgehog, other key components need to be investigated in this TTC30A KO and A375V TTC30A context. Such as GliFL, GliA and GliR, which represent the last ciliary components in the Shh pathway, before targeting Hh genes in the nucleus. Any changes in their expression level could explain the mislocalization of Smo in the TTC30A KO and mutated A375V TTC30A. Additionally, the Gli transcription factors could represent the missing link leading from increased level of phosphorylated PKA substrate to lost Smo localization and confirm the proposed interaction of Smo, Gli and PKA [154]. Regarding Smo and Ptch1, the total endogenous protein level needs to be determined, to evaluate if this strong phenotype is a mislocalization or a reduction of expression.

Upon Shh activation, Smo is entering the cilium. IFT-A and IFT-B interaction is necessary for this entry and IFT-B also facilitates the anterograde transport of Smo to the ciliary tip [155, 156]. This implies, that the observed phenotype could also originate from a transport defect. Overall, cilia were assembled in RPE1 TTC30A single KO cells and IFT88/140 localization was comparable to the control cells. Nevertheless, assembled cilia were shorter, hinting at a minor deficiency. If this mild IFT-related phenotype is sufficient to inhibit Smo completely from entering the cilium is debatable.

Also, the origin of the increase in phosphorylated PKA substrates need further investigation. It might have been caused by an increased intraciliary cAMP level but so far only PKAcat and pPKA substrate were checked. To clarify how exactly TTC30A KO is interfering in this PKA mediated phosphorylation and de-phosphorylation processes, the amount of ciliary cAMP, phosphorylated PKAcat and PKA regulatory subunits need to be determined. Impaired or absent PKA regulatory subunits, which inhibit PKAcat, are a potential source for increased cAMP level [92]. Localization studies of GPR161 would indicate if this GPCR does leave the ciliary membrane in Shh on-state. If GPR161 remains localized to the cilium this would also explain increased ciliary cAMP levels [95].

The nature of this TTC30A PRKACA interaction needs to be characterized more thoroughly, since TTC30A is a linking protein with no active sites and was not found to interact with Smo or any other part of Shh pathway in the interactome data. But as adaptor protein it is possible that TTC30A/B are involved in linking other yet unknown proteins, aside from IFT-B complex,

that result in Smo mislocalization. But most likely, the lost ciliary localization of Smo is a consequence of the increased level of PKA phosphorylated proteins. The discovered A375V TTC30B mutation found in a chinese pedigree was localized in the TTC30B gene. Shh signaling was disturbed due to reduced Smo and Gli mRNA expression level, ultimately leading to synpolydactyly [33]. Contradictory to these findings, the results shown here presented a link between Sonic hedgehog and TTC30A. Unfortunately, Du *et al.* did not present any data regarding TTC30A, further the siRNA used in the publication was not specific for TTC30B. It also inhibits TTC30A, because the targeted nucleotide sequence is identical in both paralogues (Appendix 13).

The gathered data matches to the proposed Smo, PKA, Gli interaction from Arveseth *et al.* They showed that Smo inhibits PKAcat activity and that this interaction is essential for Shh signal transduction via GliA [154]. Nevertheless, the impact of A375V TTC30A/B mutation on PKA is yet unclear and needs to be investigated. The results verified the interaction of TTC30A with PRKACA and confirmed the involvement of TTC30A in Shh signaling. This involvement could most likely result in a synpolydactyly phenotype and matches the findings in *X. tropicalis*, where TTC30A was also linked to a skeletal phenotype [135]. Furthermore, it was demonstrated that TTC30A has specific protein interactions and a non-overlapping function with TTC30B. A PKA mediated Shh downregulation in a TTC30A dependent manner could be shown.

6.4. Patient A375V mutation leads to a decreased interaction of TTC30A with IFT57 and TTC30B with TTC37

The data presented here emphasizes the impact of TTC30A, mediated by PKA, on Smo localization in Sonic hedgehog signaling. Localization studies pointed out that the A375V patient mutation, introduced in TTC30A, could not rescue Smo mislocalization observed in single KO cells. Moreover, A375V TTC30B was linked to Shh inhibition [33]. To analyze the influence of TTC30 A375V mutation on protein interactions and Sonic hedgehog a comparative mass spectrometry analysis was performed.

Therefore, HEK293T control cells were transiently transfected with either TTC30A/B wildtype sequence or the mutated A375V variant [33, 108]. Followed by a comparison of their interactomes (Table 29 and 28). The most interesting interacting partners with significantly disturbed interaction, were IFT57 for TTC30A and TTC37 for TTC30B (Figure 30). TTC37 is a

component of the SKI complex. It acts as a co-factor and regulator of the exosome mediated decay of RNA. The malfunction of SKI is linked to the trichohepatoenteric syndrome [157].

The most intriguing interaction that was impaired in A375V TTC30A in relation to TTC30A wt was IFT57. The localization of IFT57 was investigated with immunofluorescence microscopy. The signal intensity in control cells, TTC30A/B single KO cells and TTC30A/B double KO cells, rescued with either TTC30A/B wt or mutated A375V TTC30A/B, appeared comparable (**Figure 31**). Nevertheless, IFT57 signal intensity was measured, but was not significantly reduced in any condition (**Figure 32**). Regarding TTC30A/B double KO cells rescued with either A375V TTC30A or TTC30B, a tendency to decreased IFT57 signal is visible. An impaired localization of IFT57 in either A375V TTC30A or TTC30B rescue cells could be a rather mild phenotype and only five to ten cilia were measured for each condition. To increase the statistical power, the sample size will be increased.

Overall, a disturbed TTC30A IFT57 interaction caused by A375V mutation would explain how this mutation is connected to Shh. Since, IFT57 knockdown was shown to reduce the induction of Gli1 leading to dysfunctional Shh and polydactyly in humans [158]. But a total loss of IFT57, ultimately leads to disrupted ciliary assembly and was shown to be lethal [158]. The IFT-B structural model described by Petriman *et al.* shows that TTC30 and IFT57 are not directly interacting with each other. In the IFT-B1 complex TTC30 is connected to IFT88 and IFT52. IFT88/52 are then directly interacting with IFT57 and IFT38, which belong to the IFT-B2 subcomplex [13, 63]. If a minor conformational change in TTC30 due to A375V mutation would influence the binding pattern of IFT88/52 to IFT57, is up to speculation. In all IFT-B models TTC30A and TTC30B are summarized as IFT70, therefore TTC30A and B specific results are not available and up to speculation. The data gathered here indicate, that each paralogue has specific functions. These functions are either conducted as part of the IFT-B or by interaction with other proteins. It is possible but also hypothetical that there are two different IFT-B complexes. One complex consists of TTC30A/IFT70A and the other of TTC30B/IFT70B. Depending on the TTC30 paralogue these two complexes have additional individual functions, like trafficking specific proteins (e.g., Smo) into the cilium and via anterograde transport to tip.

In conclusion, results gained here showed an inhibition of Smo entering the cilium in hTERT-RPE1 TTC30A KO cells. This was mediated by PKA and ultimately leading to a downregulation of Shh. In contrast, A375V TTC30A was also suggested to downregulate Shh but in an IFT57

dependent manner. A potential involvement of PKA needs to be tested. If TTC30A can influence Sonic hedgehog signaling in various ways or if PKA and IFT57 are belonging to one unique pathway remains elusive and the underlying mechanism still has to be identified.

6.5. LCA5 knockout results in reduction of ciliary length and ciliation

To study Lebercilin function, first it was necessary to generate specific hTERT-RPE1 knockout cells. The CRISPR/Cas9 method proved effective using the suggested sgRNAs (by CCTop) for exon 3 and exon 6 [109, 110]. Sequencing revealed homozygous knockouts (**Figure 33 and 34**). Nevertheless, in western blot a faint band was still visible in KO cell lysates (**Figure 35**), implying the possibility of an incomplete knockout or the expression of a truncated Lebercilin version. To improve western blot results another antibody might be worth testing or expression of mRNA level will be determined.

The sequencing results in combination with Lebercilin localization verified the successful creation of LCA5 ex3 and ex6 knockouts (**Figure 36**). Generated RPE1 LCA5 ex3 and ex6 KO cells will further be transfected with LCA5 wt rescue constructs to revert the observed phenotype and to exclude CRISPR/Cas9 related off-target effects.

Immunofluorescence microscopy also revealed a mild reduction of ciliary length and ciliation (**Figure 37**). A possible cause is a disturbed basal body region, which was already connected to ciliogenesis defects, like reduced ciliation [20, 21]. In detail, IFT-A and IFT-B proteins bind to the transition fibers at the BB and their respective complexes are assembled. Further, cargo is bound to IFT-B and via anterograde transport delivered to the ciliary tip, where they are incorporated (e.g., tubulin) into the growing cilium [3, 54]. Interestingly, LCA5 localizes strongly to these regions of the primary cilium (BB, ciliary tip) [81]. Moreover, recent findings suggest that LCA5 forms oligomers at the basal body, in a dynein light chain (LC8) dependent manner [81]. Lebercilin was also shown to localize to the axoneme and to interact with IFT-B complex proteins [80]. Upon introduction of the identified LCA patient mutations [79] these IFT-B interactions were lost and resulted in an opsin transport defect in mouse retina [80]. Intriguingly, in LCA5 KO mice and LCA patients only retinal tissue is affected despite its ubiquitous expression [159]. The difference to other tissues is the massive need of rhodopsin in the photoreceptor's specialized retinal cilium and therefore a massive IFT-mediated transport of opsins from the inner segment (IS) along the connecting cilium to the outer

segment (OS) [79, 80]. In this extreme situation the observed mild phenotype, in RPE1 LCA5 ex3 and ex6 KO cells, might lead to subtle transport defects, protein accumulation and thereby rapid degeneration of the OS. However, the underlying mechanism remains elusive.

This specific transport defect is difficult to investigate in photoreceptor cells, the here generated RPE1 LCA5 ex3 and ex6 KO cells can be used for future studies. Therefore, a Rhodopsin fluorescence tagged overexpression construct will be transfected to visualize ciliary localization. Lebercilin KO cells will be transfected with LCA5 wt rescue constructs to reverse a possible ciliary mislocalization of Rhodopsin and the observed reduced ciliary length and ciliation. The identified LCA5 patient mutations by den Hollander *et al.* will also be investigated in this context. Further, it would be interesting to characterize the nature of LCA5 interaction with KIF7 (Syscilia). KIF7, a kinesin-4 family protein, was indicated to restrict Gli-SuFu complexes to the distal end of the cilium [160, 161]. Gli and SuFu proteins are involved in Shh signaling, which among others regulates ciliary length [3]. Hence, the possibility of KIF7 mediated influence of Lebercilin on Sonic Hedgehog will be explored.

Defects in the gene coding for X-linked retinitis pigmentosa GTPase regulator interacting protein 1, RPGRIP1 or LCA6, are similar to Lebercilin (LCA5) causing Leber congenital amaurosis. It was shown to interact with LCA5 and both proteins localize with core centriole proteins and distal appendage components in the ciliary transition zone [162]. Additionally, RPGRIP1 interacts with RPGR [163] and both localize in the rod outer segments [164]. More specifically RPGRIP1 is located at the axoneme and the basal body of the connecting cilium and is anchoring retinitis pigmentosa GTPase regulator (RPGR) to the connecting cilium [165, 166]. The major isoform RPGRorf15 is the functional significant variant in photoreceptors [167]. Interactome studies of bovine RPGRorf15 revealed IFT88 and microtubule motor protein KIF3a as possible interactors, suggesting a role of RPGRorf15 in IFT and microtubule organization [166]. Interestingly, RPGRorf15 mutations caused, like Lebercilin mutations, rapid photoreceptor degeneration [168] and a depletion of RPGR in human RPE cells led to reduced length in primary cilia [169]. The correlation of phenotypes between Lebercilin and RPGRorf15, as well as their link to RPGRIP1, suggests that RPGRorf15 might be interesting to investigate in LCA5 KO models.

6.6. SSNA1 knockout leads to Hedgehog mediated ciliary accumulation of Lebercilin

In previously described interactome studies by Syscilia, SSNA1 was found as possible interactor of LCA5, but also LCA5 was found in the SSNA1 interactome. These findings suggest a highly relevant interaction between these two proteins. To investigate the function of SSNA1 and to characterize the interaction with LCA5, specific hTERT-RPE1 KO cells were generated. The CRISPR/Cas9 system was used to target exon 1 and exon 3. Sequencing results depicted homozygous KOs (**Figure 38 and 39**). SgRNA targets were in intergenic, intronic and also exonic regions but had a minimum of three to four mismatches [125]. Total protein level was detected by western blot (**Figure 41**) and localization to the basal body by immunofluorescence microscopy (**Figure 40**). Unfortunately, in localization studies as well as western blot, the intensity of SSNA1 signal was decreased but still detectable. Meaning that these cells are either not harboring a complete SSNA1 KO, that the antibody possibly binds to other proteins or that a truncated version was detected. To improve western blot and IF results and to verify the generated knockouts another antibody might be worth testing or mRNA expression level could be determined. Another option might be the creation of a new CRISPR/Cas9 mediated KO, targeting the starting codon to delete the whole protein.

Imaging of SSNA1 KOs showed a mild increase of ciliary length, whereas ciliation was comparable to the control (**Figure 42**). This is in line with the recent findings of Lawrence *et al.* that SSNA1 accumulation was correlated with a reduction of microtubule growth but increasing microtubule stability [34]. In addition, stabilized microtubules form shorter cilia [116]. Concluding, that in the absence of SSNA1, microtubules are destabilized which ultimately results in longer cilia [34, 116]. Further, it was reported that SSNA1 severely affects cytokinesis in HeLa cells [86]. This phenotype could not be observed in hTERT-RPE1 SSNA1 KO cells but needs further quantification.

In the next step, the previously described interaction of SSNA1 with SuFu (Suppressor of Fused) was investigated [26]. SuFu is involved in the negative regulation of Shh signaling. It promotes the proteolytic truncation of full length Gli2 and Gli3 to GliR. If the ratio of GliA/GliR is shifted towards GliR, nuclear target genes are less transcribed [46, 93]. Interestingly, imaging of Shh signaling components in SSNA1 KO and control cells revealed a reduced ciliary localization of Smo and Gli2 in SSNA1 KO cells (**Figure 43**). This was in line with the findings of

Lai *et al.* who have shown a decreased localization of Smo and Gli3 to the cilium [28]. Upon activation of Shh, Smo enters the cilium and is transported (via IFT) to the ciliary tip [155]. At the tip, Smo blocks the processing of Gli to GliR and promotes the dissociation of SuFu. This relieves the inhibition on Gli resulting in GliA formation [100]. In SSNA1 KO cells with reduced localization of Smo and Gli2, the GliA/GliR ratio might be shifted towards GliR. Further, it was proposed that upon Shh activation Ptch1 might not leave the cilium and further inhibit Smo from entering the cilium [28]. This could explain the observed downregulation of Sonic hedgehog signaling which is followed by decreased transcription of nuclear target genes and would eventually lead to shorter cilia. But in contrast, in this study an increased ciliary length was observed. A possible explanation would be that the lost microtubule stabilizing effect in SSNA1 KO cells, which results in longer cilia, is stronger compared to the opposing effect of downregulated Shh leading to shorter cilia. The influence of SSNA1 on SuFu and the Sonic hedgehog pathway in this context will be determined by investigating ciliary localization of SuFu, Ptch1 and GliA respectively GliR. The observed signaling phenotype of SSNA1 KO cells as well as increased ciliary length and reduced Shh, will be rescued by ectopic expression of SSNA1 wt in KO cells. This rescue experiment serves to exclude CRISPR/Cas9 related off-target effects and for further verification of the generated KO cells.

To analyze the interaction of Lebercilin and SSNA1, previously described by the Syscilia consortium, RPE1 SSNA1 ex1 KO and control cells were treated with SAG, to activate Shh pathway. It appeared that the LCA5 signal intensity was increased in SSNA1 ex1 KO cells (**Figure 44**). This ciliary accumulation of Lebercilin related to the SSNA1 KO implies an involvement of SSNA1 in proper ciliary LCA5 localization or even expression. Whether other proteins will also accumulate or if this is LCA5 specific, needs to be determined in further experiments. In addition, this result verified the involvement of SSNA1 and Lebercilin in Sonic hedgehog signaling. It also suggests that the function of these proteins is likely influenced by the other.

At the tip of the cilium, microtubule ends are covered with ciliary cap. These caps were proposed to control axoneme length and stabilization, but their function is poorly understood [170]. Nevertheless, SSNA1 and Lebercilin localize to the ciliary tip and might have complementing roles in ciliary cap mediated microtubule stabilization. Implying, that the rapid degeneration of photoreceptors in LCA could be caused by SSNA1 dependent decreased

microtubule stability. Therefore, a potential Lebercilin dependent transport of Rhodopsin will be investigated in SSNA1 KO background.

Unfortunately, SSNA1 could not be localized in the human photoreceptors so far. Similarly, it is unclear if Sonic hedgehog signaling occurs. This is especially relevant since LCA has only a phenotype in retinal tissue. The observed severe phenotype caused by Lebercilin mutations might be caused by missing SSNA1 and its microtubule stabilizing effect. Therefore, the validation of a functional relevance of SSNA1 and Shh as well as a co-localization of Lebercilin and SSNA1 in human photoreceptors is of utmost importance for further investigating LCA.

Overall, this data gathered here highlights the importance of SSNA1/LCA5 interaction and the need to generate and analyze a specific LCA5/SSNA1 double-KO cells. To better understand LCA5 function in Leber congenital amaurosis, SSNA1 function will be further explored and the nature of SSNA1 interaction with LCA5 characterized. To unravel the mechanism resulting in Leber congenital amaurosis the nature of Lebercilin-SSNA1 interaction has yet to be understood.

7. References

1. Ishikawa, H. and W.F. Marshall, *Ciliogenesis: building the cell's antenna.* Nat Rev Mol Cell Biol, 2011. 12(4): p. 222-34.
2. Berbari, N.F., et al., *The primary cilium as a complex signaling center.* Curr Biol, 2009. 19(13): p. R526-35.
3. Wheway, G., L. Nazlamova, and J.T. Hancock, *Signaling through the Primary Cilium.* Front Cell Dev Biol, 2018. 6: p. 8.
4. Wheatley, D.N., *Primary cilia in normal and pathological tissues.* Pathobiology, 1995. 63(4): p. 222-38.
5. Satir, P. and S.T. Christensen, *Overview of structure and function of mammalian cilia.* Annu Rev Physiol, 2007. 69: p. 377-400.
6. Pazour, G.J. and G.B. Witman, *The vertebrate primary cilium is a sensory organelle.* Curr Opin Cell Biol, 2003. 15(1): p. 105-10.
7. Lee, J. and Y.D. Chung, *Ciliary subcompartments: how are they established and what are their functions?* BMB Rep, 2015. 48(7): p. 380-7.
8. Hoffmann, F., et al., *TTC30A and TTC30B Redundancy Protects IFT Complex B Integrity and Its Pivotal Role in Ciliogenesis.* Genes (Basel), 2022. 13(7).
9. Ishikawa, H. and W.F. Marshall, *Intraflagellar Transport and Ciliary Dynamics.* Cold Spring Harb Perspect Biol, 2017. 9(3).
10. Kozminski, K.G., et al., *A motility in the eukaryotic flagellum unrelated to flagellar beating.* Proc Natl Acad Sci U S A, 1993. 90(12): p. 5519-23.
11. Lechtreck, K.F., *IFT-Cargo Interactions and Protein Transport in Cilia.* Trends Biochem Sci, 2015. 40(12): p. 765-778.
12. Cole, D.G., et al., *Chlamydomonas kinesin-II-dependent intraflagellar transport (IFT): IFT particles contain proteins required for ciliary assembly in Caenorhabditis elegans sensory neurons.* J Cell Biol, 1998. 141(4): p. 993-1008.
13. Katoh, Y., et al., *Overall Architecture of the Intraflagellar Transport (IFT)-B Complex Containing Cluap1/IFT38 as an Essential Component of the IFT-B Peripheral Subcomplex.* J Biol Chem, 2016. 291(21): p. 10962-75.
14. Young, R.W., *The renewal of photoreceptor cell outer segments.* J Cell Biol, 1967. 33(1): p. 61-72.
15. Wang, J.S. and V.J. Kefalov, *The cone-specific visual cycle.* Prog Retin Eye Res, 2011. 30(2): p. 115-28.
16. Rosenbaum, J.L., D.G. Cole, and D.R. Diener, *Intraflagellar transport: the eyes have it.* J Cell Biol, 1999. 144(3): p. 385-8.
17. Besharse, J., C. Horst, and R. Bloodgood, *Ciliary and flagellar membranes.* The photoreceptor connecting cilium: a model for the transition zone. Plenum, New York, 1990: p. 389-417.
18. Pazour, G.J., et al., *The intraflagellar transport protein, IFT88, is essential for vertebrate photoreceptor assembly and maintenance.* J Cell Biol, 2002. 157(1): p. 103-13.
19. Waters, A.M. and P.L. Beales, *Ciliopathies: an expanding disease spectrum.* Pediatr Nephrol, 2011. 26(7): p. 1039-56.
20. Hildebrandt, F., T. Benzing, and N. Katsanis, *Ciliopathies.* N Engl J Med, 2011. 364(16): p. 1533-43.

21. Reiter, J.F. and M.R. Leroux, *Genes and molecular pathways underpinning ciliopathies.* Nat Rev Mol Cell Biol, 2017. **18**(9): p. 533-547.
22. Kumaran, N., et al., *Leber congenital amaurosis/early-onset severe retinal dystrophy: clinical features, molecular genetics and therapeutic interventions.* Br J Ophthalmol, 2017. **101**(9): p. 1147-1154.
23. den Hollander, A.I., et al., *Leber congenital amaurosis: genes, proteins and disease mechanisms.* Prog Retin Eye Res, 2008. **27**(4): p. 391-419.
24. Qu, Z., et al., *Knocking out lca5 in zebrafish causes cone-rod dystrophy due to impaired outer segment protein trafficking.* Biochim Biophys Acta Mol Basis Dis, 2019. **1865**(10): p. 2694-2705.
25. Viswarubhiny, S., et al., *Clinical exome sequencing facilitates the understanding of genetic heterogeneity in Leber congenital amaurosis patients with variable phenotype in southern India.* Eye Vis (Lond), 2021. **8**(1): p. 20.
26. Boldt, K., et al., *An organelle-specific protein landscape identifies novel diseases and molecular mechanisms.* Nat Commun, 2016. **7**: p. 11491.
27. Pfannenschmid, F., et al., *Chlamydomonas DIP13 and human NA14: a new class of proteins associated with microtubule structures is involved in cell division.* J Cell Sci, 2003. **116**(Pt 8): p. 1449-62.
28. Lai, C.K., et al., *Functional characterization of putative cilia genes by high-content analysis.* Mol Biol Cell, 2011. **22**(7): p. 1104-19.
29. Lettice, L.A., et al., *A long-range Shh enhancer regulates expression in the developing limb and fin and is associated with preaxial polydactyly.* Hum Mol Genet, 2003. **12**(14): p. 1725-35.
30. Robbins, D.J., D.L. Fei, and N.A. Riobo, *The Hedgehog signal transduction network.* Sci Signal, 2012. **5**(246): p. re6.
31. Takei, R., Y. Katoh, and K. Nakayama, *Robust interaction of IFT70 with IFT52-IFT88 in the IFT-B complex is required for ciliogenesis.* Biol Open, 2018. **7**(5).
32. Pathak, N., et al., *The zebrafish fleer gene encodes an essential regulator of cilia tubulin polyglutamylation.* Mol Biol Cell, 2007. **18**(11): p. 4353-64.
33. Du, Y., et al., *A rare TTC30B variant is identified as a candidate for synpolydactyly in a Chinese pedigree.* Bone, 2019. **127**: p. 503-509.
34. Lawrence, E.J., et al., *SSNA1 stabilizes dynamic microtubules and detects microtubule damage.* Elife, 2021. **10**.
35. Davenport, J.R. and B.K. Yoder, *An incredible decade for the primary cilium: a look at a once-forgotten organelle.* Am J Physiol Renal Physiol, 2005. **289**(6): p. F1159-69.
36. Porter, M.E. and W.S. Sale, *The 9 + 2 axoneme anchors multiple inner arm dyneins and a network of kinases and phosphatases that control motility.* J Cell Biol, 2000. **151**(5): p. F37-42.
37. Luck, D.J., *Genetic and biochemical dissection of the eucaryotic flagellum.* J Cell Biol, 1984. **98**(3): p. 789-94.
38. Satir, P. and M.A. Sleigh, *The physiology of cilia and mucociliary interactions.* Annu Rev Physiol, 1990. **52**: p. 137-55.
39. Afzelius, B.A., *Asymmetry of cilia and of mice and men.* Int J Dev Biol, 1999. **43**(4): p. 283-6.
40. Singla, V. and J.F. Reiter, *The primary cilium as the cell's antenna: signaling at a sensory organelle.* Science, 2006. **313**(5787): p. 629-33.

41. Eggenschwiler, J.T. and K.V. Anderson, *Cilia and developmental signaling.* Annu Rev Cell Dev Biol, 2007. **23**: p. 345-73.
42. Liang, Y., et al., *Mechanism of ciliary disassembly.* Cell Mol Life Sci, 2016. **73**(9): p. 1787-802.
43. Li, S., et al., *Three-dimensional structure of basal body triplet revealed by electron cryo-tomography.* EMBO J, 2012. **31**(3): p. 552-62.
44. Rohatgi, R. and W.J. Snell, *The ciliary membrane.* Curr Opin Cell Biol, 2010. **22**(4): p. 541-6.
45. Mitchison, H.M. and E.M. Valente, *Motile and non-motile cilia in human pathology: from function to phenotypes.* J Pathol, 2017. **241**(2): p. 294-309.
46. Anvarian, Z., et al., *Cellular signalling by primary cilia in development, organ function and disease.* Nat Rev Nephrol, 2019. **15**(4): p. 199-219.
47. Kobayashi, T. and B.D. Dynlacht, *Regulating the transition from centriole to basal body.* J Cell Biol, 2011. **193**(3): p. 435-44.
48. Huber, L.A., et al., *Rab8, a small GTPase involved in vesicular traffic between the TGN and the basolateral plasma membrane.* J Cell Biol, 1993. **123**(1): p. 35-45.
49. Nigg, E.A. and T. Stearns, *The centrosome cycle: Centriole biogenesis, duplication and inherent asymmetries.* Nat Cell Biol, 2011. **13**(10): p. 1154-60.
50. Reiter, J.F., O.E. Blacque, and M.R. Leroux, *The base of the cilium: roles for transition fibres and the transition zone in ciliary formation, maintenance and compartmentalization.* EMBO Rep, 2012. **13**(7): p. 608-18.
51. Garcia-Gonzalo, F.R. and J.F. Reiter, *Open Sesame: How Transition Fibers and the Transition Zone Control Ciliary Composition.* Cold Spring Harb Perspect Biol, 2017. **9**(2).
52. Izawa, I., et al., *Current topics of functional links between primary cilia and cell cycle.* Cilia, 2015. **4**: p. 12.
53. Gherman, A., E.E. Davis, and N. Katsanis, *The ciliary proteome database: an integrated community resource for the genetic and functional dissection of cilia.* Nat Genet, 2006. **38**(9): p. 961-2.
54. Deane, J.A., et al., *Localization of intraflagellar transport protein IFT52 identifies basal body transitional fibers as the docking site for IFT particles.* Curr Biol, 2001. **11**(20): p. 1586-90.
55. Pazour, G.J. and R.A. Bloodgood, *Targeting proteins to the ciliary membrane.* Curr Top Dev Biol, 2008. **85**: p. 115-49.
56. Kim, S. and L. Tsiokas, *Cilia and cell cycle re-entry: more than a coincidence.* Cell Cycle, 2011. **10**(16): p. 2683-90.
57. Tucker, R.W., A.B. Pardee, and K. Fujiwara, *Centriole ciliation is related to quiescence and DNA synthesis in 3T3 cells.* Cell, 1979. **17**(3): p. 527-35.
58. Tucker, R.W., C.D. Scher, and C.D. Stiles, *Centriole deciliation associated with the early response of 3T3 cells to growth factors but not to SV40.* Cell, 1979. **18**(4): p. 1065-72.
59. Rosenbaum, J., *Intraflagellar transport.* Curr Biol, 2002. **12**(4): p. R125.
60. Scholey, J.M., *Intraflagellar transport motors in cilia: moving along the cell's antenna.* J Cell Biol, 2008. **180**(1): p. 23-9.
61. Pazour, G.J., B.L. Dickert, and G.B. Witman, *The DHC1b (DHC2) isoform of cytoplasmic dynein is required for flagellar assembly.* J Cell Biol, 1999. **144**(3): p. 473-81.
62. Vashishtha, M., Z. Walther, and J.L. Hall, *The kinesin-homologous protein encoded by the Chlamydomonas FLA10 gene is associated with basal bodies and centrioles.* J Cell Sci, 1996. **109 (Pt 3)**: p. 541-9.

63. Taschner, M. and E. Lorentzen, *The Intraflagellar Transport Machinery.* Cold Spring Harb Perspect Biol, 2016. **8**(10).
64. Taschner, M., et al., *Intraflagellar transport proteins 172, 80, 57, 54, 38, and 20 form a stable tubulin-binding IFT-B2 complex.* EMBO J, 2016. **35**(7): p. 773-90.
65. Petriman, N.A., et al., *Biochemically validated structural model of the 15-subunit IFT-B complex.* bioRxiv, 2022: p. 2022.08.20.504624.
66. Taschner, M., et al., *Crystal structures of IFT70/52 and IFT52/46 provide insight into intraflagellar transport B core complex assembly.* J Cell Biol, 2014. **207**(2): p. 269-82.
67. Fan, Z.C., et al., *Chlamydomonas IFT70/CrDYF-1 is a core component of IFT particle complex B and is required for flagellar assembly.* Mol Biol Cell, 2010. **21**(15): p. 2696-706.
68. Taschner, M., et al., *Biochemical mapping of interactions within the intraflagellar transport (IFT) B core complex: IFT52 binds directly to four other IFT-B subunits.* J Biol Chem, 2011. **286**(30): p. 26344-52.
69. Bobinnec, Y., et al., *Centriole disassembly in vivo and its effect on centrosome structure and function in vertebrate cells.* J Cell Biol, 1998. **143**(6): p. 1575-89.
70. Redeker, V., et al., *Mutations of tubulin glycylation sites reveal cross-talk between the C termini of alpha- and beta-tubulin and affect the ciliary matrix in Tetrahymena.* J Biol Chem, 2005. **280**(1): p. 596-606.
71. Pathak, N., C.A. Austin, and I.A. Drummond, *Tubulin tyrosine ligase-like genes ttll3 and ttll6 maintain zebrafish cilia structure and motility.* J Biol Chem, 2011. **286**(13): p. 11685-95.
72. Pathak, N., et al., *Cytoplasmic carboxypeptidase 5 regulates tubulin glutamylation and zebrafish cilia formation and function.* Mol Biol Cell, 2014. **25**(12): p. 1836-44.
73. Khanna, H., *Photoreceptor Sensory Cilium: Traversing the Ciliary Gate.* Cells, 2015. **4**(4): p. 674-86.
74. Guo, D., et al., *Tmem138 is localized to the connecting cilium essential for rhodopsin localization and outer segment biogenesis.* Proc Natl Acad Sci U S A, 2022. **119**(15): p. e2109934119.
75. Cote, R., *Photoreceptor Phosphodiesterase (PDE6): A G-Protein-Activated PDE Regulating Visual Excitation in Rod and Cone Photoreceptor Cells*. 2006. p. 165-193.
76. Quinlan, R.J., J.L. Tobin, and P.L. Beales, *Modeling ciliopathies: Primary cilia in development and disease.* Curr Top Dev Biol, 2008. **84**: p. 249-310.
77. Arts, H.H. and N.V. Knoers, *Current insights into renal ciliopathies: what can genetics teach us?* Pediatr Nephrol, 2013. **28**(6): p. 863-74.
78. Sahel, J.A., *Spotlight on childhood blindness.* J Clin Invest, 2011. **121**(6): p. 2145-9.
79. den Hollander, A.I., et al., *Mutations in LCA5, encoding the ciliary protein lebercilin, cause Leber congenital amaurosis.* Nat Genet, 2007. **39**(7): p. 889-95.
80. Boldt, K., et al., *Disruption of intraflagellar protein transport in photoreceptor cilia causes Leber congenital amaurosis in humans and mice.* J Clin Invest, 2011. **121**(6): p. 2169-80.
81. Szaniszlo, T., et al., *The interaction between LC8 and LCA5 reveals a novel oligomerization function of LC8 in the ciliary-centrosome system.* Sci Rep, 2022. **12**(1): p. 15623.
82. Salisbury, J.L., *Centrosomes: coiled-coils organize the cell center.* Curr Biol, 2003. **13**(3): p. R88-90.

83. van Dam, T.J., et al., *The SYSCILIA gold standard (SCGSv1) of known ciliary components and its applications within a systems biology consortium.* Cilia, 2013. **2**(1): p. 7.
84. Gavin, A.C., et al., *Proteome survey reveals modularity of the yeast cell machinery.* Nature, 2006. **440**(7084): p. 631-6.
85. Ramos-Morales, F., et al., *NA14 is a novel nuclear autoantigen with a coiled-coil domain.* J Biol Chem, 1998. **273**(3): p. 1634-9.
86. Goyal, U., et al., *Spastin-interacting protein NA14/SSNA1 functions in cytokinesis and axon development.* PLoS One, 2014. **9**(11): p. e112428.
87. Basnet, N., et al., *Direct induction of microtubule branching by microtubule nucleation factor SSNA1.* Nat Cell Biol, 2018. **20**(10): p. 1172-1180.
88. Rohatgi, R., L. Milenkovic, and M.P. Scott, *Patched1 regulates hedgehog signaling at the primary cilium.* Science, 2007. **317**(5836): p. 372-6.
89. Arensdorf, A.M., S. Marada, and S.K. Ogden, *Smoothened Regulation: A Tale of Two Signals.* Trends Pharmacol Sci, 2016. **37**(1): p. 62-72.
90. Mukhopadhyay, S., et al., *The ciliary G-protein-coupled receptor Gpr161 negatively regulates the Sonic hedgehog pathway via cAMP signaling.* Cell, 2013. **152**(1-2): p. 210-23.
91. Humke, E.W., et al., *The output of Hedgehog signaling is controlled by the dynamic association between Suppressor of Fused and the Gli proteins.* Genes Dev, 2010. **24**(7): p. 670-82.
92. Taylor, S.S., et al., *PKA: lessons learned after twenty years.* Biochim Biophys Acta, 2013. **1834**(7): p. 1271-8.
93. Niewiadomski, P., et al., *Gli Proteins: Regulation in Development and Cancer.* Cells, 2019. **8**(2).
94. Wang, B. and Y. Li, *Evidence for the direct involvement of {beta}TrCP in Gli3 protein processing.* Proc Natl Acad Sci U S A, 2006. **103**(1): p. 33-8.
95. Mukhopadhyay, S. and R. Rohatgi, *G-protein-coupled receptors, Hedgehog signaling and primary cilia.* Semin Cell Dev Biol, 2014. **33**: p. 63-72.
96. Cohen, M., et al., *Ptch1 and Gli regulate Shh signalling dynamics via multiple mechanisms.* Nat Commun, 2015. **6**: p. 6709.
97. Corbit, K.C., et al., *Vertebrate Smoothened functions at the primary cilium.* Nature, 2005. **437**(7061): p. 1018-21.
98. Chen, Y., et al., *Dual Phosphorylation of suppressor of fused (Sufu) by PKA and GSK3beta regulates its stability and localization in the primary cilium.* J Biol Chem, 2011. **286**(15): p. 13502-11.
99. Wang, C., Y. Pan, and B. Wang, *Suppressor of fused and Spop regulate the stability, processing and function of Gli2 and Gli3 full-length activators but not their repressors.* Development, 2010. **137**(12): p. 2001-9.
100. Niewiadomski, P., et al., *Gli protein activity is controlled by multisite phosphorylation in vertebrate Hedgehog signaling.* Cell Rep, 2014. **6**(1): p. 168-181.
101. Goetz, S.C. and K.V. Anderson, *The primary cilium: a signalling centre during vertebrate development.* Nat Rev Genet, 2010. **11**(5): p. 331-44.
102. Huangfu, D., et al., *Hedgehog signalling in the mouse requires intraflagellar transport proteins.* Nature, 2003. **426**(6962): p. 83-7.
103. Huangfu, D. and K.V. Anderson, *Cilia and Hedgehog responsiveness in the mouse.* Proc Natl Acad Sci U S A, 2005. **102**(32): p. 11325-30.

104. Singh, J., X. Wen, and S.J. Scales, *The Orphan G Protein-coupled Receptor Gpr175 (Tpra40) Enhances Hedgehog Signaling by Modulating cAMP Levels.* J Biol Chem, 2015. 290(49): p. 29663-75.
105. Santos, N. and J.F. Reiter, *A central region of Gli2 regulates its localization to the primary cilium and transcriptional activity.* J Cell Sci, 2014. 127(Pt 7): p. 1500-10.
106. Jacob, L.S., et al., *Genome-wide RNAi screen reveals disease-associated genes that are common to Hedgehog and Wnt signaling.* Sci Signal, 2011. 4(157): p. ra4.
107. Eguether, T. and M. Hahne, *Mixed signals from the cell's antennae: primary cilia in cancer.* EMBO Rep, 2018. 19(11).
108. Gloeckner, C.J., K. Boldt, and M. Ueffing, *Strep/FLAG tandem affinity purification (SF-TAP) to study protein interactions.* Curr Protoc Protein Sci, 2009. Chapter 19: p. Unit19 20.
109. Stemmer, M., et al., *CCTop: An Intuitive, Flexible and Reliable CRISPR/Cas9 Target Prediction Tool.* PLoS One, 2015. 10(4): p. e0124633.
110. Labuhn, M., et al., *Refined sgRNA efficacy prediction improves large- and small-scale CRISPR-Cas9 applications.* Nucleic Acids Res, 2018. 46(3): p. 1375-1385.
111. Meijering, E., et al., *Design and validation of a tool for neurite tracing and analysis in fluorescence microscopy images.* Cytometry A, 2004. 58(2): p. 167-76.
112. Schindelin, J., et al., *Fiji: an open-source platform for biological-image analysis.* Nat Methods, 2012. 9(7): p. 676-82.
113. Cox, J. and M. Mann, *MaxQuant enables high peptide identification rates, individualized p.p.b.-range mass accuracies and proteome-wide protein quantification.* Nat Biotechnol, 2008. 26(12): p. 1367-72.
114. Tyanova, S., et al., *The Perseus computational platform for comprehensive analysis of (prote)omics data.* Nat Methods, 2016. 13(9): p. 731-40.
115. Cevik, S., et al., *Joubert syndrome Arl13b functions at ciliary membranes and stabilizes protein transport in Caenorhabditis elegans.* J Cell Biol, 2010. 188(6): p. 953-69.
116. Keeling, J., L. Tsiokas, and D. Maskey, *Cellular Mechanisms of Ciliary Length Control.* Cells, 2016. 5(1).
117. He, K., K. Ling, and J. Hu, *The emerging role of tubulin posttranslational modifications in cilia and ciliopathies.* Biophysics Reports, 2020. 6(4): p. 89-104.
118. Beyer, T., et al., *Tissue- and isoform-specific protein complex analysis with natively processed bait proteins.* J Proteomics, 2021. 231: p. 103947.
119. Yang, J., et al., *Rootletin, a novel coiled-coil protein, is a structural component of the ciliary rootlet.* J Cell Biol, 2002. 159(3): p. 431-40.
120. Bahe, S., et al., *Rootletin forms centriole-associated filaments and functions in centrosome cohesion.* J Cell Biol, 2005. 171(1): p. 27-33.
121. Turn, R.E., et al., *Roles for ELMOD2 and Rootletin in ciliogenesis.* Mol Biol Cell, 2021. 32(8): p. 800-822.
122. London, E. and C.A. Stratakis, *The regulation of PKA signaling in obesity and in the maintenance of metabolic health.* Pharmacol Ther, 2022. 237: p. 108113.
123. Ding, X. and J.L. Staudinger, *Induction of drug metabolism by forskolin: the role of the pregnane X receptor and the protein kinase a signal transduction pathway.* J Pharmacol Exp Ther, 2005. 312(2): p. 849-56.
124. Montminy, M., *Transcriptional regulation by cyclic AMP.* Annu Rev Biochem, 1997. 66: p. 807-22.

125. Bragina, O., et al., *Smoothened agonist augments proliferation and survival of neural cells.* Neurosci Lett, 2010. **482**(2): p. 81-5.
126. Lee, H.J., H.J. Kim, and S.J. Lee, *Mismatch Intolerance of 5'-Truncated sgRNAs in CRISPR/Cas9 Enables Efficient Microbial Single-Base Genome Editing.* Int J Mol Sci, 2021. **22**(12).
127. Adli, M., *The CRISPR tool kit for genome editing and beyond.* Nat Commun, 2018. **9**(1): p. 1911.
128. Adli, M., *The Biology and Application Areas of CRISPR Technologies.* J Mol Biol, 2019. **431**(1): p. 1-2.
129. Simon, R., et al., *The Non-Hodgkin Lymphoma Pathologic Classification Project. Long-term follow-up of 1153 patients with non-Hodgkin lymphomas.* Ann Intern Med, 1988. **109**(12): p. 939-45.
130. Gibson, T.J., M. Seiler, and R.A. Veitia, *The transience of transient overexpression.* Nat Methods, 2013. **10**(8): p. 715-21.
131. Berbari, N.F., et al., *Mutations in Traf3ip1 reveal defects in ciliogenesis, embryonic development, and altered cell size regulation.* Dev Biol, 2011. **360**(1): p. 66-76.
132. Pasek, R.C., et al., *Mammalian Clusterin associated protein 1 is an evolutionarily conserved protein required for ciliogenesis.* Cilia, 2012. **1**(1): p. 20.
133. Quelin, C., et al., *Loss of function IFT27 variants associated with an unclassified lethal fetal ciliopathy with renal agenesis.* Am J Med Genet A, 2018. **176**(7): p. 1610-1613.
134. Howard, P.W., S.F. Jue, and R.A. Maurer, *Interaction of mouse TTC30/DYF-1 with multiple intraflagellar transport complex B proteins and KIF17.* Exp Cell Res, 2013. **319**(14): p. 2275-81.
135. Getwan, M., et al., *Ttc30a affects tubulin modifications in a model for ciliary chondrodysplasia with polycystic kidney disease.* Proc Natl Acad Sci U S A, 2021. **118**(39).
136. He, K., et al., *Axoneme polyglutamylation regulated by Joubert syndrome protein ARL13B controls ciliary targeting of signaling molecules.* Nat Commun, 2018. **9**(1): p. 3310.
137. Kanamaru, T., et al., *Balancing the length of the distal tip by septins is key for stability and signalling function of primary cilia.* EMBO J, 2022. **41**(1): p. e108843.
138. Lu, Q., et al., *Early steps in primary cilium assembly require EHD1/EHD3-dependent ciliary vesicle formation.* Nat Cell Biol, 2015. **17**(4): p. 531.
139. Zhang, X., et al., *SUN1/2 and Syne/Nesprin-1/2 complexes connect centrosome to the nucleus during neurogenesis and neuronal migration in mice.* Neuron, 2009. **64**(2): p. 173-87.
140. Mojarad, B.A., et al., *CEP19 cooperates with FOP and CEP350 to drive early steps in the ciliogenesis programme.* Open Biol, 2017. **7**(6).
141. Chen, C., et al., *An ER complex of ODR-4 and ODR-8/Ufm1 specific protease 2 promotes GPCR maturation by a Ufm1-independent mechanism.* PLoS Genet, 2014. **10**(3): p. e1004082.
142. Nechipurenko, I.V., et al., *A Conserved Role for Girdin in Basal Body Positioning and Ciliogenesis.* Dev Cell, 2016. **38**(5): p. 493-506.
143. Robinson, A.M., et al., *CAMSAP3 facilitates basal body polarity and the formation of the central pair of microtubules in motile cilia.* Proc Natl Acad Sci U S A, 2020. **117**(24): p. 13571-13579.

144. Khan, S.Y., et al., *Mutations of the RDX gene cause nonsyndromic hearing loss at the DFNB24 locus.* Hum Mutat, 2007. **28**(5): p. 417-23.
145. Chen, D., et al., *SKI activates Wnt/beta-catenin signaling in human melanoma.* Cancer Res, 2003. **63**(20): p. 6626-34.
146. Takahata, M., et al., *SKI and MEL1 cooperate to inhibit transforming growth factor-beta signal in gastric cancer cells.* J Biol Chem, 2009. **284**(5): p. 3334-3344.
147. Dominguez, I., G.E. Sonenshein, and D.C. Seldin, *Protein kinase CK2 in health and disease: CK2 and its role in Wnt and NF-kappaB signaling: linking development and cancer.* Cell Mol Life Sci, 2009. **66**(11-12): p. 1850-7.
148. Tang, H.Y., et al., *EDEM2 and OS-9 are required for ER-associated degradation of non-glycosylated sonic hedgehog.* PLoS One, 2014. **9**(6): p. e92164.
149. Chen, K., et al., *Methyltransferase SETD2-Mediated Methylation of STAT1 Is Critical for Interferon Antiviral Activity.* Cell, 2017. **170**(3): p. 492-506 e14.
150. Yang, J., et al., *The ciliary rootlet maintains long-term stability of sensory cilia.* Mol Cell Biol, 2005. **25**(10): p. 4129-37.
151. Mohan, S., et al., *Striated rootlet and nonfilamentous forms of rootletin maintain ciliary function.* Curr Biol, 2013. **23**(20): p. 2016-22.
152. Bochman, M.L. and A. Schwacha, *The Mcm complex: unwinding the mechanism of a replicative helicase.* Microbiol Mol Biol Rev, 2009. **73**(4): p. 652-83.
153. Casar Tena, T., et al., *Resting cells rely on the DNA helicase component MCM2 to build cilia.* Nucleic Acids Res, 2019. **47**(1): p. 134-151.
154. Arveseth, C.D., et al., *Smoothened transduces Hedgehog signals via activity-dependent sequestration of PKA catalytic subunits.* PLoS Biol, 2021. **19**(4): p. e3001191.
155. Mourao, A., S.T. Christensen, and E. Lorentzen, *The intraflagellar transport machinery in ciliary signaling.* Curr Opin Struct Biol, 2016. **41**: p. 98-108.
156. Kobayashi, T., et al., *Cooperation of the IFT-A complex with the IFT-B complex is required for ciliary retrograde protein trafficking and GPCR import.* Mol Biol Cell, 2021. **32**(1): p. 45-56.
157. Kogel, A., et al., *The human SKI complex regulates channeling of ribosome-bound RNA to the exosome via an intrinsic gatekeeping mechanism.* Mol Cell, 2022. **82**(4): p. 756-769 e8.
158. Thevenon, J., et al., *Autosomal recessive IFT57 hypomorphic mutation cause ciliary transport defect in unclassified oral-facial-digital syndrome with short stature and brachymesophalangia.* Clin Genet, 2016. **90**(6): p. 509-517.
159. Uhlen, M., et al., *Proteomics. Tissue-based map of the human proteome.* Science, 2015. **347**(6220): p. 1260419.
160. Liem, K.F., Jr., et al., *Mouse Kif7/Costal2 is a cilia-associated protein that regulates Sonic hedgehog signaling.* Proc Natl Acad Sci U S A, 2009. **106**(32): p. 13377-82.
161. He, M., et al., *The kinesin-4 protein Kif7 regulates mammalian Hedgehog signalling by organizing the cilium tip compartment.* Nat Cell Biol, 2014. **16**(7): p. 663-72.
162. Gupta, G.D., et al., *A Dynamic Protein Interaction Landscape of the Human Centrosome-Cilium Interface.* Cell, 2015. **163**(6): p. 1484-99.
163. Boylan, J.P. and A.F. Wright, *Identification of a novel protein interacting with RPGR.* Hum Mol Genet, 2000. **9**(14): p. 2085-93.
164. Roepman, R., et al., *The retinitis pigmentosa GTPase regulator (RPGR) interacts with novel transport-like proteins in the outer segments of rod photoreceptors.* Hum Mol Genet, 2000. **9**(14): p. 2095-105.

165. Hong, D.H., et al., *Retinitis pigmentosa GTPase regulator (RPGRr)-interacting protein is stably associated with the photoreceptor ciliary axoneme and anchors RPGR to the connecting cilium.* J Biol Chem, 2001. **276**(15): p. 12091-9.
166. Khanna, H., et al., *RPGR-ORF15, which is mutated in retinitis pigmentosa, associates with SMC1, SMC3, and microtubule transport proteins.* J Biol Chem, 2005. **280**(39): p. 33580-7.
167. Hong, D.H., et al., *A single, abbreviated RPGR-ORF15 variant reconstitutes RPGR function in vivo.* Invest Ophthalmol Vis Sci, 2005. **46**(2): p. 435-41.
168. Hong, D.H., et al., *Dominant, gain-of-function mutant produced by truncation of RPGR.* Invest Ophthalmol Vis Sci, 2004. **45**(1): p. 36-41.
169. Murga-Zamalloa, C.A., et al., *Interaction of retinitis pigmentosa GTPase regulator (RPGR) with RAB8A GTPase: implications for cilia dysfunction and photoreceptor degeneration.* Hum Mol Genet, 2010. **19**(18): p. 3591-8.
170. Soares, H., et al., *Cilia Distal Domain: Diversity in Evolutionarily Conserved Structures.* Cells, 2019. **8**(2).
171. Corpet, F., *Multiple sequence alignment with hierarchical clustering.* Nucleic Acids Res, 1988. **16**(22): p. 10881-90.

8. Appendix

8.1. Additional figures and tables

1. TTC30A and TTC30B nucleotide sequences

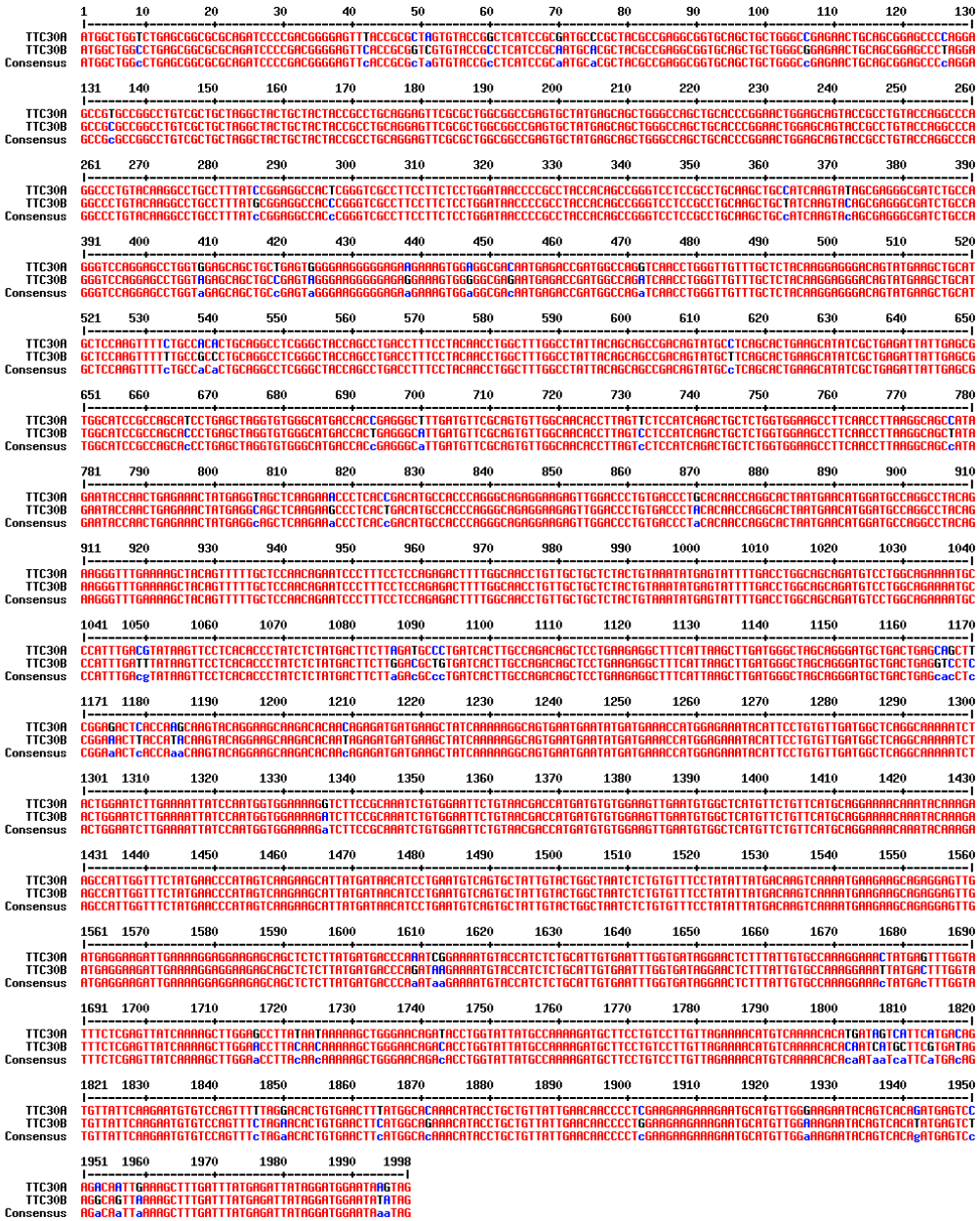

Appendix 1 – Alignment of TTC30A and TTC30B nucleotide sequences using multiple sequence alignment tool *[171]*. Different base pairs are depicted in blue, similarities in red. [8]

2. MaxQuant Settings

Parameter	Value	Machine name	ADMIN-PC
Version	1.6.1.0	Date of writing	05/22/2021 10:07:11
User name	mpcadmin	Fixed modifications	Carbamidomethyl (C)

Include contaminants	True
PSM FDR	0.01
XPSM FDR	0.01
Protein FDR	0.01
Site FDR	0.01
Use Normalized Ratios For Occupancy	True
Min. peptide Length	7
Min. score for unmodified peptides	0
Min. score for modified peptides	40
Min. delta score for unmodified peptides	0
Min. delta score for modified peptides	6
Min. unique peptides	0
Min. razor peptides	1
Min. peptides	1
Use only unmodified peptides and	False
Peptides used for protein quantification	Razor
Discard unmodified counterpart peptides	True
Label min. ratio count	2
Use delta score	False
iBAQ	False
iBAQ log fit	False
Match between runs	True
Matching time window [min]	0.7
Alignment time window [min]	20
Find dependent peptides	False
Fasta file	C:\Databases\SwissProt human 201911.fasta
Decoy mode	revert
Include contaminants	True
Advanced ratios	True
Fixed andromeda index folder	
Temporary folder	
Combined folder location	
Second peptides	True
Stabilize large LFQ ratios	True
Separate LFQ in parameter groups	False
Require MS/MS for LFQ comparisons	False
Calculate peak properties	False
Main search max. combinations	200
Advanced site intensities	True
LFQ norm for sites and peptides	False
Write msScans table	True
Write msmsScans table	True
Write ms3Scans table	True
Write allPeptides table	True
Write mzRange table	True
Write pasefMsmsScans table	True
Write accumulatedPasefMsmsScans table	True
Max. peptide mass [Da]	4600
Min. peptide length for unspecific search	8
Max. peptide length for unspecific search	25
Razor protein FDR	True
Disable MD5	False
Max mods in site table	3
Match unidentified features	True
MS/MS tol. (FTMS)	20 ppm
Top MS/MS peaks per Da interval. (FTMS)	12
Da interval. (FTMS)	100
MS/MS deisotoping (FTMS)	True
MS/MS deisotoping tolerance (FTMS)	7
MS/MS deisotoping tolerance unit (FTMS)	ppm
MS/MS higher charges (FTMS)	True
MS/MS water loss (FTMS)	True
MS/MS ammonia loss (FTMS)	True
MS/MS dependent losses (FTMS)	True
MS/MS recalibration (FTMS)	False
MS/MS tol. (ITMS)	0.5 Da
Top MS/MS peaks per Da interval. (ITMS)	8
Da interval. (ITMS)	100
MS/MS deisotoping (ITMS)	False
MS/MS deisotoping tolerance (ITMS)	0.15
MS/MS deisotoping tolerance unit (ITMS)	Da
MS/MS higher charges (ITMS)	True
MS/MS water loss (ITMS)	True
MS/MS ammonia loss (ITMS)	True
MS/MS dependent losses (ITMS)	True
MS/MS recalibration (ITMS)	False
MS/MS tol. (TOF)	40 ppm
Top MS/MS peaks per Da interval. (TOF)	10
Da interval. (TOF)	100
MS/MS deisotoping (TOF)	True
MS/MS deisotoping tolerance (TOF)	0.01
MS/MS deisotoping tolerance unit (TOF)	Da
MS/MS higher charges (TOF)	True
MS/MS water loss (TOF)	True
MS/MS ammonia loss (TOF)	True
MS/MS dependent losses (TOF)	True
MS/MS recalibration (TOF)	False
MS/MS tol. (Unknown)	0.5 Da
Top MS/MS peaks per Da interval. (Unknown)	8
Da interval. (Unknown)	100
MS/MS deisotoping (Unknown)	False
MS/MS deisotoping tolerance (Unknown)	0.15
MS/MS deisotoping tolerance unit (Unknown)	Da
MS/MS higher charges (Unknown)	True
MS/MS water loss (Unknown)	True
MS/MS ammonia loss (Unknown)	True
MS/MS dependent losses (Unknown)	True
MS/MS recalibration (Unknown)	False
Site tables	Oxidation (M)Sites.txt

Appendix 2 – Settings used for MaxQuant protein identification

3. TTC30A sgRNA off-targets

Sequence: TAGCGCGGTAAACTCCCCGTCGG
Efficacy score by CRISPRater: 0.77 HIGH
Oligo pair with 5' extension fwd: TAggTAGCGCGGTAAACTCCCCGT rev: AAACACGGGGAGTTTACCGCGCTA
Oligo pair with 5' substitution fwd: TAggGCGCGGTAAACTCCCCGT rev: AAACACGGGGAGTTTACCGCGC

Coordinates	strand	MM	target_seq	PAM	distance		gene name	gene id
chr2:177618651-177618673	+	0	TAGCGCGG[TAAACTCCCCGT]	CGG	0	E	TTC30A	ENSG00000197557
chr2:177552713-177552735	+	3	GACCGCGG[TGAACTCCCCGT]	CGG	0	E	TTC30B	ENSG00000196659
chr9:72227904-72227926	+	4	GTGAGCGG[TAAACTCCACGT]	AGG	17	I	GDA	ENSG00000119125
chr1:227952101-227952123	+	4	TAGCTCAG[TCAACTCCCAGT]	TGG	4203	-	WNT9A	ENSG00000143816
chr3:9059226-9059248	+	4	TGGCGAGG[TAAGCTCCCCGA]	GGG	0	E	SRGAP3	ENSG00000196220
chr19:15501258-15501280	-	4	TAGGGCTG[TAAACTCCACGC]	AGG	2302	-	PGLYRP2	ENSG00000161031
chr14:86725915-86725937	-	4	TTGCACGG[TAAACTCCCTGA]	AGG	NA	-	NA	NA

Appendix 3.1 – Off-targets for TTC30A sgRNA #1 – Depicted are sgRNA sequence, efficacy score and top off-target hits with gene name, number of mismatches (MM) and location according to CCTop.

Sequence: AGTTTACCGCGCTAGTGTACCGG
Efficacy score by CRISPRater: 0.73 MEDIUM
Oligo pair with 5' extension fwd: TAggAGTTTACCGCGCTAGTGTAC rev: AAACGTACACTAGCGCGGTAAACT
Oligo pair with 5' substitution fwd: TAggTTTACCGCGCTAGTGTAC rev: AAACGTACACTAGCGCGGTAAA

Coordinates	strand	MM	target_seq	PAM	distance		gene name	gene id
chr2:177618642-177618664	-	0	AGTTTACC[GCGCTAGTGTAC]	CGG	0	E	TTC30A	ENSG00000197557
chr2:172223654-172223676	+	4	AATTTGCT[GAGCTAGTGTAC]	TGG	91611	-	AC104088.1	ENSG00000232555
chr2:104078306-104078328	+	4	AATTTTCC[ACTCTAGTGTAC]	AGG	528	-	RP11-76I14.1	ENSG00000256637
chr19:39445320-39445342	+	4	GGCCTACC[GCGCTAGTGTTC]	CGG	99	I	SUPT5H	ENSG00000196235

Appendix 3.2 – Off-targets for TTC30A sgRNA #1 – Depicted are sgRNA sequence, efficacy score and top off-target hits with gene name, number of mismatches (MM) and location according to CCTop.

4. TTC30B sgRNA off-targets

Sequence: CGGGGATCTGCGCGCCGCTCAGG
Efficacy score by CRISPRater: 0.71 MEDIUM
Oligo pair with 5' extension fwd: TAggCGGGGATCTGCGCGCCGCTC rev: AAACGAGCGGCGCGCAGATCCCCG
Oligo pair with 5' substitution fwd: TAggGGGATCTGCGCGCCGCTC rev: AAACGAGCGGCGCGCAGATCCC
Top 20 offtarget sites out of 34 (including on target; for full list see xls file)

Coordinates	strand	MM	target_seq	PAM	distance		gene name	gene id
chr2:177552733-177552755	+	0	CGGGGATC[TGCGCGCCGCTC]	AGG	0	E	TTC30B	ENSG00000196659
chr13:110307541-110307563	-	4	CCAGGGTC[TGGGCGCCGCTC]	GGG	13	I	COL4A2	ENSG00000134871
chr3:120349409-120349431	+	4	CTGGGGTG[CGCGCGCCGCTC]	CGG	70	-	LRRC58	ENSG00000163428
chr14:99605094-99605116	-	3	CGGGGCTC[CGAGCGCCGCTC]	CGG	479	I	RP11-543C4.1	ENSG00000247970
chr20:63102859-63102881	+	3	CCGGGAGC[TGCGGGCCGCTC]	CGG	0	E	HAR1A	ENSG00000225978
chr3:129894011-129894033	+	4	CGGATTTC[TGCCCGCCGCTC]	TGG	84	I	TMCC1-AS1	ENSG00000271270
chr5:139648757-139648779	-	3	CAGGGAGC[TGCGCTCCGCTC]	TGG	0	E	CXXC5	ENSG00000171604
chr17:18225987-18226009	+	4	CGAGTCTC[TGCGGGCCGCTC]	TGG	224	I	LLGL1	ENSG00000131899
chr10:116742746-116742768	-	4	CGGGCCTC[GGCGGGCCGCTC]	TGG	172	-	HSPA12A	ENSG00000165868
chr10:12129893-12129915	+	4	CAGGGATG[CGCGGGCCGCTC]	CGG	99	I	SEC61A2	ENSG00000065665
chr3:74926773-74926795	+	4	CTGGAATC[TGAGAGCCGCTC]	TGG	NA	-	NA	NA
chr20:63177570-63177592	-	4	CGCGTATC[CGCGCTCCGCTC]	CGG	908	I	MIR124-3	ENSG00000207598
chr14:69829620-69829642	+	4	CTTGGATC[TGGGCCCCGCTC]	GGG	24489	-	SMOC1	ENSG00000198732
chr6:17728781-17728803	+	4	TGGGGCTG[TGCGCGGCGCTC]	GGG	6878	-	RNA5SP204	ENSG00000201415
chr1:37033105-37033127	+	4	CCGGGACA[TGCGCGGCGCTC]	AGG	867	I	GRIK3	ENSG00000163873
chr9:97574472-97574494	-	4	CGGGGAGG[TTCGGGCCGCTC]	AGG	5435	I	TMOD1	ENSG00000136842
chr4:1225417-1225439	+	3	CGCGGATC[TGCTCGACGCTC]	TGG	0	E	CTBP1	ENSG00000159692
chr10:117217764-117217786	+	4	CAGTGATC[TGCCCGTCGCTC]	TGG	7465	-	KCNK18	ENSG00000186795
chr6:136921542-136921564	-	4	CGGGATTA[TGCGCGCGGCTC]	CGG	700	-	SLC35D3	ENSG00000182747
chr17:3668323-3668345	+	4	GGGGGAAC[TGCGGCCCGCTC]	CGG	143	I	TAX1BP3	ENSG00000213977

Appendix 4.1 – Off-targets for TTC30B sgRNA #1 – Depicted are sgRNA sequence, efficacy score and top off-target hits with gene name, number of mismatches (MM) and location according to CCTop.

Sequence: CGTAGCGTGCATTGCGGATGAGG
Efficacy score by CRISPRater: 0.67 MEDIUM
Oligo pair with 5' extension fwd: TAggCGTAGCGTGCATTGCGGATG rev: AAACCATCCGCAATGCACGCTACG
Oligo pair with 5' substitution fwd: TAggTAGCGTGCATTGCGGATG rev: AAACCATCCGCAATGCACGCTA

Coordinates	strand	MM	target_seq	PAM	distance		gene name	gene id
chr2:177552682-177552704	+	0	CGTAGCGT[GCATTGCGGATG]	AGG	0	E	TTC30B	ENSG00000196659
chr5:151351487-151351509	+	4	GGGAGAGT[GAATTGCGGATG]	AGG	3897	-	SLC36A2	ENSG00000186335
chr2:126404559-126404581	-	4	CTTAGAGT[GCACTGAGGATG]	GGG	60567	-	AC023347.1	ENSG00000235774
chr4:100085672-100085694	+	4	CTTAGAGT[GCATGGTGGATG]	TGG	43568	I	DYNLL1P6	ENSG00000248820
chr10:28988154-28988176	-	4	GGTAGCCT[GCATTTGGGATG]	GGG	88670	-	RP11-492M23.2	ENSG00000229605
chr9:95773405-95773427	+	4	CATAGCTT[GCTTTGCGGAAG]	AGG	0	E	RP11-180I4.4	ENSG00000268926
chr5:118332409-118332431	+	4	AGTAGCCT[GCATTGCTGATC]	TGG	47627	-	HNCAT21	ENSG00000250427

Appendix 4.2 – Off-targets for TTC30B sgRNA #2 – Depicted are sgRNA sequence, efficacy score and top off-target hits with gene name, number of mismatches (MM) and location according to CCTop.

5. Specific TTC30A/B peptide sequences

peptide sequence	specifity	TTC30A_x/y_TTC30B
AGLSGAQIPDGEFTALVYR	TTC30A	25.64221
ALIYEIIGWNK	TTC30A	26.56001
EEEQLSYDDPNR	TTC30A	23.57260
EEEQLSYDDPNRK	TTC30A	26.29461
GNYEFGISR	TTC30A	27.89663
IEKEEEQLSYDDPNR	TTC30A	22.45543
IEKEEEQLSYDDPNRK	TTC30A	23.60411
KIEKEEEQLSYDDPNR	TTC30A	25.73300
LDGLAGMLTEQLR	TTC30A	24.61827
NYEVAQETLTDMPPR	TTC30A	44.63029
NYEVAQETLTDMPPRAEEELDPVTLHNQALMNMDAR	TTC30A	24.72231
QHPELGVGMTTEGFDVR	TTC30A	27.93952
SLVEQLLSGEGGEESGGDNETDGQVNLGCLLYK	TTC30A	26.22704
YAEAVQLLGR	TTC30A	28.68934
ACLYAEATR	TTC30B	-25.61216
AGLSGAQIPDGEFTAVVYR	TTC30B	-22.61680
DSVIQECVQFLEHCELHGR	TTC30B	-26.44459
EEEQLSYDDPDKK	TTC30B	-22.61090
EGGEESGGENETDGQINLGCLLYK	TTC30B	-26.32410
GNYDFGISR	TTC30B	-25.62171
NIPAVIEQPLEEER	TTC30B	-27.35527
NTVTYESR	TTC30B	-24.41638
QHPELGVGMTTEGIDVR	TTC30B	-23.29323
SLVEQLPSR	TTC30B	-27.06034
YAEAVQLLGGELQR	TTC30B	-27.13242

Appendix 5 – Unique amino acid sequences of unique peptide fragments for either TTC30A or TTC30B and their respective $\log_2$ ratio [8]

6. GetGo enrichment analysis for TTC30A interactome

Path/Term	Name	Direction	Ratio	Fisher-pv	Fisher-C-pv	Genes
R-HSA-176974:1	Unwinding of DNA	ENRICHED	142.27	2.700×10^{-11}	3.409×10^{-09}	MCM2 MCM3 MCM4 MCM5 MCM6 MCM7
R-HSA-69190:1	DNA strand elongation	ENRICHED	53.35	3.760×10^{-09}	4.747×10^{-07}	MCM2 MCM3 MCM4 MCM5 MCM6 MCM7

R-HSA-68962:2	Activation of the pre-replicative complex	ENRICHED	53.35	3.760×10^{-09}	4.747×10^{-07}	MCM2 MCM3 MCM4 MCM5 MCM6 MCM7
R-HSA-176187:1	Activation of ATR in response to replication stress	ENRICHED	46.141	8.170×10^{-09}	1.031×10^{-06}	MCM2 MCM3 MCM4 MCM5 MCM6 MCM7
R-HSA-72203:1	Processing of Capped Intron-Containing Pre-mRNA	ENRICHED	12.212	1.170×10^{-08}	1.477×10^{-06}	CDC40 NUP88 SF3A2 SF3A3 SF3B4 SF3B5 SNRPA1 SNRPB2 SNRPD3 SRRM2
R-HSA-72163:1	mRNA Splicing - Major Pathway	ENRICHED	14.468	1.650×10^{-08}	2.083×10^{-06}	CDC40 SF3A2 SF3A3 SF3B4 SF3B5 SNRPA1 SNRPB2 SNRPD3 SRRM2
R-HSA-72172:1	mRNA Splicing	ENRICHED	13.842	2.380×10^{-08}	3.005×10^{-06}	CDC40 SF3A2 SF3A3 SF3B4 SF3B5 SNRPA1 SNRPB2 SNRPD3 SRRM2
R-HSA-68867:2	Assembly of the pre-replicative complex	ENRICHED	25.106	2.240×10^{-07}	2.828×10^{-05}	MCM2 MCM3 MCM4 MCM5 MCM6 MCM7
R-HSA-68949:1	Orc1 removal from chromatin	ENRICHED	24.045	2.850×10^{-07}	3.598×10^{-05}	MCM2 MCM3 MCM4 MCM5 MCM6 MCM7
R-HSA-69052:1	Switching of origins to a post-replicative state	ENRICHED	24.045	2.850×10^{-07}	3.598×10^{-05}	MCM2 MCM3 MCM4 MCM5 MCM6 MCM7
R-HSA-69300:3	Removal of licensing factors from origins	ENRICHED	23.386	3.310×10^{-07}	4.179×10^{-05}	MCM2 MCM3 MCM4 MCM5 MCM6 MCM7
R-HSA-69304:1	Regulation of DNA replication	ENRICHED	22.463	4.130×10^{-07}	5.214×10^{-05}	MCM2 MCM3 MCM4 MCM5 MCM6 MCM7
R-HSA-69002:1	DNA Replication Pre-Initiation	ENRICHED	20.085	7.650×10^{-07}	9.658×10^{-05}	MCM2 MCM3 MCM4 MCM5 MCM6 MCM7
R-HSA-68874:1	M/G1 Transition	ENRICHED	20.085	7.650×10^{-07}	9.658×10^{-05}	MCM2 MCM3 MCM4 MCM5 MCM6 MCM7
R-HSA-1640170:0	Cell Cycle	ENRICHED	5.867	8.280×10^{-07}	1.045×10^{-04}	MCM2 MCM3 MCM4 MCM5 MCM6 MCM7 NUP88 PRKACA RAD50 SKA1 SUN2 SYNE1
R-HSA-69481:2	G2/M Checkpoints	ENRICHED	13.19	1.270×10^{-06}	1.603×10^{-04}	MCM2 MCM3 MCM4 MCM5 MCM6 MCM7 RAD50
R-HSA-69239:1	Synthesis of DNA	ENRICHED	17.072	1.860×10^{-06}	2.348×10^{-04}	MCM2 MCM3 MCM4 MCM5 MCM6 MCM7
R-HSA-69306:0	DNA Replication	ENRICHED	15.808	2.840×10^{-06}	3.585×10^{-04}	MCM2 MCM3 MCM4 MCM5 MCM6 MCM7
R-HSA-69620:1	Cell Cycle Checkpoints	ENRICHED	10.884	4.280×10^{-06}	5.403×10^{-04}	MCM2 MCM3 MCM4 MCM5 MCM6 MCM7 RAD50
R-HSA-69206:1	G1/S Transition	ENRICHED	14.468	4.600×10^{-06}	5.807×10^{-04}	MCM2 MCM3 MCM4 MCM5 MCM6 MCM7
R-HSA-69242:2	S Phase	ENRICHED	13.338	7.170×10^{-06}	9.052×10^{-04}	MCM2 MCM3 MCM4 MCM5 MCM6 MCM7
R-HSA-453279:2	Mitotic G1-G1/S phases	ENRICHED	12.023	1.260×10^{-05}	0.00159	MCM2 MCM3 MCM4 MCM5 MCM6 MCM7
R-HSA-74160:0	Gene Expression	enriched	2.959	1.760×10^{-05}	0.00222	APOBEC3C CDC40 EEF1A2 IGF2BP3 MBD3 NUP88 PPM1A RAD50 SF3A2 SF3A3 SF3B4 SF3B5 SNRPA1 SNRPB2 SNRPD3 SRRM2 TAF4 WDR12
R-HSA-69278:1	Cell Cycle, Mitotic	ENRICHED	5.357	4.230×10^{-05}	0.00534	MCM2 MCM3 MCM4 MCM5 MCM6 MCM7 NUP88 PRKACA SKA1

Appendix 6 – GetGo enrichment analysis for TTC30A interactome – Depicted are the found interactor proteins for TTC30A, the cellular process, where they are involved in, with the respective Fisher p-value. Modified after [26].

7. GetGo enrichment analysis for TTC30B interactome

Path/Term	Name	Direction	Ratio	Fisher-pv	Fisher-C-pv	Genes
R-HSA-74160:0	Gene Expression	ENRICHED	4.071	$9.420x10^{-17}$	$2.217x10^{-14}$	APEH APOBEC3C BOP1 CDC40 CHERP CSNK2A1 DDX42 DGCR8 DKC1 EEF1A2 FAM98B GAR1 HIST1H4A HIST2H3A HSPB1 IGF2BP3 MPHOSPH6 NAT10 NOL6 NUP210 NUP214 NUP50 NUP62 NUP85 NUP88 PES1 PIN1 PRMT1 PRPF31 RBM17 RRP7A SF3B4 SKI SNRPC SNRPD3 SRRM2 SRSF6 TBL3 TET1 TET2 TRIM28 U2SURP UBA52 USP39 WDR12
R-HSA-72203:1	Processing of Capped Intron-Containing Pre-mRNA	ENRICHED	12.098	$2.940x10^{-14}$	$6.920x10^{-12}$	CDC40 CHERP DDX42 NUP210 NUP214 NUP50 NUP62 NUP85 NUP88 PRPF31 RBM17 SF3B4 SNRPC SNRPD3 SRRM2 SRSF6 U2SURP USP39
R-HSA-5419276:2	Mitochondrial translation termination	ENRICHED	18.001	$5.640x10^{-10}$	$1.328x10^{-07}$	ERAL1 MRPS12 MRPS17 MRPS2 MRPS23 MRPS25 MRPS26 MRPS5 MRPS9 PTCD3
R-HSA-5368286:2	Mitochondrial translation initiation	ENRICHED	18.001	$5.640x10^{-10}$	$1.328x10^{-07}$	ERAL1 MRPS12 MRPS17 MRPS2 MRPS23 MRPS25 MRPS26 MRPS5 MRPS9 PTCD3
R-HSA-5389840:2	Mitochondrial translation elongation	ENRICHED	18.001	$5.640x10^{-10}$	$1.328x10^{-07}$	ERAL1 MRPS12 MRPS17 MRPS2 MRPS23 MRPS25 MRPS26 MRPS5 MRPS9 PTCD3
R-HSA-5368287:1	Mitochondrial translation	ENRICHED	16.839	$1.020x10^{-09}$	$2.401x10^{-07}$	ERAL1 MRPS12 MRPS17 MRPS2 MRPS23 MRPS25 MRPS26 MRPS5 MRPS9 PTCD3
R-HSA-176974:1	Unwinding of DNA	ENRICHED	78.302	$1.020x10^{-09}$	$2.401x10^{-07}$	MCM2 MCM3 MCM4 MCM5 MCM6 MCM7
R-HSA-1169408:1	ISG15 antiviral mechanism	ENRICHED	20.135	$1.720x10^{-09}$	$4.048x10^{-07}$	NUP210 NUP214 NUP50 NUP62 NUP85 NUP88 PIN1 STAT1 UBA52
R-HSA-1169410:3	Antiviral mechanism by IFN-stimulated genes	ENRICHED	20.135	$1.720x10^{-09}$	$4.048x10^{-07}$	NUP210 NUP214 NUP50 NUP62 NUP85 NUP88 PIN1 STAT1 UBA52
R-HSA-72163:1	mRNA Splicing - Major Pathway	ENRICHED	10.617	$2.760x10^{-09}$	$6.496x10^{-07}$	CDC40 CHERP DDX42 PRPF31 RBM17 SF3B4 SNRPC SNRPD3 SRRM2 SRSF6 U2SURP USP39
R-HSA-72172:1	mRNA Splicing	ENRICHED	10.158	$4.400x10^{-09}$	$1.036x10^{-06}$	CDC40 CHERP DDX42 PRPF31 RBM17 SF3B4 SNRPC SNRPD3 SRRM2 SRSF6 U2SURP USP39
R-HSA-69190:1	DNA strand elongation	ENRICHED	34.257	$4.510x10^{-09}$	$1.062x10^{-06}$	FEN1 MCM2 MCM3 MCM4 MCM5 MCM6 MCM7
R-HSA-69278:1	Cell Cycle, Mitotic	ENRICHED	5.57	$1.390x10^{-08}$	$3.272x10^{-06}$	CSNK2A1 FEN1 HIST1H4A HIST2H3A MCM2 MCM3 MCM4 MCM5 MCM6 MCM7 NUP210 NUP214 NUP50 NUP62 NUP85 NUP88 UBA52
R-HSA-159236:1	Transport of Mature mRNA derived from an Intron-Containing Transcript	ENRICHED	18.157	$2.970x10^{-08}$	$6.991x10^{-06}$	CDC40 NUP210 NUP214 NUP50 NUP62 NUP85 NUP88 SRSF6
R-HSA-211000:1	Gene Silencing by RNA	ENRICHED	13.955	$3.230x10^{-08}$	$7.603x10^{-06}$	DGCR8 HIST1H4A HIST2H3A NUP210 NUP214 NUP50 NUP62 NUP85 NUP88
R-HSA-1640170:0	Cell Cycle	ENRICHED	4.843	$3.910x10^{-08}$	$9.203x10^{-06}$	CSNK2A1 DKC1 FEN1 HIST1H4A HIST2H3A MCM2 MCM3 MCM4 MCM5 MCM6 MCM7 NUP210 NUP214 NUP50 NUP62 NUP85 NUP88 UBA52
R-HSA-5578749:1	Transcriptional regulation by small RNAs	ENRICHED	17.401	$4.020x10^{-08}$	$9.462x10^{-06}$	HIST1H4A HIST2H3A NUP210 NUP214 NUP50 NUP62 NUP85 NUP88
R-HSA-8868773:2	rRNA processing in the nucleus and cytosol	ENRICHED	9.413	$4.120x10^{-08}$	$9.698x10^{-06}$	BOP1 DKC1 GAR1 MPHOSPH6 NAT10 NOL6 PES1 RRP7A TBL3 UBA52 WDR12

R-HSA-194441:1	Metabolism of non-coding RNA	ENRICHED	22.372	$6.140x10^{-08}$	$1.445x10^{-05}$	NUP210 NUP214 NUP50 NUP62 NUP85 NUP88 SNRPD3
R-HSA-191859:1	snRNP Assembly	ENRICHED	22.372	$6.140x10^{-08}$	$1.445x10^{-05}$	NUP210 NUP214 NUP50 NUP62 NUP85 NUP88 SNRPD3
R-HSA-168333:3	NEP/NS2 Interacts with the Cellular Export Machinery	ENRICHED	33.558	$6.680x10^{-08}$	$1.572x10^{-05}$	NUP210 NUP214 NUP50 NUP62 NUP85 NUP88
R-HSA-170822:4	Regulation of Glucokinase by Glucokinase Regulatory Protein	ENRICHED	33.558	$6.680x10^{-08}$	$1.572x10^{-05}$	NUP210 NUP214 NUP50 NUP62 NUP85 NUP88
R-HSA-168271:2	Transport of Ribonucleoproteins into the Host Nucleus	ENRICHED	33.558	$6.680x10^{-08}$	$1.572x10^{-05}$	NUP210 NUP214 NUP50 NUP62 NUP85 NUP88
R-HSA-72312:1	rRNA processing	ENRICHED	8.926	$6.860x10^{-08}$	$1.615x10^{-05}$	BOP1 DKC1 GAR1 MPHOSPH6 NAT10 NOL6 PES1 RRP7A TBL3 UBA52 WDR12
R-HSA-72202:1	Transport of Mature Transcript to Cytoplasm	ENRICHED	16.062	$7.090x10^{-08}$	$1.669x10^{-05}$	CDC40 NUP210 NUP214 NUP50 NUP62 NUP85 NUP88 SRSF6
R-HSA-168274:2	Export of Viral Ribonucleoproteins from Nucleus	ENRICHED	32.401	$8.020x10^{-08}$	$1.888x10^{-05}$	NUP210 NUP214 NUP50 NUP62 NUP85 NUP88
R-HSA-180746:3	Nuclear import of Rev protein	ENRICHED	31.321	$9.560x10^{-08}$	$2.250x10^{-05}$	NUP210 NUP214 NUP50 NUP62 NUP85 NUP88
R-HSA-180910:3	Vpr-mediated nuclear import of PICs	ENRICHED	31.321	$9.560x10^{-08}$	$2.250x10^{-05}$	NUP210 NUP214 NUP50 NUP62 NUP85 NUP88
R-HSA-6784531:1	tRNA processing in the nucleus	ENRICHED	20.301	$1.120x10^{-07}$	$2.636x10^{-05}$	FAM98B NUP210 NUP214 NUP50 NUP62 NUP85 NUP88
R-HSA-159227:1	Transport of the SLBP independent Mature mRNA	ENRICHED	30.311	$1.130x10^{-07}$	$2.660x10^{-05}$	NUP210 NUP214 NUP50 NUP62 NUP85 NUP88
R-HSA-165054:3	Rev-mediated nuclear export of HIV RNA	ENRICHED	30.311	$1.130x10^{-07}$	$2.660x10^{-05}$	NUP210 NUP214 NUP50 NUP62 NUP85 NUP88
R-HSA-159230:1	Transport of the SLBP Dependant Mature mRNA	ENRICHED	29.363	$1.340x10^{-07}$	$3.154x10^{-05}$	NUP210 NUP214 NUP50 NUP62 NUP85 NUP88
R-HSA-3301854:1	Nuclear Pore Complex (NPC) Disassembly	ENRICHED	29.363	$1.340x10^{-07}$	$3.154x10^{-05}$	NUP210 NUP214 NUP50 NUP62 NUP85 NUP88
R-HSA-68962:2	Activation of the pre-replicative complex	ENRICHED	29.363	$1.340x10^{-07}$	$3.154x10^{-05}$	MCM2 MCM3 MCM4 MCM5 MCM6 MCM7
R-HSA-176033:2	Interactions of Vpr with host cellular proteins	ENRICHED	28.474	$1.570x10^{-07}$	$3.695x10^{-05}$	NUP210 NUP214 NUP50 NUP62 NUP85 NUP88
R-HSA-177243:2	Interactions of Rev with host cellular proteins	ENRICHED	28.474	$1.570x10^{-07}$	$3.695x10^{-05}$	NUP210 NUP214 NUP50 NUP62 NUP85 NUP88
R-HSA-176187:1	Activation of ATR in response to replication stress	ENRICHED	25.395	$2.870x10^{-07}$	$6.755x10^{-05}$	MCM2 MCM3 MCM4 MCM5 MCM6 MCM7
R-HSA-168276:2	NS1 Mediated Effects on Host Pathways	ENRICHED	25.395	$2.870x10^{-07}$	$6.755x10^{-05}$	NUP210 NUP214 NUP50 NUP62 NUP85 NUP88

R-HSA-159231:1	Transport of Mature mRNA Derived from an Intronless Transcript	ENRICHED	24.727	$3.300x10^{-07}$	$7.767x10^{-05}$	NUP210 NUP214 NUP50 NUP62 NUP85 NUP88
R-HSA-168253:1	Host Interactions with Influenza Factors	ENRICHED	24.093	$3.780x10^{-07}$	$8.897x10^{-05}$	NUP210 NUP214 NUP50 NUP62 NUP85 NUP88
R-HSA-159234:1	Transport of Mature mRNAs Derived from Intronless Transcripts	ENRICHED	24.093	$3.780x10^{-07}$	$8.897x10^{-05}$	NUP210 NUP214 NUP50 NUP62 NUP85 NUP88
R-HSA-69239:1	Synthesis of DNA	ENRICHED	12.528	$4.120x10^{-07}$	$9.698x10^{-05}$	FEN1 MCM2 MCM3 MCM4 MCM5 MCM6 MCM7 UBA52
R-HSA-3371453:2	Regulation of HSF1-mediated heat shock response	ENRICHED	16.362	$4.270x10^{-07}$	$1.005x10^{-04}$	HSPA6 NUP210 NUP214 NUP50 NUP62 NUP85 NUP88
R-HSA-168325:3	Viral Messenger RNA Synthesis	ENRICHED	23.491	$4.330x10^{-07}$	$1.019x10^{-04}$	NUP210 NUP214 NUP50 NUP62 NUP85 NUP88
R-HSA-68867:2	Assembly of the pre-replicative complex	ENRICHED	16.121	$4.680x10^{-07}$	$1.102x10^{-04}$	MCM2 MCM3 MCM4 MCM5 MCM6 MCM7 UBA52
R-HSA-68875:1	Mitotic Prophase	ENRICHED	12.283	$4.740x10^{-07}$	$1.116x10^{-04}$	HIST1H4A HIST2H3A NUP210 NUP214 NUP50 NUP62 NUP85 NUP88
R-HSA-4570464:2	SUMOylation of RNA binding proteins	ENRICHED	22.372	$5.600x10^{-07}$	$1.318x10^{-04}$	NUP210 NUP214 NUP50 NUP62 NUP85 NUP88
R-HSA-4615885:2	SUMOylation of DNA replication proteins	ENRICHED	22.372	$5.600x10^{-07}$	$1.318x10^{-04}$	NUP210 NUP214 NUP50 NUP62 NUP85 NUP88
R-HSA-68949:1	Orc1 removal from chromatin	ENRICHED	15.44	$6.120x10^{-07}$	$1.441x10^{-04}$	MCM2 MCM3 MCM4 MCM5 MCM6 MCM7 UBA52
R-HSA-69052:1	Switching of origins to a post-replicative state	ENRICHED	15.44	$6.120x10^{-07}$	$1.441x10^{-04}$	MCM2 MCM3 MCM4 MCM5 MCM6 MCM7 UBA52
R-HSA-70153:3	Glucose transport	ENRICHED	21.852	$6.340x10^{-07}$	$1.492x10^{-04}$	NUP210 NUP214 NUP50 NUP62 NUP85 NUP88
R-HSA-69306:0	DNA Replication	ENRICHED	11.6	$7.090x10^{-07}$	$1.669x10^{-04}$	FEN1 MCM2 MCM3 MCM4 MCM5 MCM6 MCM7 UBA52
R-HSA-69300:3	Removal of licensing factors from origins	ENRICHED	15.017	$7.270x10^{-07}$	$1.711x10^{-04}$	MCM2 MCM3 MCM4 MCM5 MCM6 MCM7 UBA52
R-HSA-2980766:1	Nuclear Envelope Breakdown	ENRICHED	20.427	$9.060x10^{-07}$	$2.133x10^{-04}$	NUP210 NUP214 NUP50 NUP62 NUP85 NUP88
R-HSA-69304:1	Regulation of DNA replication	ENRICHED	14.424	$9.330x10^{-07}$	$2.196x10^{-04}$	MCM2 MCM3 MCM4 MCM5 MCM6 MCM7 UBA52
R-HSA-189200:2	Hexose transport	ENRICHED	18.424	$1.570x10^{-06}$	$3.695x10^{-04}$	NUP210 NUP214 NUP50 NUP62 NUP85 NUP88
R-HSA-69002:1	DNA Replication Pre-Initiation	ENRICHED	12.897	$1.870x10^{-06}$	$4.402x10^{-04}$	MCM2 MCM3 MCM4 MCM5 MCM6 MCM7 UBA52
R-HSA-68874:1	M/G1 Transition	ENRICHED	12.897	$1.870x10^{-06}$	$4.402x10^{-04}$	MCM2 MCM3 MCM4 MCM5 MCM6 MCM7 UBA52
R-HSA-3371556:1	Cellular response to heat stress	ENRICHED	12.6	$2.150x10^{-06}$	$5.061x10^{-04}$	HSPA6 NUP210 NUP214 NUP50 NUP62 NUP85 NUP88
R-HSA-69242:2	S Phase	ENRICHED	9.788	$2.330x10^{-06}$	$5.484x10^{-04}$	FEN1 MCM2 MCM3 MCM4 MCM5 MCM6 MCM7 UBA52

R-HSA-6790901:3	rRNA modification in the nucleus and cytosol	ENRICHED	15.926	$3.400x10^{-06}$	$8.003x10^{-04}$	DKC1 GAR1 NAT10 NOL6 RRP7A TBL3
R-HSA-913531:2	Interferon Signaling	ENRICHED	7.341	$4.980x10^{-06}$	0.00117	NUP210 NUP214 NUP50 NUP62 NUP85 NUP88 PIN1 STAT1 UBA52
R-HSA-162587:1	HIV Life Cycle	ENRICHED	8.7	$5.270x10^{-06}$	0.00124	FEN1 NUP210 NUP214 NUP50 NUP62 NUP85 NUP88 UBA52
R-HSA-72306:1	tRNA processing	ENRICHED	10.747	$5.720x10^{-06}$	0.00135	FAM98B NUP210 NUP214 NUP50 NUP62 NUP85 NUP88
R-HSA-69481:2	G2/M Checkpoints	ENRICHED	8.297	$7.300x10^{-06}$	0.00172	HIST1H4A MCM2 MCM3 MCM4 MCM5 MCM6 MCM7 UBA52
R-HSA-3108214:2	SUMOylation of DNA damage response and repair proteins	ENRICHED	13.234	$9.060x10^{-06}$	0.00213	NUP210 NUP214 NUP50 NUP62 NUP85 NUP88
R-HSA-69206:1	G1/S Transition	ENRICHED	9.29	$1.390x10^{-05}$	0.00327	MCM2 MCM3 MCM4 MCM5 MCM6 MCM7 UBA52
R-HSA-68886:2	M Phase	ENRICHED	5.573	$1.460x10^{-05}$	0.00344	CSNK2A1 HIST1H4A HIST2H3A NUP210 NUP214 NUP50 NUP62 NUP85 NUP88 UBA52
R-HSA-6791226:3	Major pathway of rRNA processing in the nucleolus and cytosol	ENRICHED	7.284	$1.770x10^{-05}$	0.00417	BOP1 MPHOSPH6 NOL6 PES1 RRP7A TBL3 UBA52 WDR12
R-HSA-162909:1	Host Interactions of HIV factors	ENRICHED	8.77	$1.970x10^{-05}$	0.00464	NUP210 NUP214 NUP50 NUP62 NUP85 NUP88 UBA52
R-HSA-162599:1	Late Phase of HIV Life Cycle	ENRICHED	8.368	$2.610x10^{-05}$	0.00614	NUP210 NUP214 NUP50 NUP62 NUP85 NUP88 UBA52
R-HSA-69620:1	Cell Cycle Checkpoints	ENRICHED	6.846	$2.690x10^{-05}$	0.00633	HIST1H4A MCM2 MCM3 MCM4 MCM5 MCM6 MCM7 UBA52
R-HSA-168273:2	Influenza Viral RNA Transcription and Replication	ENRICHED	8.305	$2.730x10^{-05}$	0.00643	NUP210 NUP214 NUP50 NUP62 NUP85 NUP88 UBA52
R-HSA-3108232:1	SUMO E3 ligases SUMOylate target proteins	ENRICHED	9.996	$3.960x10^{-05}$	0.00932	NUP210 NUP214 NUP50 NUP62 NUP85 NUP88
R-HSA-168255:1	Influenza Life Cycle	ENRICHED	7.775	$4.050x10^{-05}$	0.00953	NUP210 NUP214 NUP50 NUP62 NUP85 NUP88 UBA52
R-HSA-453279:2	Mitotic G1-G1/S phases	ENRICHED	7.72	$4.230x10^{-05}$	0.00996	MCM2 MCM3 MCM4 MCM5 MCM6 MCM7 UBA52
R-HSA-2990846:2	SUMOylation	ENRICHED	9.396	$5.460x10^{-05}$	0.01285	NUP210 NUP214 NUP50 NUP62 NUP85 NUP88
R-HSA-168254:2	Influenza Infection	ENRICHED	7.212	$6.330x10^{-05}$	0.0149	NUP210 NUP214 NUP50 NUP62 NUP85 NUP88 UBA52
R-HSA-2262752:0	Cellular responses to stress	ENRICHED	4.191	$6.470x10^{-05}$	0.01523	HIST1H4A HIST2H3A HSPA6 MTMR14 NUP210 NUP214 NUP50 NUP62 NUP85 NUP88 UBA52
R-HSA-1852241:0	Organelle biogenesis and maintenance	ENRICHED	4.552	$7.300x10^{-05}$	0.01718	ERAL1 MRPS12 MRPS17 MRPS2 MRPS23 MRPS25 MRPS26 MRPS5 MRPS9 PTCD3
R-HSA-162906:2	HIV Infection	ENRICHED	5.593	$1.020x10^{-04}$	0.02401	FEN1 NUP210 NUP214 NUP50 NUP62 NUP85 NUP88 UBA52

Appendix 7 – GetGo enrichment analysis for TTC30B interactome – Depicted are the found interactor proteins for TTC30A, the cellular process, where they are involved in, with the respective Fisher p-value. Modified after [26].

8. Sequencing results of TTC30A and TTC30B single KO HEK293T cells

1)

A

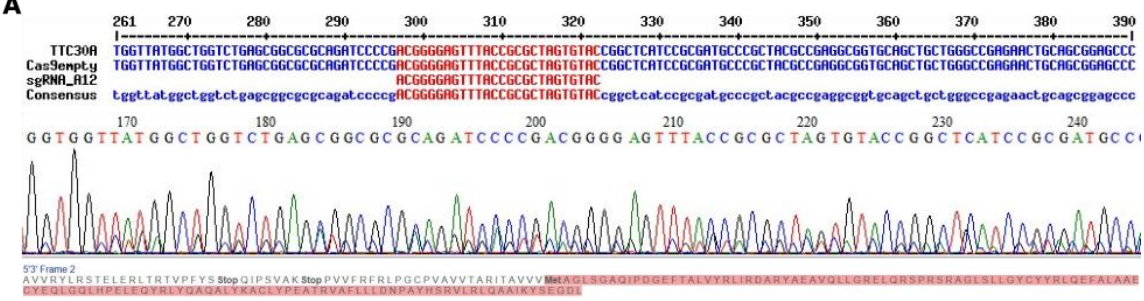

B

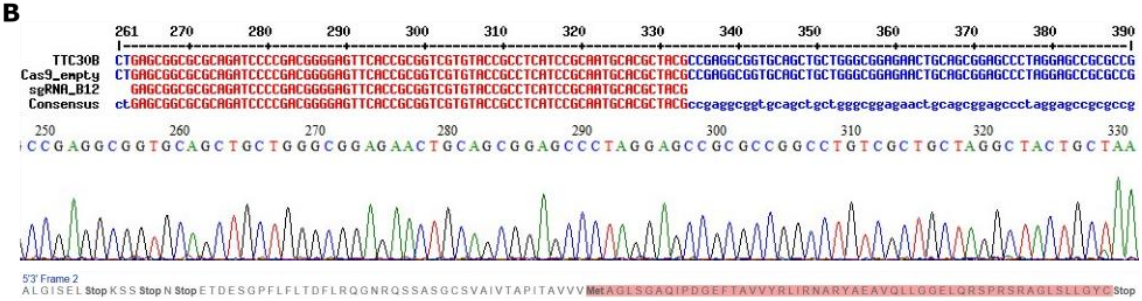

2)

A

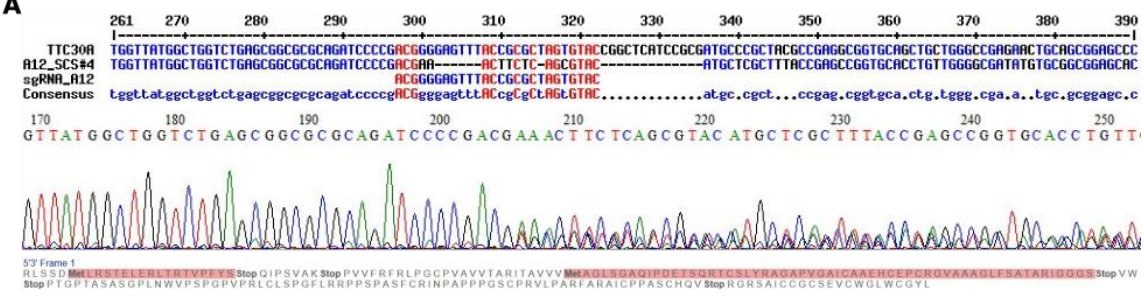

B

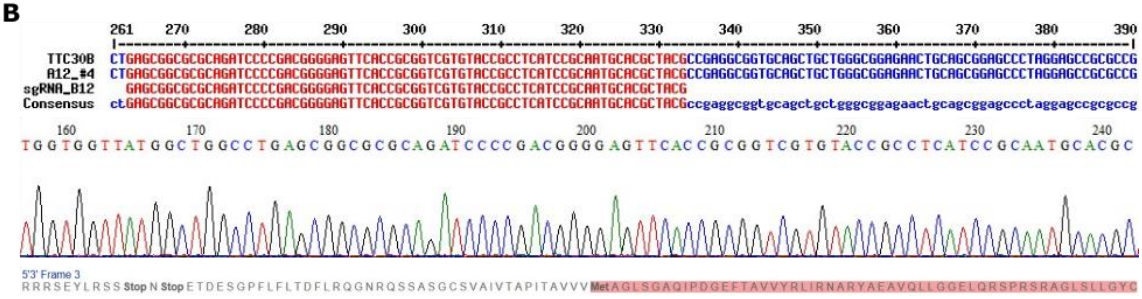

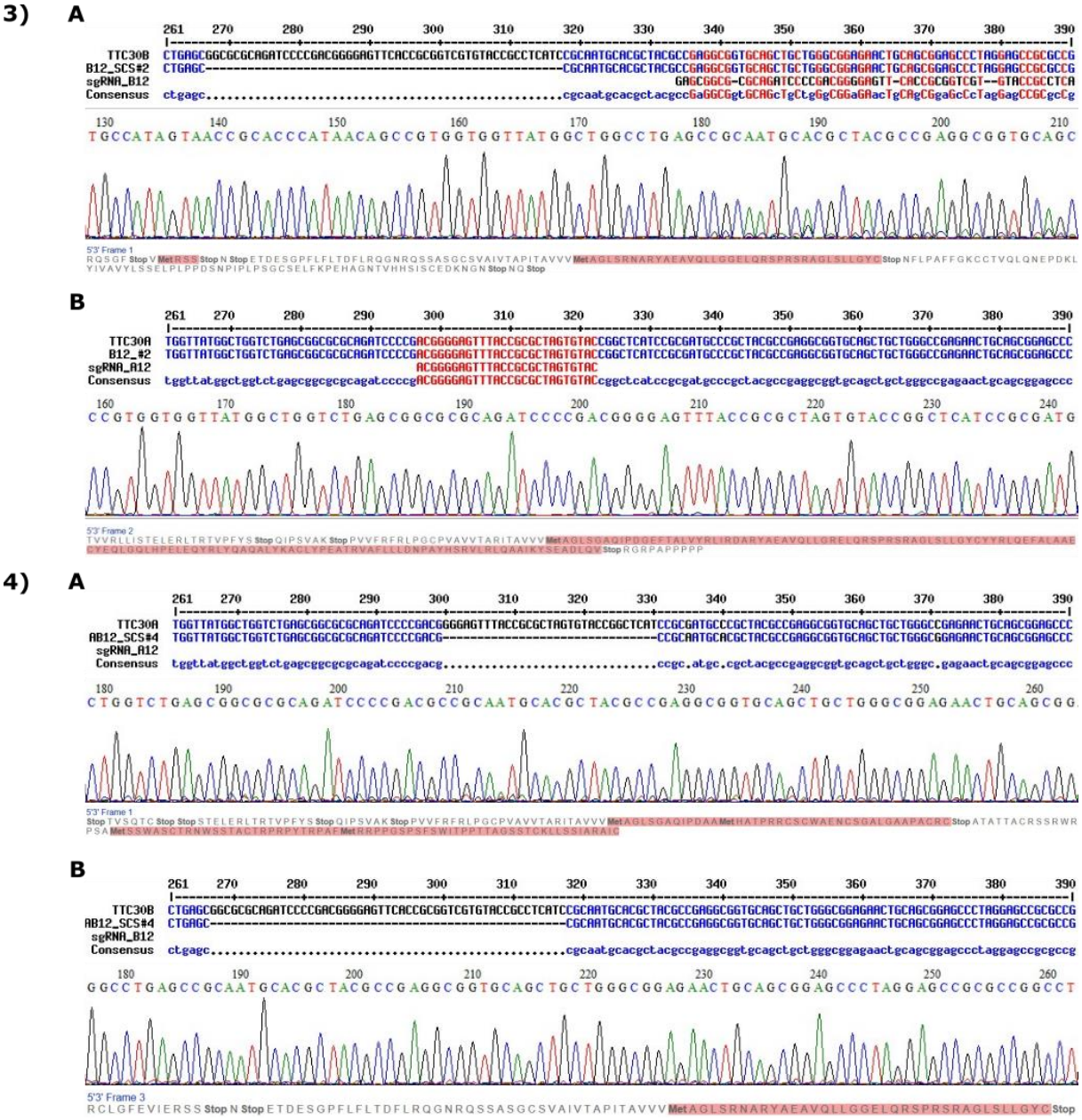

Appendix 8 – Sequencing results of Cas9 control, TTC30A/B single and double KO HEK293T cells – The figure depicts the results of (1) Cas9 empty treated HEK293T cells as well as (2) TTC30A knockout, (3) TTC30B knockout and (4) TTC30A/B double knockout cells sequenced for TTC30A (A) and TTC30B (B). Results include the alignment of TTC30 wildtype, TTC30 control or knockout sequences and used sgRNAs (top). Furthermore, the electropherogram (middle) of the respective knockout region and amino acid translation (bottom) depicting premature stop codons. [8]

9. LCA5 exon 3 sgRNA off-targets

Sequence: AAGAACTGACCAGCGATGATCGG
Efficacy score by CRISPRater: 0.59 MEDIUM
Oligo pair with 5' extension fwd: TAggAAGAACTGACCAGCGATGAT rev: AAACATCATCGCTGGTCAGTTCTT
Oligo pair with 5' substitution fwd: TAggGAACTGACCAGCGATGAT rev: AAACATCATCGCTGGTCAGTTC
Top 20 offtarget sites out of 38 (including on target; for full list see xls file)

Coordinates	strand	MM	target_seq	PAM	distance		gene name	gene id
chr6:79518771-79518793	+	0	AAGAACTG[ACCAGCGATGAT]	CGG	0	E	LCA5	ENSG00000135338
chr19:32312374-32312396	-	4	TGGACCTG[AACAGCGATGAT]	AGG	33198	-	ZNF507	ENSG00000168813
chr5:125373711-125373733	-	3	AGGAAATG[ACTAGCGATGAT]	TGG	3095	-	RP11-395P13.4	ENSG00000250402
chr2:187507552-187507574	+	4	TCTAACTG[ACCAGTGATGAT]	GGG	3782	I	TFPI	ENSG00000003436
chr10:7379145-7379167	-	4	CTGAACTG[ACTCGCGATGAT]	AGG	2632	I	SFMBT2	ENSG00000198879
chr10:104795728-104795750	+	4	CAGAAGAG[ACCAGAGATGAT]	GGG	26347	I	SORCS3	ENSG00000156395
chr14:47360915-47360937	+	4	AAGTAGTT[ACCAGGGATGAT]	GGG	17681	I	MDGA2	ENSG00000139915
chr7:79594233-79594255	-	4	AAGAGCTC[TCCAGAGATGAT]	TGG	49380	-	AC091813.2	ENSG00000226285
chr14:22144892-22144914	+	3	AATAACTG[ACCAAAGATGAT]	AGG	1889	-	AC245470.1	ENSG00000238634
chr20:28624914-28624936	-	4	AAGAAATT[TCCAGAGATGAT]	TGG	22250	-	FRG1CP	ENSG00000282826
chr17:64145918-64145940	-	4	AGGAGCAG[ACCAGCGCTGAT]	GGG	30	-	SNHG25	ENSG00000266402
chr2:27447833-27447855	+	4	AAGATCAG[CCCAGCTATGAT]	AGG	0	E	IFT172	ENSG00000138002
chr11:624350-624372	-	4	CAGCACTG[ACCACTGATGAT]	GGG	0	E	CDHR5	ENSG00000099834
chr1:91648439-91648461	+	4	AGGAATTG[ACCATGGATGAT]	GGG	4357	-	HSP90B3P	ENSG00000203914
chr19:54336088-54336110	-	4	AAGAAGGG[AGCAGCAATGAT]	AGG	662	I	LILRA4	ENSG00000239961
chr2:222633189-222633211	+	4	AATAACTC[ACCATTGATGAT]	GGG	0	E	FARSB	ENSG00000116120
chrX:107809253-107809275	-	4	AAGGGCAG[ACCAGCGAAGAT]	AGG	14571	-	NCBP2L	ENSG00000170935
chrX:38468559-38468581	+	4	AATAAATT[ACCAGCGAGGAT]	TGG	10634	I	AF241726.2	ENSG00000232370
chr7:70390700-70390722	+	4	AAGAAGGG[GCCAGCGAAGAT]	GGG	45030	I	AUTS2	ENSG00000158321
chr7:119462588-119462610	-	4	AAGAATAG[ACCAGGTATGAT]	AGG	21715	-	AC091320.1	ENSG00000263692

Appendix 9 – Off-targets for LCA5 exon 3 sgRNA – Depicted are sgRNA sequence, efficacy score and top off-target hits with gene name, number of mismatches (MM) and location according to CCTop.

10. LCA5 exon 6 sgRNA off-targets

Sequence: TCTTTATTTGGAGAGGACTTTGG
Efficacy score by CRISPRater: 0.72 MEDIUM
Oligo pair with 5' extension fwd: TAggTCTTTATTTGGAGAGGACTT rev: AAACAAGTCCTCTCCAAATAAAGA
Oligo pair with 5' substitution fwd: TAggTTTATTTGGAGAGGACTT rev: AAACAAGTCCTCTCCAAATAAA
Top 20 offtarget sites out of 149 (including on target; for full list see xls file)

Coordinates	strand	MM	target_seq	PAM	distance		gene name	gene id
chr6:79492577-79492599	+	0	TCTTTATT[TGGAGAGGACTT]	TGG	0	E	LCA5	ENSG00000135338
chr3:62156511-62156533	+	4	CTTCGATT[TGGAGAGGACTT]	GGG	534	I	PTPRG	ENSG00000144724
chr9:117139096-117139118	+	4	TGTATGTG[TGGAGAGGACTT]	AGG	2208	I	ASTN2	ENSG00000148219
chr2:124945987-124946009	-	4	TATTGTTC[TGGAGAGGACTT]	GGG	12967	-	RNA5SP102	ENSG00000252674
chr7:104799517-104799539	-	4	TGATTGTT[AGGAGAGGACTT]	AGG	0	E	LHFPL3-AS1	ENSG00000226869
chr8:27340621-27340643	+	3	TTTTTGTT[TGAAGAGGACTT]	TGG	13738	I	PTK2B	ENSG00000120899
chr11:125166380-125166402	+	3	TCTTTAGG[AGGAGAGGACTT]	GGG	1604	I	PKNOX2	ENSG00000165495
chr4:146238282-146238304	-	3	TGTTTATA[TGAAGAGGACTT]	GGG	3502	-	RP11-6L6.7	ENSG00000251010
chr15:45740129-45740151	+	4	TGATTCTT[TGTAGAGGACTT]	GGG	33359	I	RP11-718O11.1	ENSG00000259200
chr1:73679032-73679054	-	4	CCTTCTTT[TGAAGAGGACTT]	GGG	20697	I	RP4-788P17.1	ENSG00000223479
chr1:170990672-170990694	+	4	TTTTATTT[TGAAGAGGACTT]	GGG	669	I	MROH9	ENSG00000117501
chr2:195732355-195732377	+	4	TATCTAGT[TGTAGAGGACTT]	TGG	2506	I	SLC39A10	ENSG00000196950
chr13:29257319-29257341	+	4	GCTGTATG[TGCAGAGGACTT]	TGG	6765	I	MTUS2-AS2	ENSG00000236758
chr13:75428163-75428185	+	4	TATTATTT[TGGGGAGGACTT]	GGG	50869	I	RP11-182M20.2	ENSG00000225203
chr6:113786318-113786340	+	4	CCTTTGTG[TGAAGAGGACTT]	TGG	5489	-	RP1-249H1.2	ENSG00000231912
chr18:24998338-24998360	-	4	TTTTTCTC[TGTAGAGGACTT]	AGG	10656	-	RP11-958F21.1	ENSG00000264345
chr1:239522478-239522500	-	4	GTTTTGTT[TGGACAGGACTT]	AGG	23141	I	CHRM3	ENSG00000133019
chr16:76677876-76677898	+	4	ACTTTACC[TGTAGAGGACTT]	AGG	19398	I	RP11-96P7.1	ENSG00000250514
chrX:19285203-19285225	+	4	TTTGGATT[TGGAAAGGACTT]	TGG	58668	-	PDHA1	ENSG00000131828
chr11:62251338-62251360	-	3	TCTTTCTT[GGGTGAGGACTT]	TGG	6530	I	SCGB1D2	ENSG00000124935

Appendix 10 – Off-targets for LCA5 exon 6 sgRNA – Depicted are sgRNA sequence, efficacy score and top off-target hits with gene name, number of mismatches (MM) and location according to CCTop.

11. SSNA1 exon 1 sgRNA off-targets

Sequence: GCAGAACTACAACAACGAGCTGG
Efficacy score by CRISPRater: 0.58 MEDIUM
Oligo pair with 5' extension fwd: TAgGCAGAACTACAACAACGAGC rev: AAACGCTCGTTGTTGTAGTTCTG
Oligo pair with 5' substitution fwd: TAGgAGAACTACAACAACGAGC rev: AAACGCTCGTTGTTGTAGTTCT
Top 20 offtarget sites out of 92 (including on target; for full list see xls file)

Coordinates	strand	MM	target_seq	PAM	distance		gene name	gene id
chr9:137188750-137188772	+	0	GCAGAACT[ACAACAACGAGC]	TGG	0	E	SSNA1	ENSG00000176101
chr8:123433607-123433629	-	4	CTAAAAAT[ACAACAACGAGC]	CGG	1813	I	WDYHV1	ENSG00000156795
chr3:77511149-77511171	+	4	GATGAACA[AAAACAACGAGC]	TGG	11604	I	ROBO2	ENSG00000185008
chr9:20905838-20905860	-	4	GAATAAGT[ACTACAACGAGC]	AGG	1290	I	FOCAD	ENSG00000188352
chr4:186535571-186535593	-	4	ACAAAAAT[ACAAAAACGAGC]	CGG	1014	I	MTNR1A	ENSG00000168412
chr5:68168530-68168552	-	4	CCAAAAAT[ACAAAAACGAGC]	CGG	8637	-	EEF1B2P2	ENSG00000213864
chr6:31546642-31546664	-	4	GGAGGACT[GCAGCAACGAGC]	TGG	0	E	ATP6V1G2	ENSG00000213760
chr22:17004241-17004263	+	4	CCAGAGGT[ACAAAAACGAGC]	TGG	0	E	AC006548.28	ENSG00000280156
chr13:92699003-92699025	-	4	CCAGAGGT[ACAAAAACGAGC]	TGG	2364	I	GPC5-AS1	ENSG00000235984
chrX:67511790-67511812	-	4	CCAGAGGT[ACAAAAACGAGC]	TGG	21351	-	RP4-808O4.2	ENSG00000233710
chr10:102813271-102813293	+	4	GCTGAACA[CCATCAACGAGC]	AGG	0	E	WBP1L	ENSG00000166272
chr5:151391980-151392002	-	3	CCAGAAGT[ACAACAAGGAGC]	TGG	4748	I	CTB-23I7.1	ENSG00000253897
chr10:75776876-75776898	-	4	TCGGATCT[ACAACAAAGAGC]	AGG	5863	I	C10orf11	ENSG00000148655
chr18:26713169-26713191	-	4	GAATATCT[ACAACAAAGAGC]	AGG	3130	I	AQP4-AS1	ENSG00000260372
chr13:40193221-40193243	+	4	ACAAAAAT[ACAACAAAGAGC]	TGG	1266	I	LINC00548	ENSG00000278772
chr11:77248362-77248384	-	4	GTAAAAAT[ACAACAATGAGC]	TGG	2860	I	GDPD4	ENSG00000178795
chr2:9929764-9929786	-	4	TCAGAGGT[ACAACAAGGAGC]	TGG	3997	I	TAF1B	ENSG00000115750
chr6:146941511-146941533	-	4	CCAGAGGT[ACAACAAGGAGC]	TGG	6995	I	RP11-497D6.5	ENSG00000272397
chr7:19951295-19951317	-	4	CCAGAGGT[ACAACAAGGAGC]	TGG	7807	I	AC005062.2	ENSG00000243004
chr1:189016183-189016205	-	4	CCAGAGGT[ACAACAAGGAGC]	TGG	19756	I	CLPTM1LP1	ENSG00000271036

Appendix 11 – Off-targets for SSNA1 exon 1 sgRNA – Depicted are sgRNA sequence, efficacy score and top off-target hits with gene name, number of mismatches (MM) and location according to CCTop.

12. SSNA1 exon 3 sgRNA off-targets

Sequence: CTTTGCTCAGCGTTCTCAAGAGG
Efficacy score by CRISPRater: 0.78 HIGH
Oligo pair with 5' extension fwd: TAggCTTTGCTCAGCGTTCTCAAG rev: AAACCTTGAGAACGCTGAGCAAAG
Oligo pair with 5' substitution fwd: TAggTTGCTCAGCGTTCTCAAG rev: AAACCTTGAGAACGCTGAGCAA
Top 20 offtarget sites out of 60 (including on target; for full list see xls file)

Coordinates	strand	MM	target_seq	PAM	distance		gene name	gene id
chr9:137189826-137189848	+	0	CTTTGCTC[AGCGTTCTCAAG]	AGG	0	E	SSNA1	ENSG00000176101
chr9:129704154-129704176	+	4	AGTTCCTC[AGAGTTCTCAAG]	GGG	8720	I	PRRX2-AS1	ENSG00000236024
chr3:145633682-145633704	-	4	CTCTAATC[AGGGTTCTCAAG]	AGG	50868	-	GM2AP1	ENSG00000241695
chr4:127603373-127603395	+	4	GTTTACTG[AGTGTTCTCAAG]	TGG	19876	-	INTU	ENSG00000164066
chr12:72232108-72232130	+	4	TGTTGCTC[ATAGTTCTCAAG]	AGG	21378	I	TRHDE-AS1	ENSG00000236333
chr6:145540148-145540170	-	4	TGTTGCTC[ACTGTTCTCAAG]	AGG	37573	I	EPM2A	ENSG00000112425
chr11:23138596-23138618	-	4	CTTTTGAC[AGTGTTCTCAAG]	AGG	26282	-	RP11-266A24.1	ENSG00000255418
chr13:82736585-82736607	+	4	CCTTGTTC[TGAGTTCTCAAG]	GGG	86524	-	GYG1P2	ENSG00000237099
chr9:110342293-110342315	-	4	CATTTCTC[ACAGTTCTCAAG]	TGG	4409	-	TXNDC8	ENSG00000204193
chr3:20459702-20459724	+	3	CTTTTCTC[ATCTTTCTCAAG]	TGG	47920	I	RNU6-815P	ENSG00000206807
chr3:75909728-75909750	-	4	CATTGTTT[AGCATTCTCAAG]	AGG	2768	I	ROBO2	ENSG00000185008
chr1:167244039-167244061	-	3	CTGTGCTC[AGGATTCTCAAG]	AGG	2429	I	POU2F1	ENSG00000143190
chr18:11758189-11758211	-	4	CTGTTCTC[TGCCTTCTCAAG]	TGG	4244	I	GNAL	ENSG00000141404
chr15:55226325-55226347	+	4	CTTTTATC[ACCCTTCTCAAG]	AGG	2262	I	RAB27A	ENSG00000069974
chr9:107338318-107338340	+	4	ATCGGCTC[AGCGTTCCCAAG]	CGG	6124	-	RAD23B	ENSG00000119318
chr4:178438063-178438085	-	4	TTTTACTC[GGCGTTTTCAAG]	GGG	31233	-	RNA5SP173	ENSG00000201727
chr10:4554374-4554396	+	4	CATAGCTC[AGCTTTATCAAG]	AGG	39317	-	RNU6-163P	ENSG00000207124
chr7:114715887-114715909	-	4	ATGTGGTC[AGCGTTCTTAAG]	TGG	22115	-	FOXP2	ENSG00000128573
chr10:110246489-110246511	-	4	CTATGCTA[AGCCTTTTCAAG]	GGG	671	I	MXI1	ENSG00000119950
chr14:105333596-105333618	-	4	CAGTGCTC[AGCTTTCCCAAG]	TGG	2807	I	PACS2	ENSG00000179364

Appendix 12 – Off-targets for SSNA1 exon 3 sgRNA – Depicted are sgRNA sequence, efficacy score and top off-target hits with gene name, number of mismatches (MM) and location according to CCTop.

13. Nucleotide sequence alignment of TTC30A/B wildtype and siRNA described by Du *et al.*

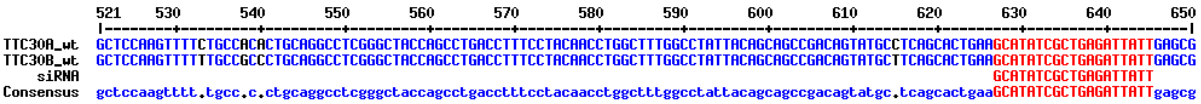

Appendix 13 – Nucleotide sequences of TTC30A/B wt aligned with the siRNA described by Du *et al.* – The graphic depicts the alignment of nucleotide sequences from TTC30A and TTC30B wt as well as the siRNA described by Du *et al.* using the multiple sequence alignment tool [171]. Different base pairs are depicted in black, similarities between TTC30A and B in blue. Additionally, similarities between TTC30A/B and the siRNA are depicted in red [33]

8.2. Acknowledgements

An dieser Stelle möchte ich mich bei denen bedanken, die mir diese Arbeit ermöglicht und zum Erfolg beigetragen haben.

An erster Stelle möchte ich mich bei Prof. Dr. Marius Ueffing bedanken, der es mir ermöglicht hat meine Doktorarbeit in seiner Arbeitsgruppe anzufertigen. Seine Fragen und konstruktive Kritik im Rahmen von Präsentationen und Besprechungen waren wertvoll für mich und meine Arbeit. Zusätzlich bedanke ich mich bei Ihm als Prüfer und Gutachter meiner Arbeit sowie für die Möglichkeit weiterhin in seiner Arbeitsgruppe an Ziliopathien zu forschen.

Ich danke Prof. Dr. Robert Lukowski für die Bereiterklärung als Prüfer und Gutachter dieser Arbeit zu fungieren. Dank unserer Besprechungen habe ich durch seine Hinweise immer neue Denkanstöße erhalten.

Ebenfalls möchte ich mich bei Prof. Dr. Peter Ruth und Prof. Dr. Frank Böckler bedanken, die sich als Prüfer im Rahmen der mündlichen Qualifikation zur Verfügung gestellt haben.

Ganz besonderer Dank gilt Dr. Karsten Boldt und Dr. Tina Beyer für die hervorragende Betreuung meiner Arbeit. Durch unsere zahlreichen Gespräche, auch zwischen Tür und Angel, habe ich zahllose Tipps, Ratschläge und neue Ideen erhalten, die mich und die Dissertation auf den richtigen Weg gelenkt haben. Dafür möchte ich mich herzlich bedanken.

Für die Unterstützung bei mikroskopischen Fragestellungen möchte ich mich bei Dr. Timm Schubert und Sylvia Bolz bedanken.

Katrin Junger und Franziska Klose, möchte ich dafür danken, dass sie sich um die Massenspektrometer und um jede zu messende Probe gekümmert haben.

Vielen lieben Dank auch an alle Kollegen der AG Ueffing, die mich während der Zeit als Doktorand immer unterstützt haben. Insbesondere bei Franziska Wörz, Tobias Leonhard und Isabel Stehle möchte ich für die großartige Arbeitsatmosphäre und ihre stetige Hilfsbereitschaft danken.

Zuletzt möchte ich mich bei meinen Freunden und Eltern bedanken. Danke dass ihr während der langen Zeit immer an meiner Seite gestanden habt und immer ein offenes Ohr hattet.

Vielen Dank!